# Nanoscale

Accepted Manuscript


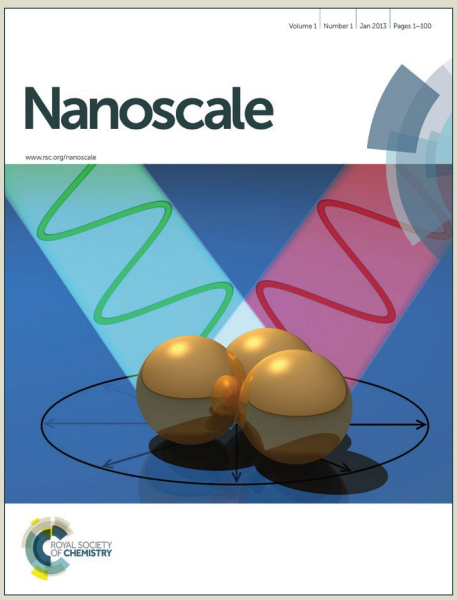





ROYAL SOCIETY OF CHEMISTRY

www.rsc.org/nanoscale

Nanoscale

REVIEW

# High Energetic Compositions Based on Functionalized Carbon Nanomaterials

Received 00th November 2015,
Accepted 00th January 2016

DOI: 10.1039/x0xx00000x

www.rsc.org/

Qi-Long Yan[a], Michael Gozin[†a], Feng-Qi Zhao[b], Adva Cohen[a], Si-Ping Pang[c]

In recent years, research in the field of carbon nanomaterials (CNMs), such as fullerenes, expanded graphite (EG), carbon nanotubes (CNTs), graphene, and graphene oxide (GO), have been widely used in energy storages, electronics, catalysts, biomaterials, as well as medical applications. Regarding energy storage, one of the most important research directions is the development of CNMs as carriers of energetic components by coating or encapsulation, thus forming safer advanced nanostructures with better performances. Meanwhile, some of the CNMs can also be functionalized to become energetic additives. This review article covers updated preparation methods for the aforementioned CNMs, with a more specific orientation towards the use of these nanomaterials in energetic compositions. Besides, the effects of these functionalized CNMs on thermal decomposition, ignition, combustion and reactivity properties of energetic compositions are significant, which are further discussed with more details. It has been shown that the use of functionalized CNMs in energetic compositions would greatly improve their combustion performances, thermal stability and sensitivity. In particular, the functionalized Fullerene, CNTs and GO are the most appropriate candidate components in nanothermites, solid propellants and gas generators, due to their superior catalytic properties as well as facile preparation methods.

## Introduction

Energetic materials (EMs) are a class of material with high amount of stored chemical energy that can be released in a fast way, and the typical classes of EMs include explosives, pyrotechnics and propellants. Gunpowder (GP), invented in ancient China, is considered as the first EMs in human history. It is a mixture of sulfur, charcoal, and potassium nitrate (saltpeter). Charcoal as form of carbon together with sulfur are fuels, while the saltpeter is an oxidizer[1,2]. Due to promising heat and gas generation properties, GP has been widely used as firearm propellant and pyrotechnic composition. As a primitive energetic composition, the GP is no longer widely in use and replaced by more advanced energetic systems both in civil and military applications, which are still under fast development. In past decades, researchers are seeking safer energetic materials with better performance, which implies four aspects: high energetic, insensitive, nontoxic, and environmental friendly[3]. In newly developed propellants and explosives, the carbon-rich materials are thereby gradually replaced by high nitrogen materials (HNMs) with higher energy content and better oxygen balance[4]. However, these HNMs are in most cases not safe enough for practical applications. Recently, a variety of carbon nanomaterials (CNMs) have been developed as carriers of EMs, combining to form advanced structures with higher performances. Some of them, as coating or encapsulating materials, is also very effective in improving the safety of energetic systems[5].

It's well known that solid carbon materials (SCMs) can be found in different forms of bulk phases (e.g. Diamonds) as well as more molecular forms (e.g. fullerenes)[6]. In fact, CNMs has a unique place in nanoscience owing to their exceptional electrical, thermal, chemical and mechanical properties. They have found application in diverse areas as composite materials, energy storage and conversion, sensors, drug delivery, field emission devices and nanoscale electronic components, due to strong adsorption capacity, chemical stability, high mechanical strength as well as easy modification[7]. Currently, several kinds of SCMs could be used in the field of EMs, which can be divided into two groups. One group is nano-powdered carbon, such as carbon black (CB) and nanodiamond, where the latter can be used as a reducing agent in energetic compositions[8]. Another one is CNMs with rich pore structure and large surface area, including fullerenes, expanded graphite (EG), carbon nanotubes (CNTs), graphene, and graphene oxide (GO). The application of these materials in the field of energetic compositions has been recently summarized[9]. In order to further expand the scope of their applications in EMs, usually nano-sized carbon materials with large surface area could be functionalized with energetic groups, or coupled with binders, energetic compounds, metal fuels, combustion catalysts, etc. to form novel advanced function nanostructures with better properties that could be used in propellants, explosives and pyrotechnics[10]. In recent years, extensive research has been done

[a] Center for Nanoscience and Nanotechnology, Faculty of Exact Science, Tel Aviv University, Tel Aviv 69978, Israel.
[b] Science and Technology on Combustion and Explosion Laboratory, Xi'an Modern Chemistry Research Institute, Xi'an 710065, China.
[c] School of Materials Science & Engineering, Beijing Institute of Technology, Beijing 100081, China.
† Corresponding authors, M. Gozin, e-maill: cogozin@gmail.com, Tel: +972-3-640-5878; Q.-L. Yan, e-mail: qilonyan@post.tau.ac.il.

on preparation and application of carbon nanomaterials in EMs[11], especially graphene, GO, CNTs and their composites as combustion catalysts or energetic components[12,13]. In addition, activated carbon fiber and graphite were also attempted in propellant manufacture and waste treatment. The relevant research topics include: design, synthesis, characterization and properties of carbon based nanomaterials; potential usage of nano-sized carbon materials in rocket propulsion; the catalytic effect and mechanisms of carbon based nano-sized catalysts on decomposition and combustion of energetic materials; application and characterization of carbon nanomaterials in purification of waste water in explosive industry[14].

In the past decades, a large amount of papers has been published regarding preparations and applications of CNMs, based on which several review papers are available mainly in Chinese literature[8,12,15-18]. Experimental and theoretical data on new carbon nanostructures using fullerenes, nanotubes as well monolithic diamond-like nanoparticles, nanofibers, various nanocomposites as starting materials are summarized in a Russian journal as well[15]. Their atomic and electronic structures, the nature of chemical bonds and physicochemical properties are compared. The applications of fullerene materials in catalytic reactions including hydrogen transfer and hydrosilylation, pyrolysis of alkanes, $H_2$-$D_2$ exchange, coupling and alkyl transfer reaction are reviewed[16]. Recent advances on the application of graphene based catalysts in energetic materials are also introduced, revealing that they have significant catalytic effect on combustion of solid propellants[17,18]. Graphene based EMs usually has larger energy release rate, meanwhile, the burning rate, mechanical properties, as well as sensitivity of propellants can be improved by using graphene or GO[19]. However, those review papers are not accessible for most of the western researchers due to language barrier. Besides, many other papers reporting CNTs, EG and CB materials and their applications in the field of EMs are still not reviewed and summarized. In order to make such a large amount of data on CNMs available to all readers especially those published in Chinese journals, this paper is trying to do an overview of preparation methods of CNMs based EMs as well as their effects on performance and sensitivity of corresponding energetic compositions.

## Classification of Carbon Nanomaterials

Carbon is one of the most important natural elements, and it has $sp^3$, $sp^2$, sp hybridizations of its orbitals. The molecular carbon atoms' anisotropy $sp^2$ may lead to anisotropy of some crystals of these materials (Table 1). Therefore, carbon materials have widely extended properties. In fact, more and more new carbon materials continue to be discovered and artificially prepared. There is no other element like carbon as a single element can form so diverse and completely different substances, in terms of structures and properties, such as 3-D diamond crystal and graphite, 2-D graphite sheets, 1-D CNTs and 0-D fullerene molecules. It has been discovered that carbon materials are mostly superior in their hardness, optical properties, heat resistance, radiation characteristics, chemical resistance, electrical insulation, electrical conductivity, surface and interface properties to many other materials. Carbon materials probably can cover the characteristics of all substances on the planet, such as "the hardest to the softest", "insulator to semiconductor, further to a super conductor", "insulation to great thermal conductivity", "fully-light absorbing to completely transparent" and so on, so these materials have a wide range of applications as listed in Table 2. In general, CNMs are attracting more and more attention in recent years due to a possibility of specific preparation of a wide range of variously-shaped nano-carbon crystals in a form of needles, tubes, spheres and many other morphologies[20]. For example, the three key conjugated CNMs are: graphene, CNTs and fullerenes. These materials have very different morphologies with unique chemical properties, but they still have much in common, especailly in terms of basic building units (Figure 1).

Table 1 Carbon compounds, carbon chemical bonds and phase formations

| Bond types | Hybridization Type | | | |
|---|---|---|---|---|
| | sp | $sp^2$ | $sp^3$ | Mixed |
| Coordination | 2 | 3 | 4 | variable |
| Average C-C Length (nm) | 0.121 | 0.133<br>0.142 | 0.154 | - |
| Binding Energy | 46 kJ $mol^{-1}$ | 35 kJ $mol^{-1}$ | 20 kJ $mol^{-1}$ | - |
| Typical Examples | Acetylene | Ethylene<br>Benzene | Adamantane,<br>Cyclododecane<br>$(CF)_n$, SiC, $B_4C$ | - |
| Identified Carbon Phases | Carbene (hexagonal facets bulk crystal C60) | Graphite (in-plane)<br>(a cubic, hexagonal) | Diamonds | $C_{60}$ |
| Undetermined carbon phases | $C_2$ to $C_{20}$<br>Carbon molecules | 1- graphite 3d-$sp^2$ bct-4<br>Polystyrene | 6H-Diamonds<br>-BC-8 | carbophene<br>graphyenes |

Table 2 The types of carbon materials.

| | Fullerenes | CNTs | Graphite | Diamond | Amorphous C |
|---|---|---|---|---|---|
| | 0-Dimension | 1-Dimension | 2-Dimension | 3-Dimension | Amorphous |
| Preparation Methods | CVD, Ablation, Discharge | Discharge, DoH, Fluoride, CVD and Ablation | CVD, Evaporation, Ablation | High-Pressure synthesis, CVD | CVD, PVD, Sputtering, Plasma |
| Morphology | Single crystal, Amorphous | Fibers | FM, Crystalline, DC | Crystalline | Amorphous, Fiber |
| Characteristics | Semi-conductive,; Catalytic, FM, SC | Conductive, High strength, Catalytic, High TC | Conductive, Catalytic, Intercalating | High hardness, High TC, HR, AR | High hardness, Conductive, CR |
| Applications | ULM, Nonlinear OM | SLM, USM, ERM, CC | Electronic, X-ray OM, CC | ULM, EEM, Coating, CC | ULM, Electronic, Coating, CC |

Notes: DoH, decomposition of hydrogen; MF, molecular fiber; DC, directional crystallization; FM, ferromagnetic; SC, superconductive; TC, thermal conductivity; HR, heat resistance; AR, abrasion resistance; CR, corrosion resistance; ULM, ultra-lubricating materials; OM, optical material; SLM, super lightweight material; USM, ultra-high strength material; PVD, Physical vapor deposition; CVD, Chemical vapor deposition; ERM, energy raw materials; EEM, electricity - electronic materials; CC, catalyst carrier

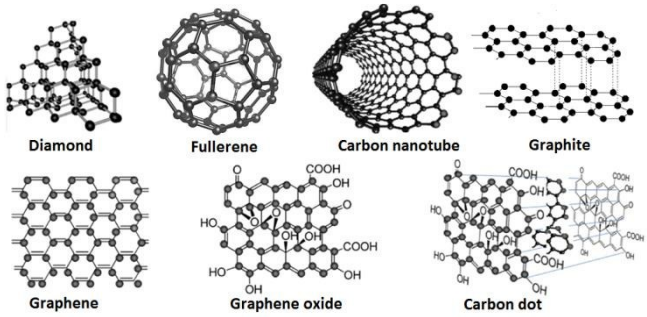


Figure 1. Various forms of carbon nanomaterials.

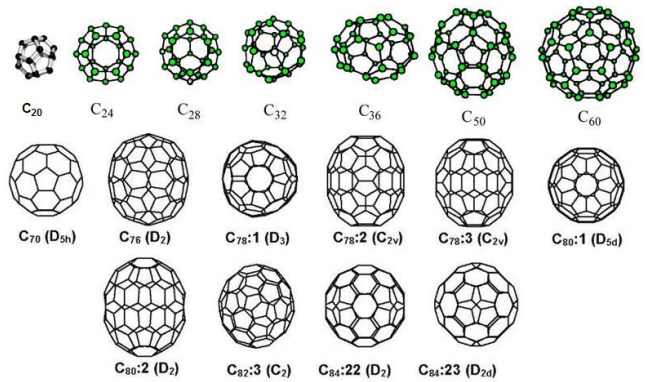


Figure 2. Fullerene structures and their symmetry.

These CNMs can transform to each other under a certain experimental condition, and hence, initial work on CNTs has origins in a fullerene research. There are many kinds of fullerene derivatives ($C_{20}$, $C_{32}$, $C_{60}$, $C_{70}$, $C_{84}$, etc.), where Buckminsterfullerene ($C_{60}$) is a typical and well-known example[21]. Each fullerene possesses the characteristic of being a pure carbon cage, each atom bonded to three others, as in the graphite (Figure 2).

Table 2 shows examples of various typical carbon materials. As mentioned in the Introduction part, current CNMs, including fullerene, graphene, CNTs and carbon materials have many excellent physical and chemical properties, and some of them are widely used in the field of EMs. Unlike graphene, every fullerene has exactly 12 pentagonal faces with a different number of hexagonal faces (e.g., $C_{60}$ has 20). The CNTs could be seen as graphene sheets rolled into hollow tubes, which could be divided into single-walled, double-walled and multi-walled nanotubes. As a special cylindrical form of fullerene, CNTs were discovered more than 30 years earlier than fullerenes, but this discovery was not fully appreciated at that time. Recently, CNTs production exceeded several thousand tons per year, and these materials are used for applications in energy storage, automotive parts, boat hulls, sporting goods, filters, electronics, coatings, carrier of catalysts and electromagnetic shields.[22] CNT-related publications were more than tripled during the past decade, while a rate of patent applications was also dramatically increased. Although most of the CNMs production output was of unorganized structure, organized CNT architectures such as "forests", yarns and regular sheets were manufactured in smaller volumes[23]. Except for fullerenes and CNTs, some other CNMs, including graphene and GO, are also under intensive investigation[24-28]. In the following sections, newly developed preparation methods for several mentioned CNMs, together with the functionalized EMs and energetic compositions based on these materials are summarized with more details.

## CNMs Based Energetic Nanomaterials

### Energetic Composites Containing Carbon Black

***Manufacturing Processes of CB:*** Carbon black (CB) material is composed mostly of fine particles of amorphous carbon. Various features of CB are controlled during its production by partially combusting oil or natural gases[29,30]. It is widely used in various applications from black coloring pigment (resin coloring, dyes and printing inks) to electric conductive agents for high-technology materials, including antistatic films, fibers and magnetic media. A large amount of CB is used in automobile tires as an excellent rubber reinforcement agent[31,32].

CBs could be produced by thermal decomposition or partial combustion of hydrocarbons, such as oil and natural gas[33]. The characteristics of a particular CB vary depending on manufacturing

process. The material produced by furnace process, currently the most widely used method, is called "furnace black", distinguishing it from CB manufactured by the other processes. The latter is usually used in energetic compositions. Furnace black is obtained by blowing an aerosol of petroleum or coal into a high-temperature chamber. This method is efficient for mass production of CB due to high yields as well as better particle size and structure control. The other preparation methods include channel process (by bringing partially combusted fuel), acetylene black process (by thermally decomposing acetylene gas) and lampblack process (by collecting soot from fumes, generated by burning oils or pine wood). Recently, a new method has been developed to produce CB from hydrolysis, carbonization and pyrolysis of rice husk[34]. The specific surface area (SSA) of CB obtained from the rice husk was increased from 389 (of the previous starting materials) to 1034 $cm^2\ g^{-1}$ and pore volume from 0.258 to 0.487 $cm^3\ g^{-1}$, respectively. This method is also applicable to preparation of CB from other types of biomass. For better applications of CB in different industrial products, it has to be dispersed by some solvents. For example, stable high-load dispersions of CB in PMA (propyleneglycol methylether acetate) could be prepared by a ball-milling process. Another type of CB materials is Graphitized carbon black (GCB), which is a non-porous form of amorphous carbon. The GCB powder is made up of highly agglomerated nanoparticles with a spherical morphology, and it has been shown from the high-resolution TEM images that it has a core-shell structure. A 5 nm graphitic shell is covering an amorphous carbon core (Figure 3).

A highly graphitized CB has been used to evaluate isosteric heat of adsorption in order to determine the difference in adsorption mechanism of strong polar and non-polar fluids[35-38], allowing its use in chemical residue analysis[39]. GCB materials are hydrophobic and frequently used to effectively trap organic compounds from water or water vapours.

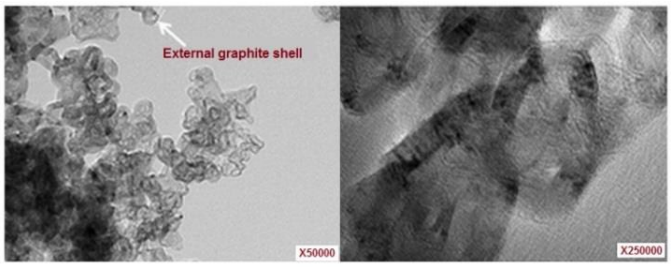


Figure 3. TEM images of the GCB material (crystallized in a 3H graphitic structure with a $d_{002}$ interlayer space of 0.346 nm, which is slightly larger than that of an ideal graphitic structure, 0.335 nm). Reprinted from Ref. 37 published in *J Aoac Int* (2009) with permission of Publishing Technology.

As a super adsorbent, CB could be easily combined with nano-sized Ems[36], forming a new type of energetic mixtures with better performances, which are described in the following section.

***Energetic Compositions Containing CB*:** CB is usually used as an additive in solid rocket propellants to modify their combustion properties due to its large surface area with strong adsorption effect[39]. CB is considered as an important additive in energetic compositions, and its effect on performances of EMs is significant even with the content of less than 5 wt.%. In fact, graphite, CB and fullerene differ by their structure as well as surface properties in terms of defects and surface groups, which affect surface free energy characteristics and surface energetic heterogeneity[40]. Therefore, these CNMs may have different effects on solid rocket propellants' performance. As mentioned above, GCB has larger SSA and the commercial one has SSA from 6 to 225 $m^2g^{-1}$. It was shown that the GCBs with lower SSA exhibited a higher degree of graphite crystallinity, resulting in higher average adsorption energy to $N_2$[41]. Before adding CB to solid propellants, it must be homogeneously mixed with polymer binders. The homogeneity of CB dispersion in several polymers has been evaluated by electric conductivity of the resulted mixture. It has been shown that the minimum viscosity during curing is critical to CB dispersion morphology[42]. However, no data is available regarding the mixtures of CB with polymers, such as hydroxyl-terminated polybutadiene (HTPB) and glycidyl azide polymer (GAP) that are used in propellants. The CB may also be used as flame retardant for interpenetrating polymer networks based on unsaturated polyester/epoxy, where the CB maintains the mechanical properties of the polymer as compared with the other additives[43]. In order to achieve better mechanical strength, CB is usually used together with Carbon Fiber (CF) in polymer blends. It was indicated that the surface roughness of CB and CF strongly affects the carbon-polymer interactions, and the entropy penalty plays a determining role in competitive adsorption of polymers on the rough carbon surfaces[44]. This may also be the case for energetic polymer binders, such as poly-BAMMO and poly-NIMMO. It has been found that the surface of CB is energetically heterogeneous. The level of roughness (or heterogeneity) of CB could be evaluated theoretically using lattice density functional theory (DFT), where two lattice DFT models have been developed and experimentally verified[45]. The surface activity of commercial and lab-produced CBs is varying in their particle size. It consists of at least four different adsorption sites, while the fraction of which depends on production process of CB and its particle sizes[46]. The fraction of high-energy sites largely decreases with decrease of the particle sizes, and completely disappears during graphitisation.

The reinforcing potential of CB is closely related to the amount of high energetic sites. Therefore, it can be used as active filler in the rubber industry including rubber based propellants to improve their physical and dynamic properties. The surface energy difference between rubbers and CB is large, which has a negative influence on the stability of the CB dispersion in the rubber matrix and on its distribution in blends of different rubbers. It was suggested to use plasma polymerization in modification of CB's surface by depositing a thin film of polymer over it[47]. The fullerene soot as a by-product of fullerene production can be used in this plasma modification process[48]. In this case, both CB and polymer matrix would have a comparable surface energy, where the polymer matrix could be elastomers like Styrene-Butadiene Rubber (SBR), Butadiene Rubber (BR) and Ethylene-Propylene Diene Rubber (EPDR), which are widely used in polymer bonded explosives (PBXs) and propellants[49]. There is an alternative way to improve the mechanical strength of CB-containing polymer blends, which are ball-mill mixing, annealing and quenching heat treatment[50]. The



 

first process can break down highly structured CB into finer particles, while the latter two make CB form a coagulation structure again in the polymers.

The shock wave generated from detonation of EMs may in turn cause phase transition in CB, due to extreme pressure and high temperature. Such phase transitions provide a way for preparation of nanodiamond from CBs, where a cubic crystal diamond structure is obtained. This method is significantly different from the preparation of diamonds using graphite as a carbon source[51]. In the past, CB was commonly used in solid propellants, but recently it was also used in primary explosives in order to improve their ignition delays as well as to reduce sensitivity. For example, a primary explosive, tetramine-bis(5-nitrotetrazolato) cobalt(III) perchlorate (BNCP) has been combined with CB[52]. It was proved that CB can decrease laser initiation threshold of BNCP, the detailed mechanism of which will be discussed in a later section. CB can also be combined with potassium nitrate (KN) to form a new kind of propellant (CBKN) for special application in blasting valves[53]. Such blasting valves are used at nuclear power stations in pressurized water reactors. Comparing black powder (HY6) and sulfur-free black powder (WHY6) to CBKN propellant it was shown that he latter has higher auto-ignition temperature (over 321 °C) and lower burn rate, indicating that the CBKN has better thermal stability. In addition to the abovementioned application, CB may have further applications in EMs. For instance, in the development of nanothermites, the requirements for their mechanical and electrostatic sensitivities are high. Such sensitivities may be modulated by using pristine or chemically modified CB as additives, as it was already shown for performance improvement of $WO_3$/Al nanothermite[54].

## Energetic Mixtures Based on Nanodiamonds (nD)

***New preparation methods for nD*:** Diamond has a variety of promising physico-chemical properties, such as high density (among carbon-based materials), and low thermal sensitivity[55]. Nanodiamonds (nDs) are diamonds with size in the range of several nanometers. The nDs were found inside meteorites and can be easily produced by explosion methodology. In past decades, a variety of techniques have been developed for the production of nD[56], including radio-frequency plasma-aided decomposition of hydrocarbon[57], plasma-assisted CVD, using hydrocarbons[58], transformation of graphite under shock compression (SCP)[59], transformation of $C_{60}$ films under SCP[60], transformation of graphite at high pressure and temperature[61], plasma-based chemical synthesis by using a carbon plasma jet, treatment of the diamond surface in hydrogen plasma and annealing of silica wafer embedded with carbon atoms[62,63]. Furthermore, it can be synthesized by catalysing CB at ambient pressure and a temperature of 1100 °C[64-66]. As mentioned earlier, CB is composed of fragments of carbon network, either single layers (bent, curved or flat) or small, assembled packs[67-71]. Since nDs could be synthesized from CB as a carbon source, one could speculate that it is also possible to prepare nDs from CNTs. In fact, a unique experimental procedure was designed to synthesize nDs by using CNTs as a raw material[72]. It was suggested, on the basis of ultradispersed diamond optical analysis, to consider chemical part of detonation processes as superposition of three basic processes: destruction of "explosophoric groups", the endothermic and exothermic reactions[73]. Trinitrotoluene (TNT) and RDX are the explosives primarily used to synthesize nDs by detonation. It was shown that the use of nanostructured explosive charges may lead to formation of detonation nDs (DnDs) with smaller particle sizes, which provides new understanding of nanodiamond formation-mechanisms[74]. The discontinuity of the explosive at a nanoscale level may play a key role in modifying the particle size of DnDs. Upon using TNT/RDX mixture as the shock wave source, nD particles with the initial diameter of 2-12 nm were obtained[75]. These nD particles would agglomerate during storage with a significant decrease in SSA from 360 to 255 $m^2$ $g^{-1}$ due to aging. An updated mechanism for formation of nD particles during TNT detonation synthesis was recently proposed[76]. This mechanism includes the following steps: (a) decomposition of TNT into radicals, such as dimer $C_2$ and $CO_3$; (b) formation of cyclohexane from $C_2$ or radical of molecules; (c) interaction of diamond-like core (adamantane radical) with methyl; and (d) growth of DnD particles similar to the CVD process. The nD particles could be formed during detonation of EMs, while they can also be used as an ingredient of energetic compositions.

***Energetic Mixtures Based on nD*:** The thermal decomposition of chlorate-based mixtures is initiated by the decomposition of the reducing components. This mechanism was observed in saccharose (Sa)- and thiourea-based compositions[77,78]. This decomposition is started by melting of chlorate while the reducing agent is thermally stable. Therefore, the thermal insensitivity of the reducing agent is the key point of desensitization of chlorate-based energetic formulations. The nDs were suggested to replace Sa for improving the sensitivity of potassium chlorate (KC)-based compositions[79]. It was shown that the nDs/KC formulations are much less sensitive to thermal stress. The TEM image and XRD spectra of nDs incorporated into KC matrix are shown in Figure 4.

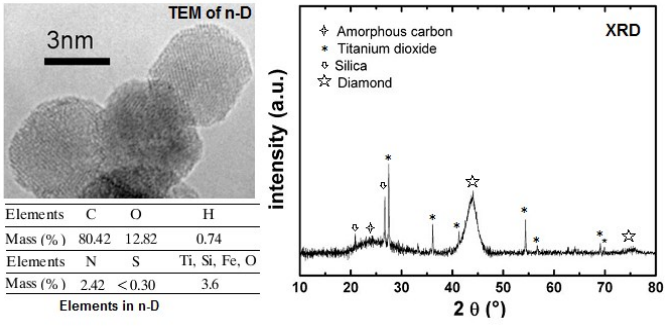


Figure 4, TEM picture, XRD pattern chemical composition of nDs used to form the nDs/PC compositions. Reprinted from Ref. 79 published in *Propellants Explos Pyrotech* (2009) with permission of John Wiley & Sons, Inc.

It could be seen that the diameter of nDs is less than 5 nm, with carbon content of about 80% and O content of 12.8%. It seems that the Sa content in Sa/KC mixtures has little effect on their impact sensitivity (IS), while the IS of nDs/KC compositions strongly depends on the nDs content. However, the nDs/KC compositions

with larger content of nDs are very sensitive to friction, due to the hardness of the diamond. The nDs/KC compositions were found to be deflagrating primary explosives with maximum propagation rate of 3,960 m $s^{-1}$ at 12.3 MPa when the content of nDs is 22 wt.%. Such compositions are considered as "green" primers. The nDs/KC reactive formulations usually decompose in two possible combustion modes, i.e. (i) continuous or (ii) intermittent, depending on the proportion and pressing level of nDs used to shape the pellets[80].

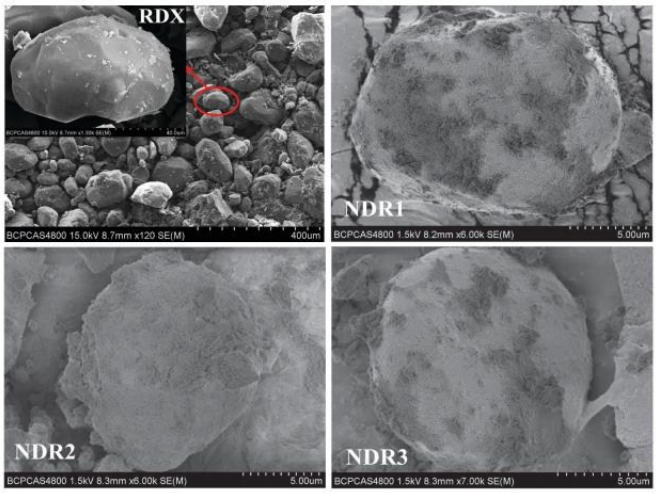


Figure 5, SEM images of RDX and the n-D, where n-D to RDX are kept at 1:8 (NDR1), 1:6 (NDR2), and 1:4 (NDR3) which correspond to increasing the mass proportions of n-D coating of 1/9, 1/7, and 1/5, respectively. Reproduced from Ref. 81 with permission from the PCCP Owner Societies.

In addition to direct use of nDs as an ingredient in energetic compositions, it could also be used to coat particles of high EMs. It was reported that a well-dispersed and uniformly shaped DnDs were produced and used in coating of micron-sized RDX particles[81]. SEM images of these materials are shown in Figure 5. It has been found that the DnDs could reduce the energy barrier of thermal decomposition of RDX and improve its reactivity. However, excessive coating over 1/3 of nDs would hinder the decomposition and gas diffusion, as an inert shell.

Similar to the other CNMs, except for physically combining with energetic components, nDs could also be functionalized with energetic or other functional groups. However, this topic is unexplored and no data has been published in opened literature on this issue till today. The most important reason for chemical functionalization of nDs is that detailed and unambiguous characterization of the surface structure of nD particles remains to be a very challenging task. In fact, it was shown that treating the nD particles in a reduction reaction, resulted in enrichment of hydroxyl and hydroxymethyl functional groups, paving a way for new generation of nD-based EMs.

## Energetic Composites Based on Expanded Graphite

***Development of Expanded Graphite*:** Due to the layered structure of graphite, atoms, ions and even small molecules could be inserted (intercalated) between the graphene layers of graphite, and it is a quite easy process for the case of expandable graphite ($E_bG$). There are several popular ways to prepare $E_bG$ as an excellent halogen-free flame retardant, including liquid phase synthesis, ultrasonic irradiation, and hydrothermal methods[82,83].

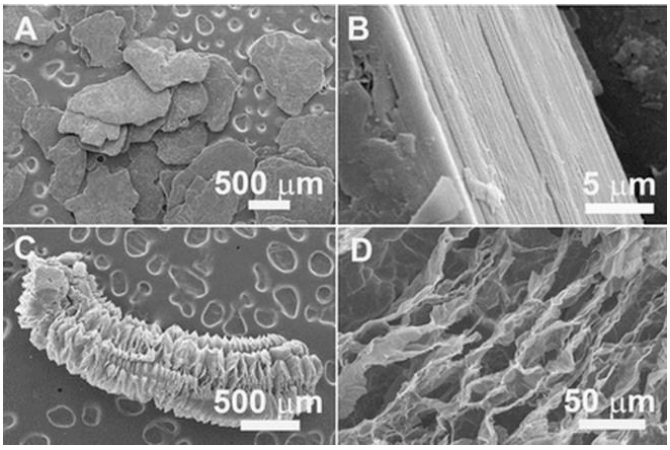


Figure 6, SEM images of the characteristic structures of flake graphite (A, B) and expanded graphite (C, D). Reproduced from Ref. 85 with permission of Copyright 2013, The Electrochemical Society.

Recently, a new preparation procedure was developed, where the natural graphite was initially dispersed in $H_2O_2$ and then introduced into an autoclave to proceed with the hydrothermal process[84]. In all cases, under the influence of heat, the graphite layers are separated like in an accordion, expanding the graphite flakes (Figure 6)[85]. High quality $E_bG$ has a large proportion of intercalated layers, where sulphur- or nitrogen-containing compounds are used as intercalating agents. Depending on a nature of graphite and intercalating agent, expansion can commence at as low as 180°C and can occur suddenly and rapidly. In the case of a free expansion, the final volume between the layers can be several hundred times greater than the initial one. It is well known that electrochemical insertion of $Na^+$ into graphite is greatly hindered by the insufficient interlayer spacing, while the EG could be a good option to replace graphite used in a $Na^+$ battery anode (Figure 7).[86] EG can usually be prepared from fine expandable graphite flakes (160 μm in size), using acetic anhydride as inserting agent and potassium dichromate as oxidant[87]. The best known conditions for this process are: mole fractions of a graphite, acetic anhydride, concentrated sulfuric acid, potassium dichromate should be 1:1:3.1:0.6, with reaction time of 50 min and reaction temperature of 45 °C. Similarly, the micron-sized EG is prepared by chemical oxidation method, using sulfuric and glacial acetic acids as inserting reagents and potassium dichromate as oxidizing agent[88]. The optimum mass ratio of raw materials for the latter process is: $E_bG/H_2SO_4/CH_3COOH/K_2CrO_7$ (1:5:3:0.5), while the reaction time is 60 min at room temperature. The micron-sized EG has stronger infrared extinction coefficient than the raw graphite, due to inclusion of some open or semi-open small holes that can absorb infrared radiation. The expansion usually occurs at the very beginning of the reaction, and the extension of the reaction times has little effect on the microstructure of the final EG[89]. After its preparation, the EG



 

material is ready for applications in various fields including preparation of advanced EMs.

***Preparation of EG-containing Materials*:** EG can be used in heat-generating energetic compositions to enhance thermal conductivity in packed bed reactors (PBR) of chemical heat pumps (CHP)[90,91]. The PBR is fabricated using a certain energetic mixture. The corresponding CHP is based on reversible solid-gas reactions, where the energetic density and energy content are the key factors that determine its performances, depending on the reactive medium implementation. It has been shown that the solid-gas pair $CaCl_2/CH_3NH_2$ can be optimized by adding EG as a filling material, which could improve the heat and mass transfer[90]. It is also the case for packed bed reactor system MgO-$H_2O$[91]. In both dehydration and hydration, the EG/MgO-$H_2O$ pellets have higher reaction rates and reactivity than the pure $Mg(OH)_2$ pellets. The temperature distribution is also more homogeneous in the packed bed. As mentioned above, EG is currently widely used as a flame-retardant in many kinds of polymers. Moreover, a novel flame-retardant EVA/IFR/Synergist composite containing $CaCO_3$, EG and graphite was developed[92]. Because of its properties, this composite material may have a great potential application in solid propellant cladding materials. Except for its flame-retardancy, EG also found its application in electromagnetic materials. Recently, nano γ-$Fe_2O_3$/EG magnetic composite was prepared by sol-gel and low temperature self-combustion techniques[93]. This magnetic composite may be very useful as a combustion catalyst in solid propellants as well. In order to make a mutual comparison, the preparation methods of EG and its composites are summarized in Table 3.

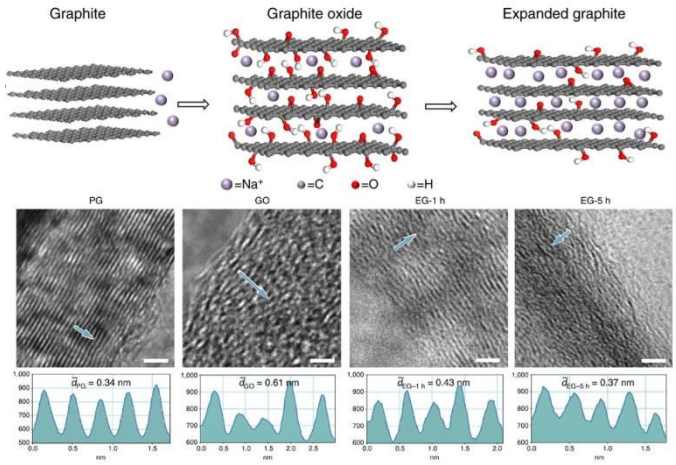


Figure 7, upper is a schematic diagram: (left) $Na^+$ cannot be electrochemically intercalated into graphite because of the small interlayer spacing, (middle) Electrochemical intercalation of $Na^+$ into GO is enabled by the enlarged interlayer distance because of oxidation; However, the intercalation is limited by steric hindering from large amounts of oxygen-containing groups; (right) a significant amount of $Na^+$ can be electrochemically intercalated into EG owing to suitable interlayer distance and reduced oxygen-containing groups in the interlayers.; below is the high-resolution TEM images showing cross-sectional layered structures for PG, GO, EG-1 h and EG-5 hrs. Reprinted from Ref. 79 with permission of Copyright © 2014, Nature Publishing Group.

## EMs Based on Functionalized $C_{60}$ Fullerene

***Introduction of Functional Materials Based on $C_{60}$:*** $C_{60}$ has been very extensively investigated in terms of its functionalization and corresponding applications[94]. The application field depends on functionalization reactions, which can be one of the followings: hydrogenation reduction by electron addition, reaction of fullerene radical anions with electrophiles, nucleophilic addition, nucleophilic substitution, forming its organometallic derivatives, polymers, dendrimers and related structures[95]. The applications of fullerene materials in catalytic reactions, such as singlet oxygen oxidation, non-metal nitrogen-fixation, graphite-diamond transition, as well as EMs combustion processes. Several new functionalization reactions have been developed by using molecular catalysis, such as (a) organoboron addition to fullerenes, (b) C-H bond allylation and arylation of hydroxyfullerenes, (c) C-H/C-C bond cleavage of alkynyl-hydoxyfullerenes, (d) regioselective tetraallylation of fullerenes, (e) nucleophilic substitution of aziridinofullerene, and (f) cycloaddition of alynes to aziridinofullerene[96]. An new interdisciplinary field was created when supramolecular chemistry and fullerenes crossed with each other, whereby many unprecedented fullerene-based supramolecular architectures have been designed and constructed[97]. For example, rotaxanes[98], catenanes[99], self-assembled coordination compounds[100], liquid crystalline inclusion complexes[101], and photoactive supramolecular devices[102] were prepared and characterized. Later on, a stable supramolecular complex was synthesized from a bis-crown ether receptor and a bis-ammonium fullerene ligand[103]. First, fullerenes have extraordinary capabilities to coordinate metal atoms, both inside (endohedral) and outside (exohedral) the carbon cage[104]. Many exohedral compounds have been synthesized, such as the Pd and Ir complexes. The fullerene ligands in these cases are acting in a similar manner to olefins (Figure 6) [105,106].

The exohedral metallofullerenes may open a new way to prepare a variety of novel energetic materials and combustion catalysts. A certain functionalized fullerenes can be heated to their ignition temperature with low-intensity, continuous-wave (c.w.) laser irradiation[107]. Laser-induced ignition was demonstrated with various laser radiation at intensities as low as 100 W $cm^{-2}$. As shown in Figure 9, processes ***a*** means Laser-induced cleavage of functional groups induces acoustic shock-waves or otherwise imparts kinetic energy to the fullerene cages; ***b***, Energetic fullerene cages collide, leading to coalescence or disintegration ***c***, Coalescence of SWCNTs into larger SWCNTs, MWCNTs and carbon onions is promoted by the heat generated by the incident laser, cleavage of the functional groups and the exothermic coalescence processes, together with the catalytic action of cleaved functional groups and defects on the nanostructures; ***d***, Alternatively, disintegration of fullerene cages supplies carbon for the simultaneous formation of SWCNTs, MWCNTs and carbon onions, with intact fullerene cages acting as nucleation sites. The simultaneous formation of various carbon nanostructures can be catalysed by cleaved functional groups and the defects present on intact fullerene cages. The energetic fullerene cages collide, leading to coalescence or disintegration.

Table 3 the preparation methods and application of expanded graphite based energetic materials

| Materials | Preparation methods | Application fields | Contributors |
|---|---|---|---|
| EG | 1, using natural graphite flakes as raw material, acetic anhydride as inserting agent and potassium dichromate as oxidant; | Antistatic and anti-electromagnetic material, Electronic devices, Flame retardant, Energetic materials | Ji, et al., 2006 |
| | 2, By dispersing natural graphite in $H_2O_2$ with subsequent hydrothermal treatment in autoclave; | | Kuan, et al., 2012 |
| | 3, Micron-sized EG can be prepared by the method of chemical oxidation, using sulfuric acid and glacial acetic as inserting reagent and potassium dichromate as oxidizing agent | | Ba, et al., 2011 |
| Porous carbon | Prepared from energetic carbon precursors, alkali propiolates, via ultrasonic spray pyrolysis; | Purification, catalysts | Xu, et al., 2012 |
| EG/PP | EG/polypropylene (PP) nanocomposites are prepared by solid-state ball-milling followed by low-temperature melt mixing | Engineering materials, Binders | Mohammad, et al., 2013 |
| EG/$Mg(OH)_2$ | By mixing $Mg(OH)_2$ powder and EG | Chemical heat pumps | Zamengo, et al., 2014 |
| γ-$Fe_2O_3$/EG | Nano γ-$Fe_2O_3$/EG is prepared by sol-gel and low temperature self-combustion technique | Magnetic materials | Zhang, et al., 2011 |
| $CaCl_2/CH_3NH_2$/EG | Mixed using a cylindrical solid-gas reactor | Chemical heat pumps | Balat, et al., 1993 |

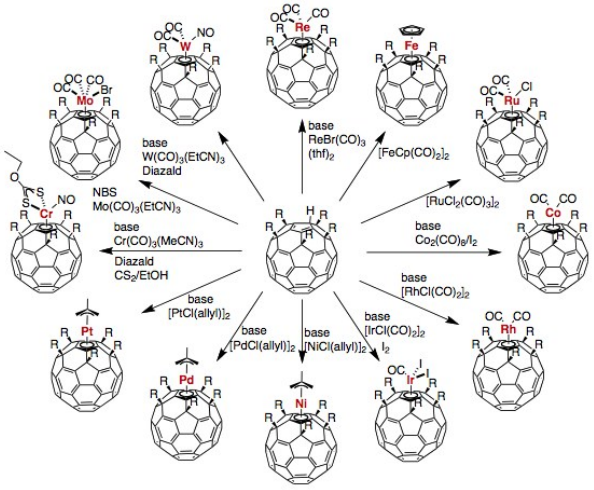


Figure 8, syntheses paths exohedral metal fullerene complexes. Reprinted from Ref. 106 with permission from the Copyright © 2011, Royal Society of Chemistry.

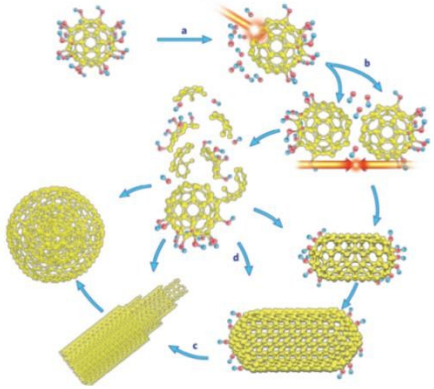


Figure 9. Proposed mechanism for laser-induced transformation of functionalized fullerenes. Reprinted from Ref. 107 with permission of Copyright © 2008, American Chemical Society.

***Functionalization of Fullerenes by Energetic Moieties***: The preparation of energetic fullerene can trace back to 1990s in China, while the first compound of this kind available in the literature might be trinitrophenyl $C_{60}$ derivative (Cp-1, TNPF), by reacting of trinitrochlorobenzene with sodium azide[108]. There were no further reports on this issue until 2006, when a new fullerene derivative containing energetic moiety N-methyl-2-(1,3-dinitrophenyl) fulleropyrrolidine (MDFP) was prepared by the Prato reaction (Scheme 1).

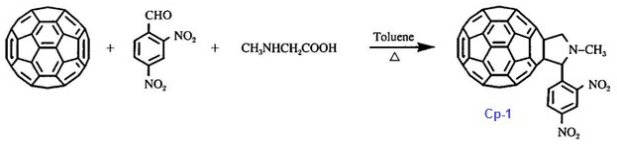


Scheme 1: Preparation procedure of MDFP[108]

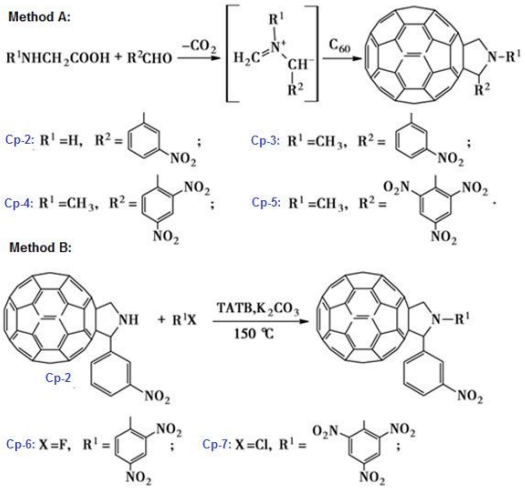


Scheme 2: Preparation methods of N-unsubstituted fullerpy- rrolidine. Reprinted from Ref. 110 published in *Chin J Energet Mater* (2009) with permission.

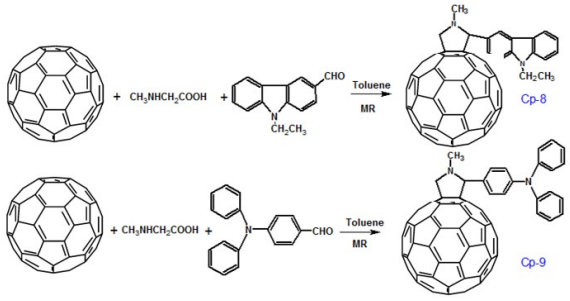


Scheme 3: Preparation method of N-methyl-2-(4'-N, N-diphenylaminophenyl)-fulleropyrrolidine under microwave irradiation.

The optimum molar ratio of $C_{60}$, 2,4-dinitrobenzaldehyde and N-methylglycine reactants was 1:2:6, while the reaction was conducted at 95 °C for 40 hrs[109]. After the latter publication, the preparation of energetic fullerene derivatives became a popular topic and many new compounds were synthesized. Typical representatives of this family of compounds are nitro-fulleropyrrolidine derivatives, which are synthesized by the 1,3-dipolar cycloaddition reactions of $C_{60}$ and the nucleophilic substitution reaction of N-unsubstituted fulleropyrrolidine[110] (Scheme 2). More specifically, Cp-1 to Cp-4 compounds are prepared by 1,3-dipolar cycloaddition, while the Cp-6 and Cp-7 are prepared from Cp-2 via necleophilic substitution.

It has been found that the mechanical sensitivity of HMX could be greatly reduced when it was mixed with 1% of N-methyl-2-(3-nitrophenyl) fulleropyrrolidine (Cp-3, MNPFP). Also, N-Methyl-2-(N-ethylcarbozole)-fullero- pyrrolidine (Cp-8, MECFP) and N-methyl-2-(4'-N,N-diphenylaminophenyl)- fulleropyrrolidine (Cp-9, MDPAFP) were synthesized via microwave irradiation (MR; Scheme 3)[111]. Photoinduced intramolecular electron transfer process from $C_{60}$ moiety to carbazole moiety has been studied by nanosecond laser flash photolysis. The performance of N-methyl-3-(2',4',6'-trinitrobenzene)-fulleropyrrolidine (Cp-5, MTNBFP) has been estimated by using self-consistent field calculation method based on the following overall isodesmic reaction.

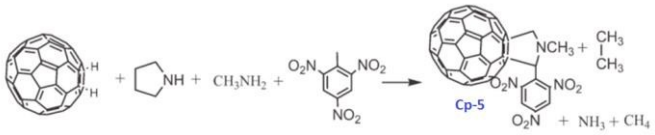


Scheme 4: Preparation of Cp-5

It has been calculated that the enthalpy of formation of Cp-5 is 2782.2 kJ $mol^{-1}$, while its detonation velocity and pressure are 3282 km $s^{-1}$ and 4.443 GPa, respectively[112]. Upon complete combustion, the total heat of combustion for Cp-5 is $2.17\times10^5$ kJ $mol^{-1}$ due to its high carbon content. It seems that this compound may not be useful as the main ingredient of an explosive or a propellant, but it might be good additive for heat generating energetic compositions. In order to improve the energetic content of fullerene derivatives, a promising way is introduction of more nitro groups on the fullerene skeleton. Such strategy has been attempted recently, where a high nitrogen content derivative $C_{60}(NO_2)_{14}$ (FP, CP-10) was prepared and characterized[113], using a prolonged treatment of $C_{60}$ in benzene with very high concentrations of $N_2O_4$. However, Cp-10 is not so thermally stable and it deflagrates when heated above 170 °C in nitrogen or air, releasing a considerable amount of heat. This compound may be used as a powerful explosive, depending on its sensitivity, which has not been reported. Except for the nitro-derivatives of fullerene, there are also fullerene nitrates that can be used in propellant compositions as energetic burn rate modifier. As a typical example, fullerene ethylenediamine nitrate (Cp-11, FEDN) was synthesized by reacting fullerene and ethylenediamine in diluted nitric acid (Scheme 5)[114].

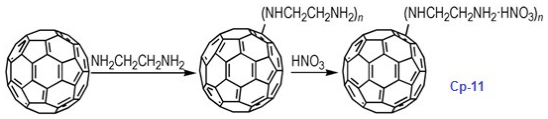


Scheme 5: Synthesis of Cp-11.

Cp-11 can undergo three-step decomposition process starting at about 100 °C. The details about its decomposition mechanism will be described in a later section. Energetic fullerene catalysts may improve the specific impulse of solid propellants, meanwhile decrease their pressure exponents. There is another type of polymeric catalyst based on fullerene, so-called fullerene itaconic acid copolymer lead salt (FIAL, Cp-12), which may have better effect on combustion[115]. It was prepared via a two-step reaction by using $C_{60}$, itaconic acid and lead nitrate as starting materials (Scheme 6).

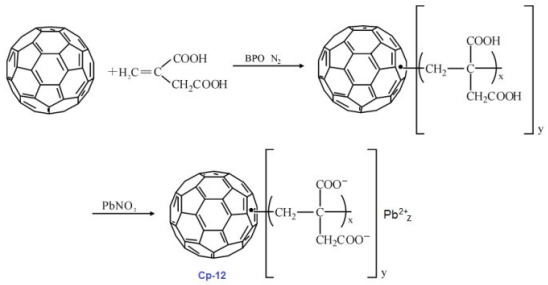


Scheme 6: Synthesis method of Cp-12.

As shown in Scheme 6, the reaction time and temperature had little effect on the final content of lead. However, the optimum reaction conditions for the preparation of Cp-12 were found to be at 25 °C with pH value of 6.9. The resulting catalyst Cp-12 is quite thermally stable, with decomposition temperature peak at 304 °C. Based on aforementioned fullerene nitrate (FN, Cp-11), a more energetic derivate, fullerene ethylenediamine dinitramide (FED, Cp-13) could be obtained via ion exchange reaction with ammonium dinitramide in 84% yield (ADN; Scheme 7)[116].

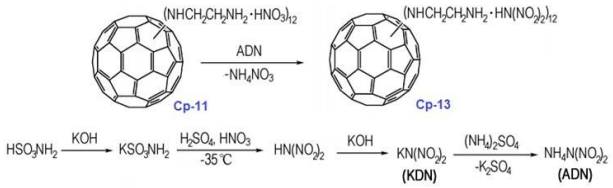


Scheme 7. Synthesis method of Cp-13 and ADN.

The Cp-13 product has appearance of yellowish solid and its structure was analyzed by UV-vis, FT-IR, elemental analysis and XPS techniques. Based on these analyses, Cp-13 was found to have a formula of $H_{12}C_{60}(HNCH_2CH_2NH_2{\cdot}HN(NO_2)_2)_{12}$, and it was proposed for use as an oxidizer in solid propellants like ADN. In order to combine the advantages of fullerene and lead salts as propellant catalysts, another lead salt based on fullerene phenylalanine (FPL, Cp-14) was prepared. Analogously to Cp-12, Cp-14 can be prepared by using the same strategy, where the Pb cation comes from $Pb(NO_3)_2$ (Scheme 8)[117,118].

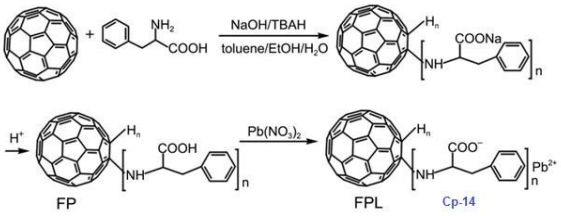


Scheme 8: Synthesis of Cp-14

FPL was found to have a significant catalytic effect on decomposition of 1,3,5-trinitroperhydro-1,3,5-triazine (RDX), and it may be used as an efficient combustion catalyst in solid propellants. On the basis of abovementioned synthetic method, a new potential energetic combustion catalyst, fullerene hydrazine nitrate (FHN, Cp-15) was designed and prepared in a two-step process. First, fullerene hydrazine (FH) was prepared in 84% yield from fullerene and hydrazine hydrate, and then the obtained FH was reacted with concentrated nitric acid to form FHN salt in (Scheme 9)[119].

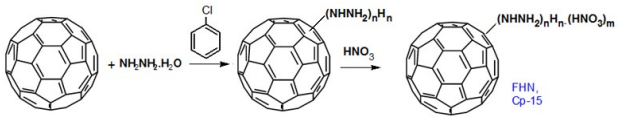


Scheme 9: Synthesis of Cp-15

The elemental and other chemical analyses of FH showed composition of C, 69.38%, N, 26.86% and H, 3.76%, strongly indicating that the formula of FH, obtained under these reaction conditions is $C_{60}(NHNH_2)_{10}H_{10}$. The corresponding formula of FHN salt was found to be $C_{60}(NHNH_2)_{10}H_{10}{\cdot}4HNO_3$ with the oxygen content of 14.9%. In general, $C_{60}$ can either be combined with energetic moieties, as shown above, or be functionalized with energetic polymers. Two novel fullerence-based energetic polymers have been prepared recently, including $C_{60}$-poly(glycidyl nitrate) ($C_{60}$-PGN, Cp-16)[120] and $C_{60}$-glycidyl azide polymer ($C_{60}$-GAP, Cp-17)[121]. The former polymer was synthesized through a modified Bingel reaction of $C_{60}$ with bromomalonic acid PGN ester, in presence of amino acid in dimethyl sulfoxide, while the latter was prepared by using the same reaction between $C_{60}$ and bromomalonic acid glycidyl azide polymer ester (Scheme 10). Both Cp-16 and Cp-17 have great thermal stability over 200 °C and could be used as energetic binders of solid propellants.

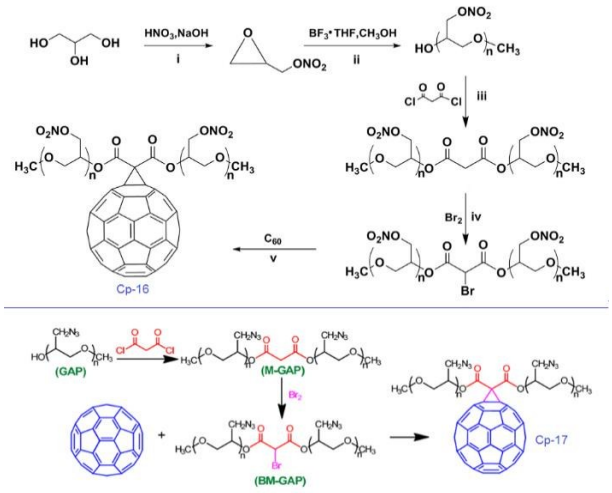


Scheme 10, Synthesis of $C_{60}$-PGN and $C_{60}$-GAP.

For better comparisons, the preparation methods and applications of abovementioned energetic fullerene derivatives are summarized in Table 3.

As shown in Table 3, it is clear that most of the energetic fullerene derivatives were obtained directly by reacting $C_{60}$ with corresponding energetic precursors. Almost all the work has been carried out during the past 5 years, strongly indicating that this research field is in its infancy. Those energetic fullerene derivatives could either be used as combustion catalysts or as energetic binders. However, the compatibility and sensitivity were not systematically investigated yet for all these materials, which is very important for their practical applications.

## EMs Based on Graphene, GO or Reduced GO

***Improved methods of Graphene, GO and rGO preparations*:** Graphene is a carbon-based material that is typically a one atom thick sheet of graphite. It has been widely investigated in past decades starting with a report by Novoselov et al. on its isolation and unique electronic properties[122]. Soon after its discovery, graphene was mainly applied in electronic devices[123,124]. The high quality graphene sheets are usually prepared by CVD process[125,126], requiring very expensive facilities, and hence new alternative methods for graphene preparation need to be developed. The exfoliation of alkali metal graphite intercalation compounds (GIC), as one of promising ways, is therefore designed to prepare non-functionalized and functionalized graphene sheets retaining the $sp^2$ network. For example, alkali metal-based GICs readily exfoliate in N-methylpyrrolidone (NMP), giving stable solutions of negatively charged graphene sheets[127], and soluble functionalized graphenes with minimum $sp^2$ disruption were synthesized by reacting exfoliated alkali metal-based GICs with electrophiles[128].

GO is another form of graphene that is also very attractive for preparation of graphene-based materials[129-131]. In fact, thin films of GO could be reduced in solution under various reducing conditions, and the reduction converts GO into a reduced-GO (rGO) material, which exhibits better electrical conductivity[131,132]. In addition to its

use in making rGO for electronic devices, GO has been used in catalytic oxidation[133-135], biotechnology[136-139] and as a surfactant[140].

Table 3 the preparation methods and application of fullerene based energetic materials

| Materials | Preparation method | Application field | Contributors |
|---|---|---|---|
| FPGN | Through a modified Bingel reaction of $C_{60}$ and bromomalonic acid PGN ester in the presence of amino acid and dimethyl sulfoxide; | Energetic binder; | Gong, et al., 2015 |
| FFGAP | Using a modified Bingel reaction of [60]fullerene ($C_{60}$) and bromomalonic acid glycidyl azide polymer ester (BM-GAP); | Energetic binder; | Huang, et al., 2015 |
| FPL | Fullerene phenylalanine (FP) was dissolved in 10 mL water, then the pH of FP water solution was adjusted to 6.96 using 1 mol/L $HNO_3$, adding $Pb(NO_3)_2$ (0.01 mol) and the mixture was stirred at 30 °C for 3 h; | Propellant catalyst; | Guan, et al., 2014 |
| FHN | Fullerene hydrazine is synthesized from fullerene and hydrazine hydrate, and then it reacts with concentrated nitric acid to form fullerene hydrazine nitrate; | Energetic combustion catalyst; | Guan, et al., 2014 |
| FEN | Using fullerene, ethylenediamine and dilute nitric acid as raw materials; | Propellant catalysts; | Chen, et al., 2014 |
| FED | via ion exchange reaction of fullerene ethylenediamine nitrate and ammonium dinitramide (ADN); | Energetic components; | Chen, et al., 2014 |
| mPF | Gycyl-porphyrin (20 mg) and $C_{60}$ (42 mg) are dissolved in 45 ml of anhydrous toluene under, then add three-fold excess of benzaldehyde; | Catalyst of explosives; | Jin, et al., 2014 |
| FIA-Pb | Prepared via two steps reaction using $C_{60}$, itaconic acid and lead nitrate as raw materials; | Propellant catalyst; | Liu, et al., 2013 |
| PF | Prolonged treatment of $C_{60}$ in benzene with very high concentrations of $N_2O_4$; | Magnetic material; | Cataldo, et al., 2011 |
| MTNBFP | Not available in the literature; | Primary explosive; | Tan, et al., 2010 |
| NFD | Synthesized by the 1, 3-dipolar cycloaddition reactions of $C_{60}$ and the nucleophilic substitution reaction of N-unsubstituted fulleropyrrolidine; | Propellant catalyst; | Jin, et al., 2009 |
| FDFP | Prepared by the Prato reaction with reactants molar ratio of $C_{60}$, 2,4-dinitrobenzaldehyde and N-methylglycine 1:2:6; | Energetic catalyst; | Jin, et al., 2006 |
| NPF | Prepared via $C_{60}$ reacts with trinitrochlorobenzene and sodium azide; | Energetic components | Wang, et al., 1996 |

Notes: FEN, fullerene ethylenediamine nitrate; FED, Fullerene ethylenediamine dinitramide $H_{12}C_{60}(HNCH_2\ CH_2NH_2{\cdot}HN(NO_2)_2)_{12}$; mNPF, N-methyl-2-(3-nitrophenyl) pyrrolidino-[3',4':1,2] fullerene; NFD, nitro fulleropyrrolidine derivatives; PF, polynitro[60]fullerene, $C_{60}(NO_2)_{14}$; MTNBFP, N-methyl-3-(2',4',6'-trinitrobenzene)-fulleropyrrolidine; FPGN, [60]Fullerene- Poly(glycidyl nitrate); MDFP, N-methyl-2-(1,3-dinitrophenyl) fulleropyrrolidine; FIA-Pb, Fullerene itaconic acid copolymer lead salt; FFGAP, functionalized [60]fullerene-glycidyl azide polymer; FPL, fullerene phenylalanine lead salt; FHN, fullerene hydrazine nitrate;; NPF, trinitrophenyl $C_{60}$ derivative.

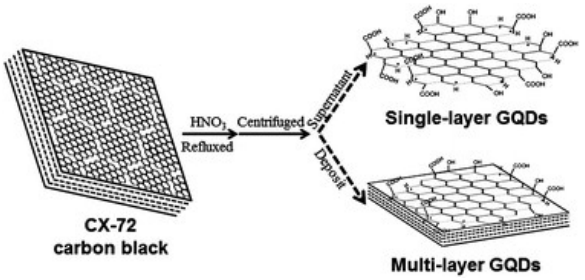


Figure 10. The preparation procedures for single- and multi-layer GQDs. Reprinted with permission from Ref. 141 with permission of © 2009 IOP Publishing Ltd.

Recently, a facile and scalable liquid-phase preparation method for aqueous solutions of isolated graphene sheets from low-temperature EG, was reported[141]. It has been shown that graphene sheets exfoliated from EG could be restored to an extended conjugated $sp^2$ network. Later on, noval single- and multi-layer graphene quantum dots (GQDs) were prepared from CX-72 CB by chemical oxidation (Figure 10)[142]. Single-layer GQDs were demonstrated to be excellent probes for cellular imaging, while the multi-layer GQDs may offer great applications in optoelectronic devices.

Preparation of GO was already reported more than a century ago and it could be done by several approaches. In general, the conversion of graphite to GO is conducted in two steps: (1) the oxidation of graphite to GO; (2) the removal of impurities (acids, manganese salts, etc). Brodie's method, reported in 1859, was the pioneering one, where he used fuming $HNO_3$ and $KClO_3$ as the intercalatant and oxidant[143]. Nevertheless, this method has several flaws, including too long reaction time and generation of toxic gases during the reaction. In 1958, Hummers and Offeman developed another method, which is the most widely employed for synthesis way of GO nowadays[144]. They used $H_2SO_4$ to intercalate graphite in presence of $NaNO_3$, while using $KMnO_4$ as an oxidizer. Recently, Tour et al. improved Hummers method by excluding $NaNO_3$, while increasing the amount of $KMnO_4$ and performing the reaction in a 9:1 mixture of $H_2SO_4/H_3PO_4$[145]. However, there are still several problems in this method. To solve these problems, an improved Hummer's method has been recently developed[146]. In the latter method, GO was prepared with a simple purification process in a high yield, using small graphite flakes as a raw material. In fact, GO in solid state is gradually "reduced" and become darker in its colour upon prolonged storage in air at room temperature. Such disproportionation reactions are highly exothermic[147]. In the past,

thermal reduction/exfoliation of GO was a typical method for rGO production, which however has a drawback of requiring specialized equipment for rapid thermal shock absorption. Currently, a new alternative method is available, based on vacuum and microwave-assisted exfoliation, which has solved the problem of poor reduction of GO with low C/O ratio[148]. Microwave irradiation of GO in vacuum leads to outgassing from GO and the creation of plasma, which aids temperature distribution and hydrogenation. As mentioned earlier, graphene, GO and rGO derivatives are well-known in the field of electronic technology and biotechnology. Although many of these functionalized carbonaceous nanomaterials could be used in various energetic compositions, the number of publications in this field is limited[149]. For instance, GO itself is highly energetic material, thermally unstable and can readily undergo exothermic disproportionation reactions to produce chemically modified graphene under mild heating conditions.

***EMs Based on Graphene:*** Functionalized graphene can be a multidentate ligand to coordinate many metals or metal ions on its surface[150]. Structures of graphene ligands are similar to metal-porphyrin, metal-phthalocyanine, and metal-phenanthroline complexes. The most-commonly used metal ions for coordination to functionalized graphene ligands include copper and nickel[151,152]. Graphene can be combined with EMs or functionalized with energetic groups. The first reported case showed that graphene can be a good carrier for laying molecular monolayers of an insensitive explosive, 1,3,5-triamino-2,4,6-trinitrobenzene (TATB), which was attributed to the strong π-π attraction between the TATB and graphene sheets (Figure 11)[153].

The calculated detonation enthalpy of TATB/graphene complex is 1.61 kJ $g^{-1}$ with a density of 2.1 g $cm^3$, while the detonation pressure and detonation velocity are 10.5 GPa and 2.40 km $s^{-1}$, respectively. The lubricating property of graphene is better than graphite, and a series of complexes with adjustable properties could be obtained by adjusting the proportion and the order of overlaying layers. However, this kind of materials is still in a design stage. In common practice, EMs should be safe enough to be handled even in the case of primary explosives. In order to improve the electrostatic sensitivity of lead styphnate (LS), graphene nanoplatelet-lead styphnate composites (GLS) were prepared either by adding graphene nanoplatelets (GNP) to the reaction solution or by coating normal LS with GNP. The composites showed an excellent anti-electrostatic performance with depressed electrostatic spark sensitivity and static electricity accumulation[154].

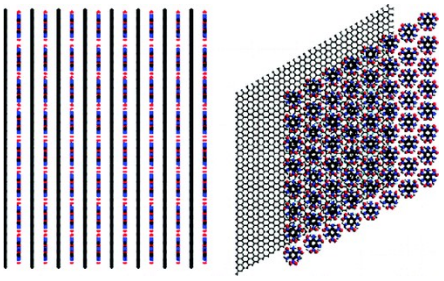

Figure 11. Structure of sandwich complex of TATB/Graphene layer formed due to strong π–π attraction. Reprinted from Ref. 153 with permission of Copyright © 2010, American Chemical Society.

Although potassium picrate (KPA) is less powerful explosive than LS, it has many important applications. KPA is somewhat shock-sensitive and even more sensitive than the parent picric acid. If ignited in confined space, KPA will detonate. The ultrafine KPA was prepared under the action of crystalline controlling agent, and its thermal sensitivity can be improved by graphene-doping. The KPA doped with graphene nanoparticles (having a larger surface area) may partially hinder the effective collisions of KPA particles and accelerate the heat dispersion[155], and hence the mechanical sensitivity of KPA may be decreased. Except for primary explosives, high energy solid propellants also need to be safer in order to be used in low vulnerable (LOVA) munitions.

In particular, ammonium perchlorate (AP) is the main ingredient of high energy composite propellants. Yet, its surface properties need to be improved for better safety. A nano-composite based on AP and graphene aerogels (AP/GA, Figure 12) was prepared by a sol-gel method and characterized by scanning electron microscope (SEM), elemental analysis and X-ray diffraction (XRD) techniques[156]. It has been seen in Figures 12a and 12b that (similarly to GA), there are still many voids inside AP/GA nano-composite material with SSA of 49.18 $m^2g^{-1}$. However, a large amount of AP particles, with an average particle size of 69.4 nm, are attached to the skeleton of graphene. The elemental analysis of this material shows that the content of AP may reach 94%, which is very promising as the main energetic component[157]. Based on AP/GA nanocomposites, a novel GA/$Fe_2O_3$/AP nanostructured energetic material was prepared by a sol-gel method, which was followed by a supercritical $CO_2$ drying technique (Figure 13)[158]. It has been demonstrated that $Fe_2O_3$ and AP are well dispersed in GA layers on a nanometer scale, where $Fe_2O_3$ exhibits a catalytic effect on thermal decomposition of AP.

Figure 14 shows the SEM images of GA and GA/$Fe_2O_3$/AP nano-structured energetic composite. It is apparent that the morphology of GA is uniform on large scale and exhibits a three-dimensional network of randomly oriented sheet-like structures with wrinkled texture as well as rich hierarchical pores. It is very similar to AP/GA, a plenty of AP crystallizes on the networks of GA and covers the surface. $N_2$ adsorption-desorption isotherms of GA and the corresponding nanocomposites are shown in Figures 14c and 14d.

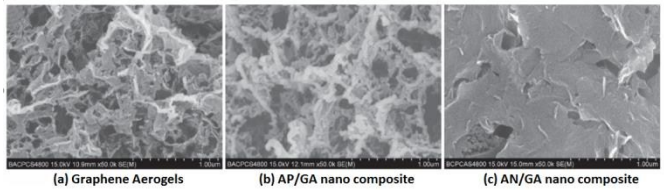


Figure 12. the SEM photos of GA and AP/GA nano composite. Reprinted from Ref. 156 with permission of Copyright © 2012, *Chin. J. Explos. Propellants*.

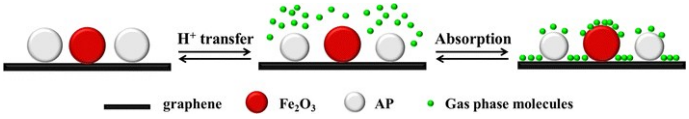


Figure 13. the principle of GA/$Fe_2O_3$/AP nanostructured energetic composite formation, where $Fe_2O_3$ and AP nanoparticles are added and trapped in the porous three-dimensional networks of GA. Reprinted from Ref. 158 with permission of Copyright © 2014, Springer Science.

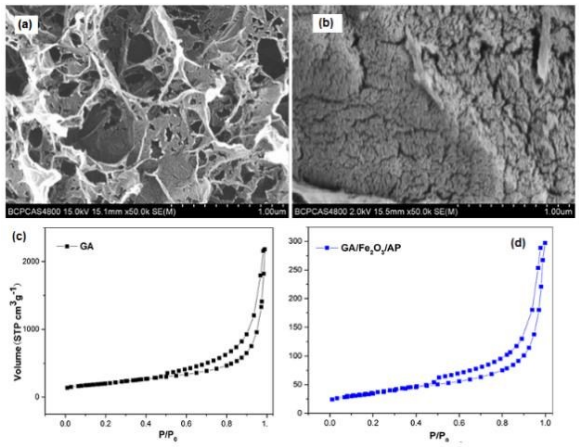


Figure 14. The SEM images of GA (a) and GA/$Fe_2O_3$/AP nanostructured energetic composite (b); Nitrogen adsorption–desorption isotherms for GA (c) and GA/$Fe_2O_3$/AP nanostructured energetic composite (d). (reproduced from Lan, J. Sol-Gel. Sci. Tech., 2015, 74,161-167.) Reprinted from Ref. 158 with permission of Copyright © 2014, Springer Science.

For GA/$Fe_2O_3$/AP nano-structured energetic composites and GA, the adsorption-desorption curves indicate an open wedge-shaped meso-porous structure of this material, resulting from the presence of the graphene sheets[159]. The tested SSAs of GA and the nano-composite are 717 and 123 $m^2 g^{-1}$, respectively, while the total pore volumes ($V_{tot}$) determined by the Barret-Joyner-Halenda (BJH) method for GA and the nano-composite are 3.37 and 0.46 $cm^3 g^{-1}$, respectively. After filling GA with AP, the nano-composite shows significant decreases in its SSA and $V_{tot}$, indicating that AP may decrease the SSA of the product.

Except for AP, GA can also be used to prepare nanocomposites of ammonium nitrate (AN), another common oxidant used in propellants and explosives. Similarly, it can be prepared by the sol-gel method followed by a supercritical $CO_2$ drying process[160]. According to SEM and elemental analysis, nano-sized AN uniformly disperses in the GA, with an average particle size of 71 nm and mass fraction of 92.7% (Figure 12c). All the above-mentioned materials are metastable intermolecular composites (MICs), which are among the most attractive EMs in terms of their performance. MICs are generally composed of a fuel and an oxidizer with particle sizes in nanometer range. The heat and mass transfer are greatly enhanced due to nanoscale contact of oxidizer and fuel particles. The most promising application for MIC composites is nanothermites. On the basis of graphene functionalization, long-range electrostatic and short-range covalent interactions could be harnessed to produce multifunctional EMs through hierarchical self-assembly of nanoscale oxidizer and fuel into highly reactive macrostructures.

A self-assembly method of Al and $Bi_2O_3$ nanoparticles on functionalized graphene sheets (FGS) was recently reported[161]. The self-assembly process and the chemical bonds formed are shown in Figure 15. Such nanocomposite structure was formed in a colloidal suspension phase that ultimately condense into ultra-dense macrostructures, which contains 5 wt.% of GO. The TEM and SEM photos of GO/Al/$Bi_2O_3$ composites, as well as Al and $Bi_2O_3$ nanoparticles are shown in Figure 15. In this case, the oxygen atom from the OH group on Al is protonated by the hydrogen of the COOH group on GO, which creates a carboxylate anion (GO-$COO^-$) group on the GO (Figure 15).

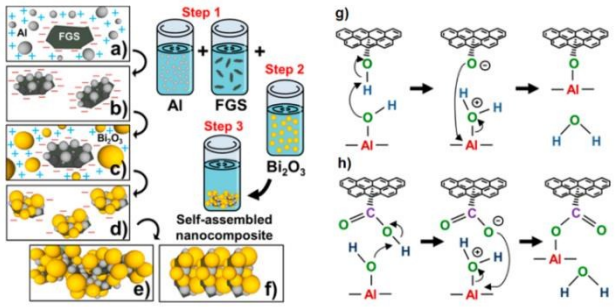


Figure 15, Schematic of the self-assembly process: (a) electrostatic attraction of Al to GO, (b) covalent bonding of GO/Al existing as a stable GO/Al dispersion, (c) electrostatic attraction of $Bi_2O_3$ to GO/Al nanostructures, and (d) noncovalent assembly of $Bi_2O_3$ on GO/Al; instability of GO/Al/$Bi_2O_3$ dispersion continues the self-assembly process to form ultradense macrostructures; Chemical interactions between (g) hydroxyl groups of GO and surface hydroxyl groups of Al nanoparticles leading to C–O–Al covalent bond and (h) carboxylic groups of GO and hydroxyl groups of Al nanoparticles leading to O=C–O–Al covalent bond. Reprinted from Ref. 161 with permission of Copyright © 2014, American Chemical Society.

The covalent bonding between Al and GO, and the absence of covalent bonding between $Bi_2O_3$ and GO, were shown by various spectroscopic methods.The Figure 16 shows the orientation of the GO/Al/$Bi_2O_3$ nanostructures within the larger macrostructures. The formation of this structure is suggested to be driven by the two-particle-size modes, where the smaller sized and less planar GO/Al/$Bi_2O_3$ forms randomly oriented macrostructures, while more planar one tends to condense into layered macrostructures for larger-sized assembles. Layered assembly probably arises from the preference of larger 2-D GO/Al/$Bi_2O_3$, and they geometrically align with one another due to van der Waals interactions. Regardless of their structure, the GO/Al/$Bi_2O_3$ nanocomposites have excellent fuel/oxidizer contact in comparison to randomly mixed Al/$Bi_2O_3$, resulting in enhanced reactivity.

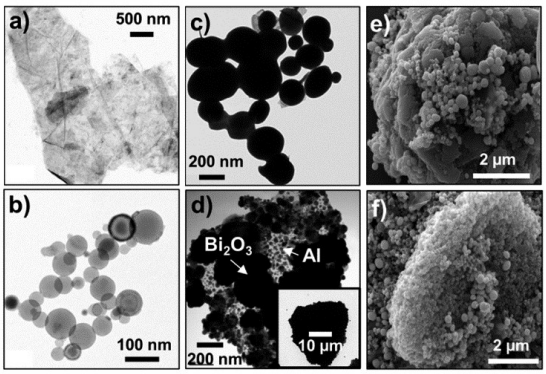


Figure 16, TEM (a–d) and SEM (e, f) images of GO(5%)/Al/$Bi_2O_3$ composites self-assembled from nano to macro length scales: (a) a few layered GO sheets, (b) Al nanoparticles with 80 nm average diameter, (c) $Bi_2O_3$ nanoparticles with 90–210 nm size range, and (d) layered nanoscale building block of a GO densely decorated with Al first and then $Bi_2O_3$; The inset in (d) shows a ultradense assembly of Al and $Bi_2O_3$ on GO; ultradense macro structures self-assembled from GO/Al/$Bi_2O_3$ nano-composites in layered (e) and random (f) orientations. Reprinted from Ref. 161 with permission of Copyright © 2014, American Chemical Society.

It was found that a remarkable enhancement in measured energy release from 739 to 1421 J $g^{-1}$ for this novel composite than for normal $Al/Bi_2O_3$ mechanical mixture. Except for the aforementioned method, pyrocarbon (PyC) coating can also be introduced to $Al_2O_3$-$SiO_2$ system, using *in situ* oxidation of PyC by thermolysis of AN.[162] The formation of nitrogen oxides during the decomposition of AN could enable the oxidation of PyC at relatively low temperature. In this way, PyC coating can be easily introduced to three-dimensional all-oxide fiber-reinforced composite (Figure 17). For the composites without PyC interphases (Figure 17a), the fracture surface was very homogeneous and nearly without pull-out fibers. As shown in Figure 17b, the fibers were tightly surrounded by the matrix and no fiber/matrix (F/M) debonding occurred, suggesting strong interfacial bonding. A large number of micro-pores are distributed on the fiber surface due to chemical corrosion of matrix. Obvious fiber pull-out behaviour is shown for the composites with PyC interphases (Figure 17c) due to weak interfacial bonding, which has been confirmed by SEM imaging (Figure 15d). It indicates that the porous coating is favourable to the F/M debonding, thereby improving the performances. As mentioned earlier in this section, insensitive energetic materials are greatly desirable for LOVA ammunition compositions. The capability to control compositions and properties for target EMs is essential toget optimal performance, controlled energy release, and low sensitivity. With these goals in mind, a new work on relatively insensitive explosive 1,1-diamino-2,2-dinitroethylene (FOX-7) has been done[163]. The FOX-7 nanocrystals were prepared under confinement of mesoporous carbon FDU-15 via a self-assembly process. It has been indicated that a complete impregnation can be achieved in N-methyl-2-pyrrolidone at 100-110 °C, and the maximum amount of FOX-7 in the FOX-7/FDU-15 composites could be 43.8 wt.%. There are many other functionalized graphene that are only used in energy storages such as batteries and fuel cells. One could refer to a comprehensive review on graphene derivatives in energy storage applications for further details[164].

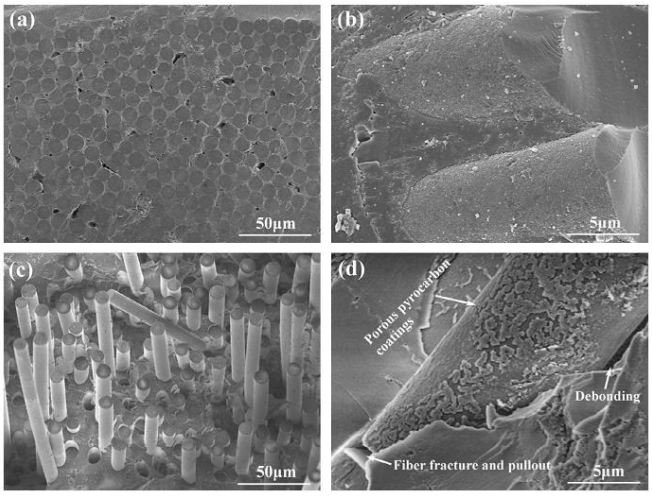


Figure 17. Fracture surfaces of the N440/AS composites without (a, b) and with (c, d) PyC interphases. Reprinted from Ref. 162 with permission of Copyright © 2015, Elsevier Ltd.

## EMs Based on GO and rGO

As compared with graphene, GO seems to be more suitable and easier for functionalization into energetic compounds. First, GO itself is considered as a potential EM. Upon heating, GO can readily undergo violent exothermic decomposition due to the extensive oxygenic functional groups on the basal plane (phenol, hydroxyl, and epoxide) and at the edges (carboxylic)[165]. It is also the case for rGO, which is confirmed to retain some oxygenic groups resulting from the imperfect reduction. Therefore, rGO is energetic as well, yet not as energetic as GO. The DSC results suggest that GO may take up to 0.8 kJ $g^{-1}$ of heat to trigger its deoxygenating reaction. Since the heavy addition of inert graphite would impair the energy output of the composite explosives, GO and rGO could be promising candidates to substitute graphite in the insensitive high energy PBX compositions.

On the one hand, GO and rGO may act as space-qualified lubricants, which could strongly improve the low-temperature performance of hypergolic ionic liquids by reduction of their viscosity[166]. However, to match the type of graphene to the specific ionic-liquid functionality is very important to achieve the optimized performance. On the other hand, GO and rGO may enhance the ignition and burning properties of hypergolic ionic liquids. For example, it has been found that the laser ignition and burn rates of Nitrocellulose (NC) microfilms can be enhanced upon doping with GO[167], where a Nd:YAG (1064 nm, 20 ns) laser was used to ignite GO-doped NC films at low temperatures. The researchers studied several kinds of NC microfilms doped with different concentration of GO, (e.g. 0.1 wt.%, 0.5 wt.%, 1 wt.% and 2 wt.%). Some of the morphologies these films are shown in Figure 18. The pure NC films are continuous, smooth, and homogeneous (Figure 18a). After introducing the GO into NC films, the morphology of the latter varies significantly and its surface becomes rough.

Moreover, the increase in the concentration of GO would lead to formation of highly porous structure (Figures 18b and 18c). AFM imaging and comparion of GO-doped NC containing 0.5 wt.% of GO with the one containing 1 wt.% shows the latter has larger pores with diameters from 0.5 μm to 3 μm (Figure 18e).

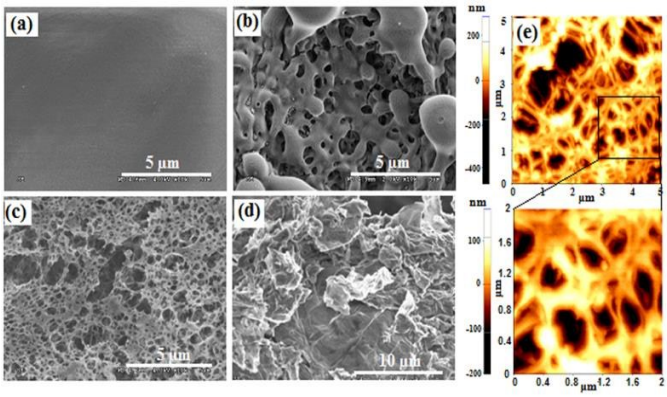


Figure 18. SEM and AFM images of pure and GO doped NC films. SEM image of (a) pure NC film, (b) 0.5%, and (c) 2% GO doped NC film; (d) as-produced GO; (e) AFM images of 1% GO doped NC film. (Reproduced from Zhang, et al., Appl. Phys. Lett., 2013, 102, 141905) Reprinted from Ref. 165 with permission of Copyright © 2013, AIP Publishing LLC.



 

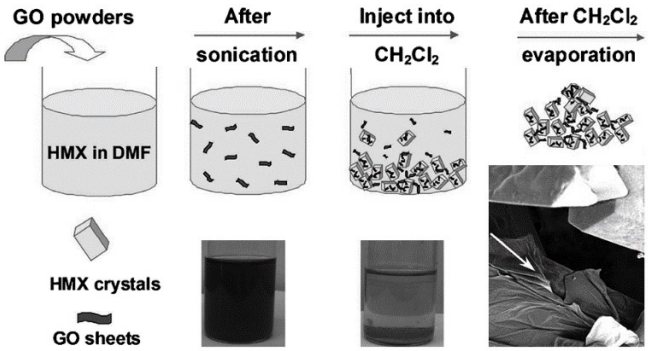


Figure 19. procedures for the formation of the HMX/GO composites. Reprinted from Ref. 168 published with permission of Copyright © 2013, John Wiley & Sons, Inc.

In addition to burn rate enhancement, GO can also be used to decrease the sensitivity of energetic crystals. For instance, to improve the safety of 1,3,5,7-tetranitro-1,3,5,7-tetrazocine (HMX), GO was introduced by a solvent-antisolvent method (Figure 19)[168]. In a typical procedure, HMX was dissolved in DMF at 40 °C, and then GO (about 2 wt.%) was added. After GO was completely dispersed in HMX solution in DMF by sonication, the mixture was injected into $CH_2Cl_2$ (in which GO is much less soluble). After filtration, washing, and dying at 40 °C, the HMX/GO composite was obtained. The SEM images of this material are shown in Figure 20. It can be seen that GO is not capable of changing the shape of HMX crystals. The morphology difference between HMX and HMX/GO was found to be considerable. The surfaces of unmodified HMX crystals are smooth and clean, while some wrinkles are observed in composite HMX/GO, which may significantly improve the safety properties of HMX. It was also shown that GO sheets exhibited even better desensitizing effect than $C_{60}$ and CNTs.

Except for simple coating of energetic crystals, GO can also be funcationalized with energetic moieties. It has been reported that tetrazine derivatives can be covalently grafted to GO through nucleophilic substitution, forming a new type of materials (FGs-Tz)[169]. The general synthetic route, leading to the grafting of substituted chlorotetrazines to $FGS_2$, which is GO with a norminal C/O of 2, is shown in Scheme 6. The reactions of $FGS_2$ with chlorotetrazines take a long time (48 hrs) requiring a temperature of 120 °C. The reaction between Tz1 and $FGS_2$ was found to be unsuccessful and undesirable side reactions took place between the Tz1 and the other components of the suspension. It has been shown by DSC that the unmodified $FGS_2$ has a strong exotherm peak at ~230 °C due to rapid thermal reduction releasing $H_2O$ vapour and $CO_2$. This exotherm was not present in thermally reduced FGS and in the FGS-Tz compounds, indicating that the $FGS_2$ was reduced during the reaction between chlorotetrazines and $FGS_2$. There might be some exotherm above 300 °C for FGS-Tz3 and FGS -Tz4, because the decomposition was not complete below that temperature.

It is, therefore, not clear that these functionalized FGS -Tz can be considered as energetic materials. In contrast to the GO grafted with tetrazines, the pure tetrazines are less stable, indicating the GO has stabilization effect on these tetrazine molecules. In order to make a complete comparison of all graphene, GO and rGO based EMs, their preparation methods together with the potential applications are summarized in Table 4.

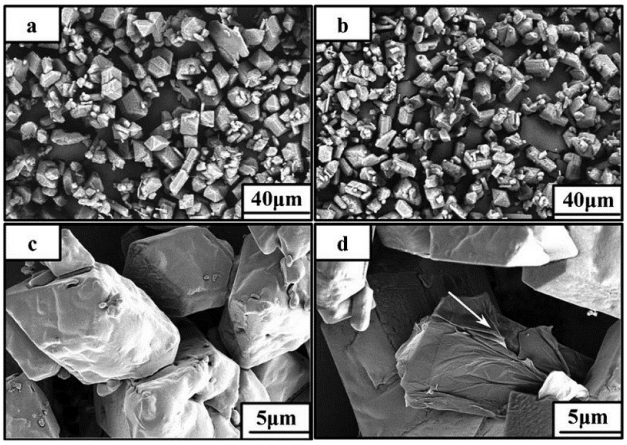


Figure 20. The SEM images of HMX and HMX/GO-2 at low-magnification (a, b) and high-magnification (c, d). Reprinted from Ref. 168 with permission of Copyright © 2013, John Wiley & Sons, Inc.

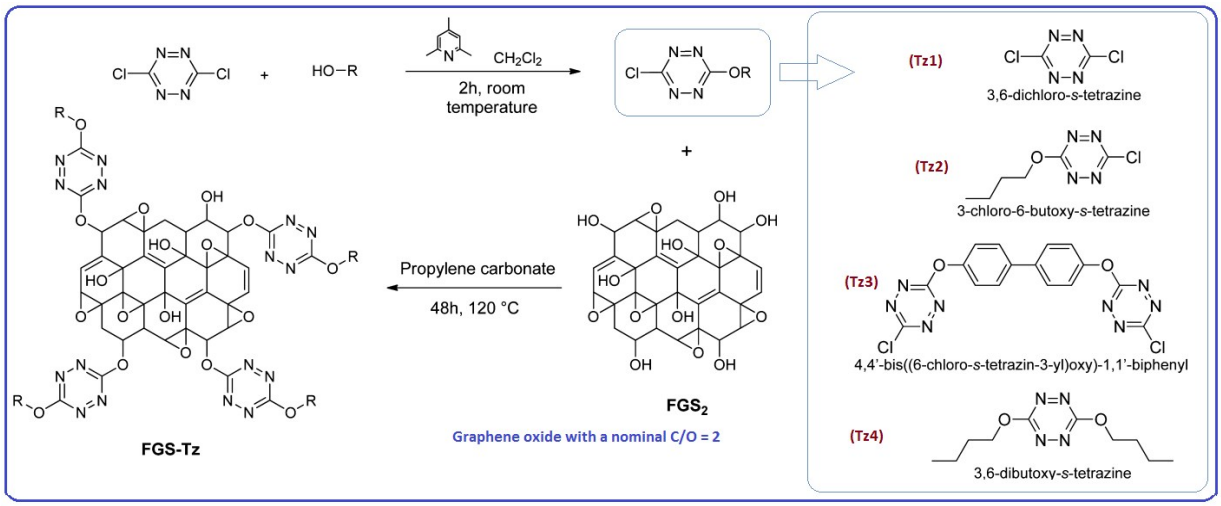


Scheme 11. General synthetic route leading to the grafting of substituted chlorotetrazines to $FGS_2$

Table 4 the preparation methods and application of graphene, GO and reduced GO based energetic materials

| Materials | Preparation method | Applications | Contributors |
|---|---|---|---|
| GA/$Fe_2O_3$/AP | By a facile sol-gel method and supercritical carbon dioxide drying technique; | Propellants; | Lan, et al., 2015 |
| GA/AN | By a sol-gel and supercritical $CO_2$ drying method; | Propellants; | Lan, et al., 2015 |
| $Cu_2O$/rGO | $Cu_2O$ nanoparticles are deposited on graphene by chemical reduction of $CuSO_4$ in the presence of GO; | Treatment of waste explosives; | Shen B., et al., 2015 |
| GO-Tzs | The tetrazine derivatives covalently grafted to GO through nucleophilic substitution, at 120 °C for 48 hrs in propylene carbonate; | Not clear; | Li Y. et al., 2015 |
| CL-20/GL/rGO | Graded CL-20 particles are coated with 551 glue by emulsion polymerization method and then mixed with reduced GO; | Energetic compositions; | Yu, L., et al., 2014 |
| Al/$Bi_2O_3$/FGS | Formed in a colloidal suspension phase that ultimately condense into ultra-dense macrostructures; | Energetic devices; | Thiruvengadathan, et al., 2014 |
| AP/GA | The nanostructured energetic composite is prepared by the sol-gel method; | Solid propellants; | Wang, et al., 2014, 2012 |
| GKPA | Prepared under the action of crystalline controlling agent and modified by graphene; | Energetics; | Liu, et al., 2014 |
| HMX/GO | A two-dimensional GO was introduced to HMX by the solvent-nonsolvent method; | Propellants and explosives; | Li R., et al., 2013 |
| GLS | Prepared either by adding graphene nanoplatelets (GNP) to the reaction solution or by coating normal lead styphnate (LS) with GNP; | Primary explosives; | Li Z.-M., et al., 2013 |
| GO/NC | Pure and GO-doped NC films are obtained through mixing pure NC-acetone solution and various weight ratios of GO water solution; | Propellants; | Zhang X., et al., 2013 |
| GO/FOX-7 | FOX-7 nanocrystals are synthesized in mesoporous carbon FDU-15 through self-assembly impregnation in N-methyl-2-pyrrolidone at 100-110 °C; | Explosives and propellants; | Cai H., et al., 2013 |
| NdG | Through supercritical (SC) reaction in acetonitrile at temperature as low as 310 °C, using expanded graphite as starting material; | Nano electronic devices, and catalyst; | Qian, et al., 2011 |

Notes: NdG, N-doped graphene; GA, graphene aerogel; AP, Ammonium Perchlorate; GKPA, graphene-doped ultrafine potassium picrate; FOX-7, 1,1-diamino-2,2-dinitroethylene; GL, 551 glue; FGS-Tz, tetrazine derivatives functionalized GO with a nominal C/O of 2.

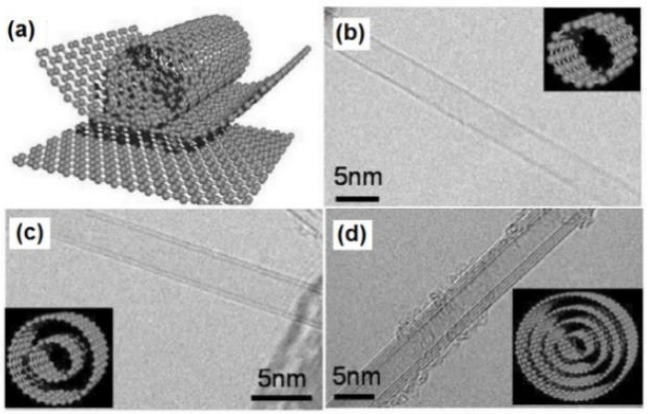


Figure 21. (a) Schematic diagram of an individual layer of honeycomb-like carbon called graphene, and how this could be rolled in order to form a CNT; (b)–(d) HR-TEM images of single-, double- and multi-walled carbon nanotubes (insets are their corresponding images). Reprinted from Ref. 170 with permission of Copyright © 2006, International Union of Pure and Applied Chemistry.

According to Table 4, graphene or its aerogels could be combined with either catalysts, or oxidizers. Sol-gel method is commonly used for preparation of these materials. Pure GO and rGO are energetic, but there are not so many energetic nanomaterials or composites based on them yet, except for composites with HMX, NC and FOX-7. These energetic components were either deposited on the skeleton of GO or coated by thin layers of GO or rGO. All abovementioned composite materials are novel, and were reported very recently. All these materials could be considered as promising candidate components of energetic compositions, as combustion catalysts or main ingredients.

## EMs Based on Functionalized CNTs

***New Preparation Methods for CNTs*:** CNTs could be visualized as rolled sheets of graphene ($sp^2$ carbon honeycomb lattice) (Figure 21a), that are sometimes capped at each end of a tube[170]. They could be either single-walled, with diameters as small as about 0.4 nm (SWCNTs), or multi-walled consisting of nested tubes (MWCNTs, e.g., 2-30 concentric tubes, positioned one inside another) with outer diameters ranging from 5 to 100 nm (Figures 21b-21d). There are three possible CNT chiralities: zigzag, armchair, and chiral, defined by their chiral angle and wrapping integers. For example, MWCNTs could be found in carbon soot on graphite anodes, which may have more attractive application potential than the SWCNT form. There are many different methods to synthesize CNTs, including electric arc discharge, laser ablation and CVD methods. However, currently the CVD method is the dominant one, which can be used with liquid, solid, or gas carbon sources. This method should be used in combination with proper catalysts, pre-deposited in a form of a thin layers on various substrates,[171–175] or through vapor-phase catalyst delivery.[176–181]

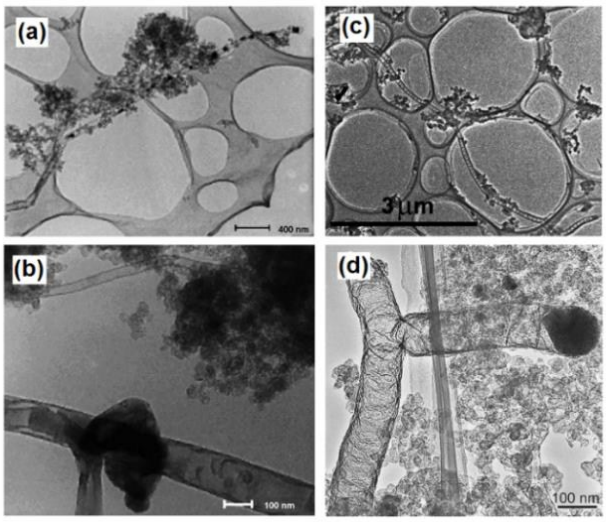


Figure 22. TEMs image of an end capped CNT with Cu-particles (a), a tube-within-a-tube CNT (b), a segmented CNT with length of a dozen microns (c) and a CNT–T-junction with a crystalline Fe-particle at its end (d). Reprinted from Ref. 188 with permission of Copyright © 2004 Elsevier Ltd.

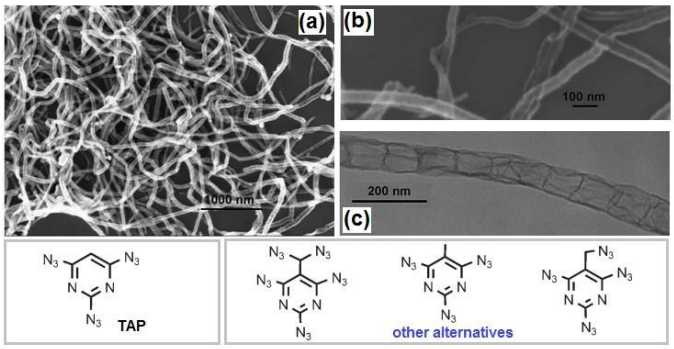


Figure 23. SEM (a, b) and TEM (c) images of CNTs generated by catalytic detonation of TAP (the other polyazidopyrimidines that can be used for this purpose) (Reproduced from Ye, et al., 2006, Angewandte Chem. – Int. Ed., 45, 7262-7265.) Reprinted from Ref. 191 with permission of Copyright © 2006, WILEY-VCH Verlag GmbH & Co. KGaA.

The CNTs can end capped by Cu and Fe nanoparticles for energetic and catalytyst applications (Figure 22). It is essential for large-scale production of high-purity SWCNTs[182], double-walled CNTs (DWCNTs)[183], as well as MWCNTs[184]. Preparation of DWCNTs, with length of up to 2.2 mm, were achieved with selectivity of 85% by precisely controlling the thickness of iron catalyst[183]. A variety of aligned CNT structures have been prepared predominately on non-conducting substrates, posing limitations on applications where conductive substrates/contacts are required[172,173,177]. To circumvent this problem, aligned MWCNTs can be directly grown on Inconel 600 metallic alloy, using vapor-phase catalyst delivery[185]. Controlled synthesis has endowed SWCNTs with narrow distributions of tube diameter and a large fraction of a predetermined tube type[186,187].

It is possible that the CNTs, formed in the detonation processes of high nitrogen compound – cyanuric triazide (TAT), contain a small amount of nitrogen atoms. Elemental analysis showed that less than 3 wt.% nitrogen was present when using C/N containing material as the precursor[188, 189]. It was reported that the nitrogen atoms in $CN_x$ nanotubes can be inhomogeneously distributed with an enrichment of carbon on the external surface[190]. All tubes prepared using nickel, copper or steel cartridges were of a multi-walled type, but the morphology and the yield depended on a metal. For Ti-based catalysts, there was no CNTs formation being detected, indicating that this metal has no catalytic effect on nanotube formation. In addition to TAT, polyazidopyrimidines and metal/fluorocarbon pyrolants can also be used to prepare CNTs[191,192]. 2,4,6-Triazidopyrimidine (TAP) was found to be a good precursor for CNTs in the presence of $Ni(ClO_4)_2$. The SEM and TEM images of CNTs generated by catalytic detonation of TAP are presented in Figure 23. It could be seen that the hollow-channel CNT structures, with length of 3-20 µm, and diameters of 60-80 nm are obtained. The yield of CNTs is estimated to be greater than 90%. They have a bamboo-like morphology and these "compart-metalized nanotubes" are segmented with a relatively uniform length of about 90 nm. Except for detonation synthesis method, the SWCNTs and "carbon nano-carpet rolls" (CNCR) were found in the combustion residue of a pyrolant-based on poly(carbon-monofluoride) (PMF, $(CF_x)_n$) and rich in Mg particles[192]. More investigations should be done to clarify the mechanism of CNTs formation during combustion of EMs. In addition to organized CNT structures, a variety of tailored structures with enhanced properties have been synthesized for special applications, such as: 1-D yarns, fibers, ropes, brushes, 2D sheets, buckypapers, and 3D foams and sponges. 1-D nitrogen-containing CNTs (1-D NCNSs) have emerged in the past two decades as exceptionally promising nanomaterials due to their unique physical and chemical properties, which enables a broad range of applications in various fields of modern technology [193]. All these CNTs or NCNSs materials can be used in the field of EMs in the following ways: 1) functionalized with polymeric binders, 2) coupled with pyrotechnics, 3) used as carriers of combustion catalysts, 4) combined with metal fuels and 5) functionalized with energetic moieties/groups.

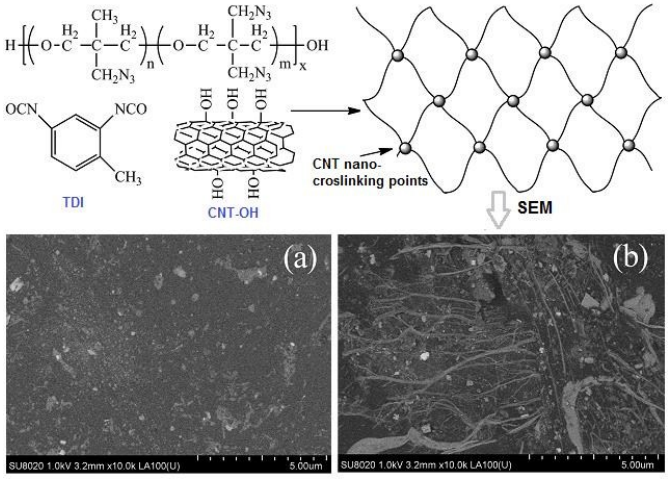


Figure 24. Synthetic scheme for CNT/BAMO-AMMO thermoset polyurethane elastomer and its SEM images with different CNT mass fractions: (a) 0.5 wt.%; (b) 1.0 wt.%; (reproduced from Zhang, et al., J. Energet. Mater. 33, 2015, 305-314.) Reprinted from Ref. 195 with permission of Copyright © 2015 Taylor & Francis.

***CNTs Functionalized with Polymeric Binders*:** Polymeric materials, expecially energetic polymers are very important ingredients in composition of explosives and propellants. The functionalization of CNTs by using energetic polymers may be one of the promising ways to improve the performances of corresponding energetic compositions. For example, recently, a nano-modified energetic binder films were prepared from GAP using hydroxylated CNTs (CNT-OH) as a crosslinking agent and toluene diisocyanate (TDI) as a curing agent[194]. When the content of CNT-OH was 1 wt.% and the R value (mole ratio of NCO and OH) was 1.4, the obtained binder film exhibited a tensile trength of 7.2 MPa with failure elongation of 375%, which is much higher than that of normal GAP binder film.

Besides, the thermal stability was increased, while its glass transition temperature ($T_g$) was decreased to below -40 °C. Later on, another similar energetic binder – 3,3′-bisazidomethyloxetane-3-azidomethyl-3′-methyloxetane (BAMO-AMMO) covalently modified with CNTs was synthesized by the same research group[195]. Their preparation schemes as well as the SEM images of the obtained BAMO-AMMO films are shown in Figure 24. During preparation, BAMO-AMMO random copolymer (or TME) was added to a reactor under $N_2$ atmosphere, followed by mixing with TDI and dibutyltin dilaurate (DBD). Then, the reaction mixture was blended uniformly and cured at 60 °C for 7 days. Similarly to GAP-CNTs composite, upon using 1 wt.% of CNT-OH with R value of 1.4, the elongation ratio of CNTs/BAMO-AMMO binder was 380% and the tensile strength was 10.4 MPa, which was 82.5% higher than that of the traditional trimethylolethane (TME)/BAMO-AMMO energetic binder. However, the $T_g$ of CNTs/BAMO -AMMO binder (-34 °C) is slightly higher than that of GAP-CNTs.

Except for energetic polymers, CNTs can also be used to enhance inert polymers such as fluoropolymer, which is very important binder for PBXs[196,197]. The mechanical strength of PBXs has to be improved for applications in penetration warheads and nuclear bombs. MWCNTs/fluoropolymer (F2314) composites were prepared via a melt blending process, and the effect of MWCNTs content on the viscoelastic properties of MWCNTs/F2314 were explored by using a dynamic mechanical analysis (DMA) method[198]. It has been shown that at 80 °C and 0.1 MPa, when the MWCNTs content was increased from 2 wt.% to 20 wt.%, the constant creep strain rate of MWCNTs/F2314 composites was decreased by 84.7%.

***CNTs Coupled with Pyrotechnics*:** It has been mentioned in the former section that one could use GO in pyrotechnic compositions to improve the heat generation. For this purpose, CNTs as the analogue of GO could be better. In fact, CNTs were introduced into pyrotechnics based on potassium perchlorate (KP) or potassium nitrate (KN) for the first time in 2009, using water-mixing and acetone-mixing methods[199]. Maximum reaction rate of KP was increased to 8.2 $min^{-1}$, which is about 4 times faster than that without CNTs. Meanwhile, its time to maximum rate was decreased to 52.1 $min^{-1}$, which is 56.4% lower than that of pyrotechnics without CNTs. The improvement for KP was not as significant as for KN. Generally, samples obtained from water-mixing method are better, but both methods are not adequate to make the contact of CNTs with KN at a molecular level.

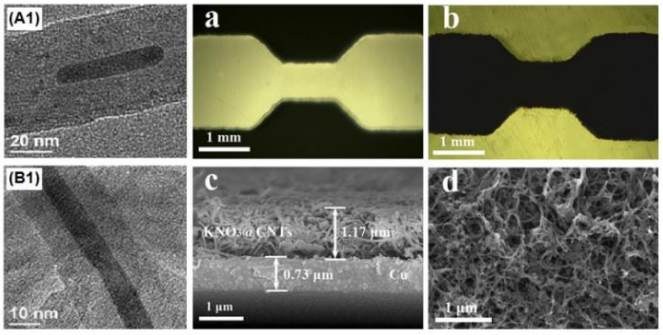


Figure 25. TEM images of the KN/CNTs nano energetic materials (nEMs) achieved by wet chemical method (A1 and B1), showing the legible lattice stripe (B1); micrographs of the Cu thin-film microbridge (a), the micro-initiator after EPD (b); SEM images of the sectional view (c) and the surface morphology of the micro-initiator after EPD (d). Reprinted from Ref. 200 with permission of Copyright © 2012 Elsevier B.V.

In order to achieve the goal of a molecular level mixing, a new wet chemical method was proposed to embed $KNO_3$ in CNTs, forming a uniform novel $KNO_3$/CNTs nanoenergetic materials[200, 201]. The latter material can be integrated into a copper thin-film microbridge (CTFM) positioned on a glass substrate. It has been shown that the hollow cavities of the CNTs were filled with crystalline $KNO_3$, and that the entire surface of the micro-initiator was well distributed without large aglomeration. Compared with single-layer CTFM, the micro-initiator exhibited more violent electrical explosion process than the micro-initiator without CNTs. Also, the CNTs-containing micro-initiator had longer duration of an electrical explosion and higher peak temperature, due to enhancement of heat generation by CNTs. It has been shown that the decomposition heat of CNTs-based micro-initiators is about 876.1 J $g^{-1}$ (peak temperature: 386.8 °C). High-speed photography of these micro-initiators' ignition process showed that fast chemical reaction of CNTs was involved in the electric explosion process resulting in a more heat release. Figure 23 shows the TEM images of the KN/CNTs nEMs as well as SEM images of the sectional view and surface morphology of the micro-initiator, after ElectroPhoretic Deposition (EPD).

It can be seen in Figure 25 that the KN nanocrystals are homogeneously filled inside the hollow cavities of CNTs, without impurities attaching on the exterior wall. The average proportion of CNTs:KN is estimated at about 10:1 from TEM images. The bulk density of KN is 2.109 g $cm^{-3}$, and the density of MWCNT is typically observed to be around the same as KN. It is clear that the $KNO_3$/CNTs nEMs tightly covered the CTFM. The whole surface was well distributed without large agglomeration. The CNTs arrays showed excellent electron field emission properties[202]. When $KNO_3$/CNTs nEMs was integrated with a CTFM deposited onto a ceramic substrate, the electro-explosion performance was greatly improved. It means that due to superior electric and thermal conductivities of CNTs, the enhanced chemical reaction of the $KNO_3$/CNTs nEMs is beneficial for the miniaturization of electro-pyrotechnics. In fact, there are several reported techniques for integrating EMs on an electronics or microelectromechanical



 

system (MEMS) chip. It includes modifications to the bulk substrate material, deposition of thin films, and growth of nanotubes on the top of the substrate[203].

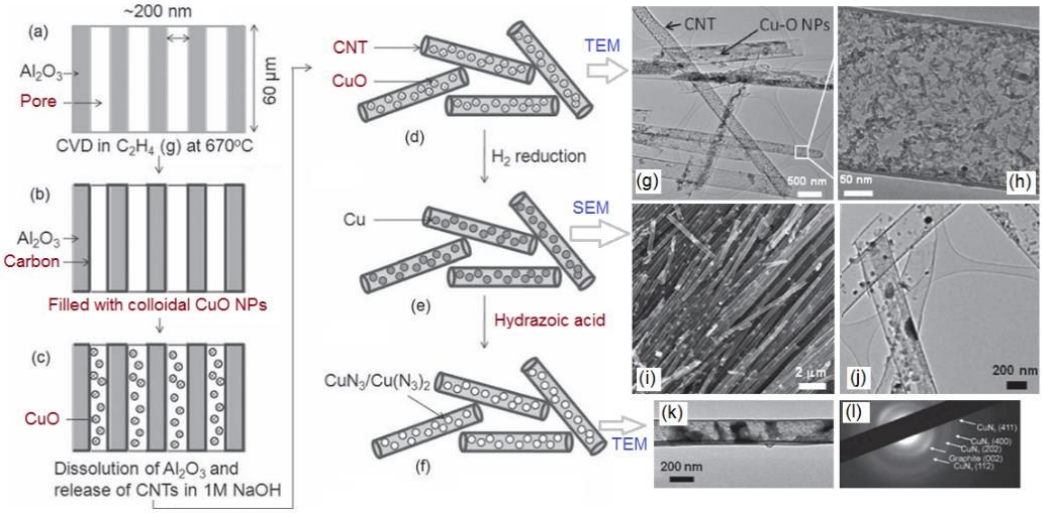


Figure 26. Schematics of the chronological steps of the synthesis process: a) commercial alumina membrane; b) carbon coated alumina membrane; c) pores of the carbon coated membrane filled with colloidal Cu-O NP solution; d) Cu-O NP filled CNTs after dissolution of the alumina membrane; e) Cu NP filled CNTs after $H_2$ reduction; f) CA NPs inside the CNTs. g) TEM image of Cu-O NPs filled CNTs, (h) an enlarged view showing rod-like NPs inside the CNT framed in (g); TEM micrograph of i) $CuN_3/Cu(N_3)_2$ filled CNT and j) SAED pattern of the $CuN_3$ filled CNTs. Reprinted from Ref. 204 with permission of Copyright © 2010 WILEY-VCH Verlag GmbH & Co. KGaA.

The involved EMs systems could be nanoporous energetic silicon, energetic CNTs, and solution-deposited nitramines (e.g. RDX). Except for microignitor application, CNTs can also be used to stabilize the extremely sensitive new "green" primary explosives. The currently used ones, such as lead azide (LA) and lead styphnate (LS), are very toxic and harmful to the people who work with them. Nowadays, more and more novel environmentally friendly EMs have been developed to replace LA and LS, but many of the materials are simply too sensitive to handle. Copper azide (CA) is one of the cases and it detonates easily from electrostatic charges during handling. It has been found that the sensitivity of CA can be suppressed when it is encapsulated in conducting containers, such as anodic aluminium oxide (AAO)-templated CNTs[204]. The preparation procedure of CA/AAO-CNTs composites and the morphologies of involved intermediates are shown in Figure 26.

It has been shown in Figure 26 that the colloidal copper oxide nanoparticles (nano Cu-O) of ~5 nm are synthesized and filled into CNTs with diameter of ~200 nm, produced by template synthesis. The Cu-O inside the CNTs is reduced by hydrogen to elemental copper, and reacted with hydronic acid gas to produce copper azide. It was found that upon ignition, the 60 µm long straight, open-ended CNTs guide decomposition gases along the tube channel, without fracturing the nanotube walls. These novel materials are potentially useful as nano-detonators and "green" primary explosives. It is also the case for BNCP, which can either be coupled with CB, or encapsulated by CNTs (Figure 27)[52].

The encapsulating material should be electrically conducting in order to dissipate electric charges and prevent detonation due to static electricity. If the CNTs are straight and open-ended, nanotube channels can potentially drive the shock waves along its length, increasing the efficiency of initiation of the secondary explosives, thus retaining the initiated particles within the nanotube[205]. In addition to primary explosives, the properties of pyrotechnic compositions used in flashbang or solid state laser pump sources can also be modified by CNTs. To improve the pump efficiency of $Zr/KClO_4$ pyrotechnic reagent, the high strength CNTs with strong adsorption capacity was introduced[206]. It has been shown that the inclusion of CNTs had a significant effect on the thermal behavior and light radiation energy. When the content of CNTs is 0.5 wt.%, the total radiation energy of the pyrotechnics can reach 1830 J $g^{-1}$.

***CNTs as Carriers of Combustion Catalysts***: Combustion catalysts can influence a radical chemical reaction by changing its mechanism, and they are chemical compounds that can change reaction pathway to products through routes with lower activation energy[207]. As a reagent, the amount of catalyst doesn't change before and after the combustion. Heterogeneous catalysts may catalyse gas phase chemical reactions that would take place on a surface of this catalyst. Prepferably, to enchance the active surface of such catalysts, it should have a porous or nanoparticles structure.

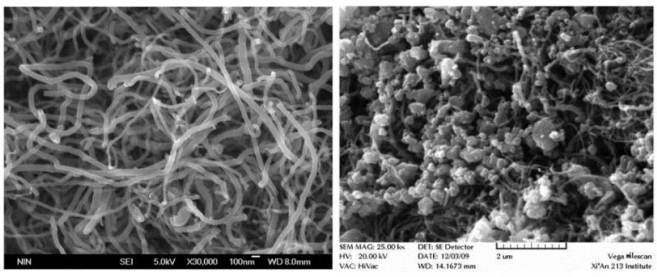

Figure 27, The SEM photos of CNTs and BNCP/CNTs. Reprinted from Ref. 52 published in *Chin. J. Energet. Mater.* (2013) with permission.

Regarding combustion catalysts for propellants, on one hand, they should maintain their activity during propellants' production

processes, which means that the catalyst should be chemically compatible with various ingredients of propellants[208,209]. On the other hand, the particle size of catalysts should be as small as possible with surface structure that could be uniformly dispersed in the propellant matrix. Nano-sized catalysts or additives are highly promising for improving combustion performance of propellants, but they are very active and need to be coated with inert materials. A combination of these nano-sized catalysts with CNTs could be one of the promising solutions. For instance, a nano Cu/CNTs composite catalyst (see Figure 28) was prepared by liquid reductive deposition method, using the CNTs as the carrier[210]. The researchers used $CuCl_2{\cdot}2H_2O$ as the source of Cu ions and $KBH_4$ as a reducing agent. The reaction was conducted at 50 °C with addition of disodium EDTA and PVP as surfactant and complexing agents. It has been shown that Cu/CNTs can remarkably decrease the peak decomposition temperature ($T_p$) of AP/HTPB propellant.

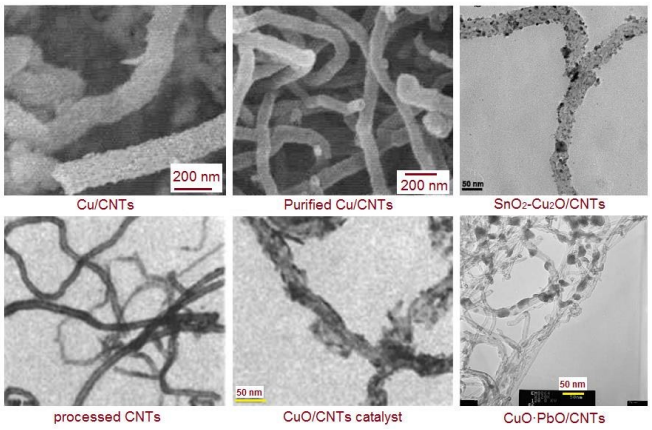


Figure 28, The SEM and TEM images of CNTs, Cu/CTNs and CuO/CTNs combustion catalysts. Reconstructed from several figures appeared in References 210, 211, 215, and 216 with permission.

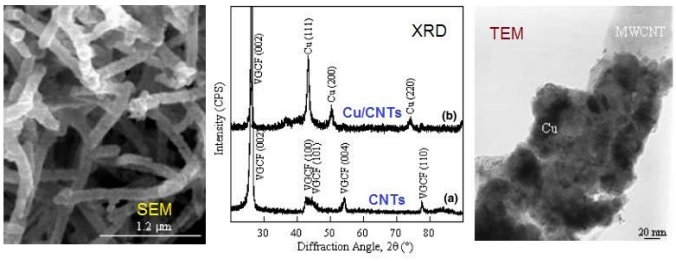


Figure 29, the SEM and TEM images, XRD spectra of CNTs and Cu/CNTs prepared by eletroless deposition method. Reprinted from several figures published in Ref. 213 with permission of Copyright © 2004 Elsevier B.V.

Similarly, catalyst CuO can also be carried by CNTs, forming a novel CuO/CNTs composites (black powder, Figure 28)[211]. Taking cupric acetate and CNTs as the reactants, CuO/CNTs could be also prepared by solvent-infusion method at normal pressure and temperature of 100°C. The catalytic effect of this material on N-guanylurea-dinitramide (FOX-12 or GUDN) was found to be significant and the resulted composite material had excellent thermal stability and low sensitivity. In addition to abovementioned composites, metal fuels or catalyst may also be encapsulated inside CNTs. The SWCNT was proposed to be the best protective coating for energetic metal nanoparticles and as a base for propellants' catalysts[211]. An advanced technology has been developed to prepare metalized CNTs using a $CO_2$ laser for ablation of the composite graphite target[212] or eletroless deposition on top of MWCNTs[213]. The SEM and TEM images of the resulted product, as well as its XRD spectra are shown in Figure 29.

It has been shown in Figure 29 that the copper layers with the average thickness of 40 nm have been deposited on the surfaces of MWCNTs. It provides an effective means to fabricate powder metal-coated CNT composites. Based on this principle, $Fe_2O_3$/MWCNTs composite particles were also produced by a mild physical absorption method using molten $Fe(NO_3)_3{\cdot}9H_2O$ as a precursor[214]. It has been shown that a large number of hematite phase $Fe_2O_3$ is uniformly filled inside the MWCNTs, where the fraction of $Fe_2O_3$ is about 25.8 wt.%. In fact, this concept is also applicable to binary catalysts. For instance, the $SnO_2$-$Cu_2O$/CNTs composite catalyst was prepared by an integrative infusion method based on a liquid phase deposition, using $CuCl_2{\cdot}2H_2O$, $SnCl_4{\cdot}2H_2O$, and CNTs as reactants[215]. It was shown that $SnO_2$ and $Cu_2O$ nanoparticles were attached on CNTs uniformly with oval morphologies and 5-10 nm of layer thickness (Figure 28). It has positive catalytic effect on decomposition of FOX-12, which could be catalyzed by aforementioned CuO/CNTs as well. The catalytic effects of these materials will be further discussed in a separate section, in conjunction with the thermal behavior of several other related materials.

There is another binary catalyst being widely used in solid propellants, which is CuO·PbO. The catalyst could be also modified to by addition of CNTs, forming CuO·PbO/CNTs composite material by a microemulsion method[216]. The obtained catalyst has particle sizes of below 50 nm (Figure 28). In addition to copper and lead oxides, the cobalt and aluminum oxides can also be deposited onto CNTs for better catalytic activity. It was reported that Co-Al mixed metal oxides/CNTs (CoAl-MMO/CNT) nanocomposite could be synthesized from Co-Al layered double hydroxide/CNTs composite precursor[217]. It has been shown that that in this nanocomposite, the cobalt oxide nanoparticles and Co-containing spinel-type complex metal oxides are well-dispersed on the surface of CNTs, forming heterostructure of CoAl-MMO and CNTs, which has great catalytic effect on energetic oxidizers such as AP.

***CNTs Combined with Metal Fuels*:** The metal fuels are very important ingredients in energetic compositions. In solid rocket propellants, the most widely used elemental fuels are aluminium, boron and magnesium[218,219]. For explosives, Al is more effective than the others, especially in thermobaric compositions. The inclusion of the CNTs to metal fuels may improve their combustion efficiency. The first attempt on combination of metals with CNTs was made by Syvain et. al, who invented novel flash-ignitable EMs based on metal fuels (including Pd, Fe, Ni, Co, Al, Cu, Zn, K, Na and Ti) in combination with CNTs or activated carbon[220]. Recently, Ag and Al particles were deposited on CNTs, and their catalytic behavior of the resulted materials was investigated[221,222]. The



 

Ag/CNTs composites could be prepared by two methods: silver mirror reaction and hydrothermal methods, where the former methodology uses $AgNO_3$ in ammonia solution (as the source of Ag) mixed with CNTs and formaldehyde, and the latter uses $AgNO_3$ in ammonia solution is reacted with CNTs dispersed in polyvinyl-pyrrolidone (PVP)[221]. The content of carbon in Ag/CNTs, obtained from these two methods, were found to be different (Figure 30), where the fomer has 37.2 wt.%, with particle size of 29.3 nm and the latter has only 8.1 wt.% (35.4 nm). The lower amount of CNT in composition typically results in higher energy content of the material.

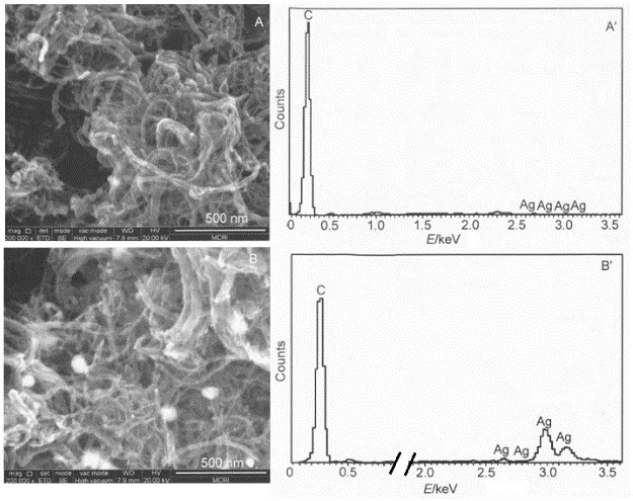


Figure 30, the SEM images and EDS spectra of Ag/CNTs prepared by two different methods: (A) silver mirror reaction and (B) hydrothermal method. Reprinted from several figures published in Ref. 221 with permission of *Acta Phys.-Chim. Sinica*.

As the most widely used metal fuels, Al has been intensively investigated regarding its oxidation and combustion behavior, which have great effect on final performance of Al-containing propellants and explosives. Controlling Al oxidation rate and temperature, as well as reaction enthalpy is important for its practical use. The CNTs was introduced to Al initially for enhancing its mechanical strength, due to large tensile strength of CNTs (150 GPa)[223-225]. However, the thermal behavior could also be tailored by CNTs according to a recent report[222]. There are several functions of CNTs, which can control the sizes and thermal properties of Al particles by changing the contents of CNTs. The morphological modifications of Al/CNT mixtures during different stages of ball-milling of Al particles with CNTs are shown in Figure 31. This figure shows the morphological changes that undergo Al/CNTs mixtures with the progress of milling time. The morphology can be categorized to three types based on milling time: in Stage I, where Al particles were coated by CNTs and spherical Al particles were distorted into platelets. In the Stage II, Al particles are disintegrated into smaller sizes and CNTs were partially embedded inside Al particles, which look like urchins and in the Stage III, Al/CNTs particles aggregated into larger sizes with CNTs homogeneously dispersed inside the Al matrix.

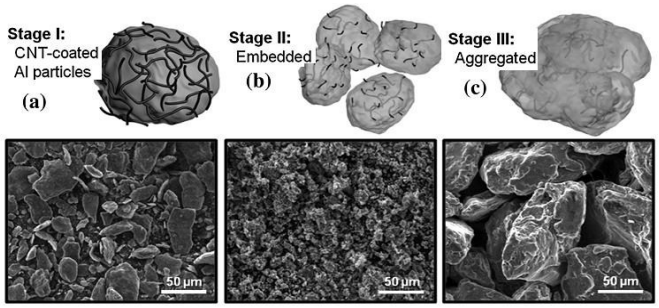


Figure 31, Morphological modifications of Al/CNT mixtures with ball-mill time: (a) Stage I (30 min); CNTs coated on the surface of Al particles, (b) Stage II (120 min); CNTs embedded inside Al particles while portion of CNTs remain on the Al surface, and (c) Stage III (180 min); Aggregation of Al particles with embedded CNTs inside. Reprinted from Ref. 222 with permission of Crown copyright © 2013, Published by Elsevier Ltd.

***CNTs Functionalized with Energetic Moieties/groups*:** As described earlier in this paper, fullerens could be functionalized with various energetic groups to from a new type of EMs, which is also the case for CNTs, as another carbon's allotrope. In 2003, metallic laser-synthesized SWCNTs were electrochemically-induced functionalized with $NO_2$ groups. This modification was confirmed by Raman spectroscopy[226]. The nitration process was carried out by acidification of CNTs to form -COOH groups on their surface and was followed by reaction of the resulted material with thionyl chloride and then with 4-nitroaniline[226, 227].

Except for $NO_2$ groups, many other energetic groups can be introduced to CNTs as well. In fact, the SWCNT modified with tetrazoly groups (SWCNTs-$CN_4$) was prepared by diazo-reaction, where covalent bonds were formed to hold the structure of five-membered ring[228]. It was indicated by X-ray photoelectron spectroscopy (XPS) that the nitrogen content in this SWCNTs-$CN_4$ material was about 14.8%, while the ratio of tetrazolyl groups to carbon atoms was about 4.9%. Similarly, on a basis of diazonium chemistry, SWCNTs could be decorated with nitrobenzenes, using microwave irradiation of the reaction mixture[229]. It has been found that even covalent functionalization introduces defects that could reduce conductivity, and thermo-power waves would rapidly propagate along fuel-coated decorated nanotubes, producing electrical power. The schematic presentation of reaction propagation on a SWCNT, decorated with trinitrobenzenes and the reaction conditions to produce different nitrobenzenes functionalized SWCNTs, as well as their Raman spectra and DSC thermograms are shown in Figure 32. It is clear that the energy from a chemical reaction at one end may propagate through the 1-D conductor, initiating reactions in the attached molecules at the wave-front. The energetically decorated SWCNTs appear to generate considerable heat when decomposing at high temperatures. It can be seen from Figure 30d that MNP-, DNP-, and TNP-SWCNTs can undergo exothermic reaction between 300 and 330 °C during linear heating, except of the BrP-SWCNTs (functionalized with non-energetic 4-bromophenyl group).

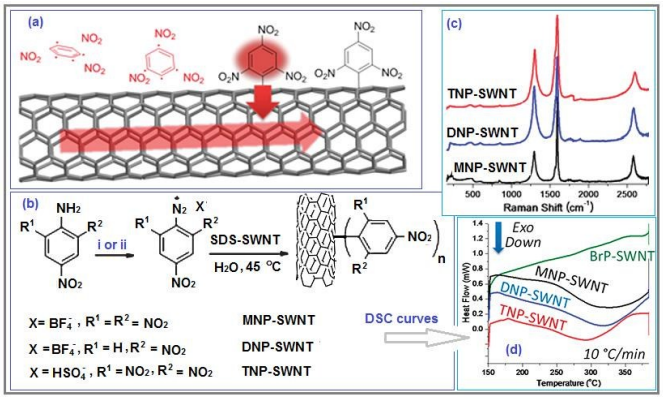


Figure 32, (a) Schematic representation of reaction propagation on a single-walled carbon nanotube decorated with trinitrobenzenes; (b) synthesis of nitrophenyl-SWNTs via diazonium reactions, where "i" represents $NOBF_4$, acetonitrile, 0 °C, 4 hrs (for MNP- and DNP-SWNT), while "ii" denotes $NOHSO_4$ ($NaNO_2$+$H_2SO_4$), $H_2O$, room temperature, 3 hrs (for TNP-SWCNT); (c) Raman spectra of energetically decorated SWNTs with modes at 1200 $cm^{-1}$ increased in the Raman spectra after covalent functionalization (excited at 785 nm); d) DSC curves at 10 °C $min^{-1}$ under nitrogen where all the nitrophenyl-SWCNTs decompose with slow heat release, whereas the BrP-SWCNTs do not release the heat at all. Recombination of several figures from Ref. 229 with permission of Copyright © 2011, American Chemical Society.

In addition to covalently functionalized CNTs with energetic groups, energetic compounds may non-covalently functionalize CNTs via doping or adsorption. For instance, BNCP could be doped by CB or CNTs[52], whereas TATB could be adsorbed by CNTs[230]. Theoretical calculation shows that TATB deforms remarkably when it is non-covalently attached to the surface of CNTs, especially on its inner wall. The diameter of the CNT determines the distortion degree of TATB molecule inside, but it has little effect on the deformation of the TATB molecule bound outside the CNTs. The non-covalent combination of TATB with CNTs is exothermic due to the negative adsorption energy. TATB adsorption on the inner wall of CNTs was energetically more favourable than that of the TATB-bound outside. In both cases, more stable adsorption occurs with the increase of nanotube's diameter. As a comparison, these researchers also theoretically investigated the structure, adsorption energy, and initial dissociation reaction of the energetic 3,3'-diamino-4,4'-azofurazan (DAAzF) assembled inside or outside SWCNTs[231]. They found that most of the adsorption processes of SWCNTs with larger diameters are exothermic and thermodynamically favourable, indicating that DAAzF may spontaneously assemble inside the CNTs. Based on those theoretical findings, the CNTs were successfully used as the host of some high-nitrogen content compounds. For instance, CNTs (10,10) were selected as a nanoscale matrix to host N-oxides of 3,3'-azo-bis(6-amino-1,2,4,5-tetrazine) (DAATO) molecules, using CVD (chemical vopor deposition) method for obtaining so-called nitrogen-doped CNTs (N-CNTs)[232]. Their SEM and TEM images, as well as XPS spectra are shown in Figure 31. It has been stated that the DAATO contains an average of 3.2-3.6 oxygen atoms per molecule[233], resulting in five possibilities for positioning and quantifying oxygen atoms per molecule (Figure 33c).

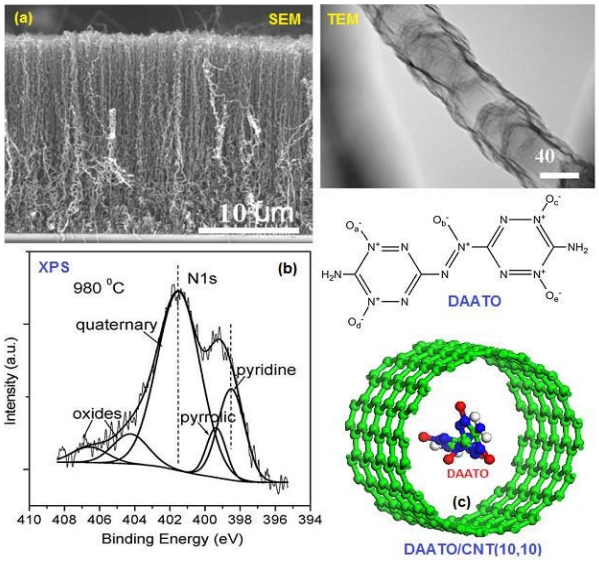


Figure 33, SEM and TEM images for the morphology (a), N1s XPS spectra (b) of N-CNTs synthesized at 980 °C and the structural geometry of DAATO/CNT (10, 10). Recombination of several figures from Ref. 232 with permission of Copyright © 2009 Elsevier Ltd.

Diameter and growth rate of these novel hybrid materials are obviously temperature dependent. It has been found that a single N-CNT has a diameter of 60 nm when its preparation temperature is 980 °C (Figure 33), while it is only around 30 nm at 800 °C, because as temperature decreases, agglomeration of the catalyst becomes smaller, resulting in thinner formed N-CNTs. It also indicates that the lower synthesis temperature usually results in curled and disordered graphitic layers, but the higher temperature favours the formation of a better-organized layered graphitic structure[234]. N-CNTs have a nitrogen content of 10.4 % when the temperature is 800 °C. Except for tetrazine, triazole moieties can also be used to functionalize MWCNTs using 'click' chemistry[235]. The resulting product was successfully incorporated into a polyurethane (PU) matrix by in situ polymerization, where interactions with the PU polymer were enhanced. As a result, the heat of decomposition of the PU/MWCNTs nano-composites was significantly increases due to inclusion of triazole moieties.

In addition to the abovementioned CNTs-based energetic materials, more and more other novel EMs have been under development. As a comparison, the preparation and applications of existing CNTs-based EMs are summarized in Table 5. It can be seen that most of the functionalized CNTs are used for catalysts or energetic additives of propellants and explosives due to relatively lower energy content and promising catalytic activity. Several of them may be used as ingredients of pyrotechnics, such as thermites and ignitors. The preparation procedures of these materials are typically facile, including microemulsion, hydrothermal, reductive deposition, ultrasonic, CVD, as well as straightforward chemical reaction methods. Combination of CNTs with sensitive EMs provides a way to improve sensitivity and performance of the parent EMs. It has been reported that N-doping of CNTs can create well-localized and highly active sites on the CNT surface[236]. When CNTs are filled with high EMs, e.g. a polymeric nitrogen chain, an



 

effective electric field would be created between the CNT surface and the nitrogen chain with minimal C–N distance. This inclusion process would stabilize the high energetic polynitrogen chain that is unstable under the ambient conditions[237]. This approach helps in utilization of highly unstable EMs.

## Effects of CNMs on Performances of EMs

### Catalytic Decomposition, Ignition and Combustion

***CNMs-promoted Thermal Decomposition of EMs:*** It is essential to evaluate thermal properties of newly developed energetic ingredients of propellants, explosives and pyrotechnics, since these parameters have intrinsic connections to the combustion and detonation performances of the final charges made of this new material[238-242]. There are several parameters need to be evaluated, including thermal stability, heat of decomposition, activation energy ($E_a$), reaction models as well as chemical pathways of thermolysis[243-247]. As mentioned above, CNMs have larger SSAs, great thermal conductivity and superior electroconductivity. Therefore, they are better capable to promote thermochemical reactions, such as catalyzing decomposition of energetic compounds including RDX, HMX and AP. The new nEMs based on functionalized fullerene, CNTs and graphene could either be used as catalysts or main energetic ingredients in explosive charges and propellants.

Table 5. The preparation methods and application areas of CNTs based energetic materials.

| CNTs based EMs | Preparation methods | Applications | Contributors |
|---|---|---|---|
| SWCNTs-$CN_4$ | Prepared by a diazo-reaction on the wall of SWCNTs; | Energetic mateials; | Ji, et al., 2015 |
| MWCNTs/F2314 | Obtained from the melt blending of Fluoropolymer and MWCNTs mixture; | PBXs, Pyrotechnics; | Lin, et al., 2015 |
| $KNO_3$/CNTs | By mechanically mixing and grinding to nanosize; | Energetic initiator; | Guo, et al., 2012, & 2015 |
| Zr/$KClO_4$/CNTs | By grinding the mixture of Zr and $KClO_4$ for 20 min; | Pyrotechnic reagent; | Liu, et al., 2015 |
| CNT/BAMO-AMMO | Using CNT-OH as a crosslinking agent, covalently modified BAMO-AMMO; | Energetic binder; | 2010; Chi, et al., 2015 |
| $Fe_2O_3$/MWCNTs | By mild and superior physical absorption method using molten $Fe(NO_3)_3{\cdot}9H_2O$ as the precursor; | Thermites, pyrophoric substrates; | Doorenbos, et al., Wang, et al., 2014 |
| GAP/CNTs binder films | Using hydroxylation CNTs as crosslinking agent, GAP as prepolymer, TDI as curing agent; | Propellants, PBXs; | Zhang, et al., 2013 |
| Al/CNT composites | Al/CNT mixture were engineered by a mechanical pulverization; | Thermites, Propellants; | Jeong, et al., 2013 |
| Nano BNCP/CNT | Prepared from tetraamnine BNCP doped with CNTs; | Detonators, Pyrotechnics; | Chen, et al., 2013 |
| CoAl-MMO/CNT | Synthesized from Co-Al layered double hydroxide/CNTs precursor; | Propellant catalyst; | Fan, et al., 2013 |
| HMX/CNTs | Prepared with an ultrasonic compositing method; | Energetic compositions, | Zeng, et al., 2012 |
| Ag/CNTs | Using silver mirror reaction and hydrothermal methods; | Explosive catalyst; | An, et al., 2012 |
| Al/Teflon/CNTs | By blending of Al with Teflon and CNTs; | Energetic binder; | Kappagantula, et al., 2012 |
| Nitro-SWNTs | Prepared by chemical transformation of the carboxylic acid groups introduced on the wall of CNTs; | Energetic materials; | Forohar, et al., 2012 |
| HMX-P/MCNTs | HMX-polymeric binder system doped with a small mass fraction (1 wt%) multiwalled CNTs or graphite; | Microwave materials; | Duque, et al., 2011 |
| NB-SWNTs | Single-walled CNTs decorated with mono-, di-, and TNB via diazonium chemistry; | Thermopower wave generators; | Abrahamson, et al., 2011 |
| $SnO_2$-$Cu_2O$/CNTs | Prepared by integrate infusioning with liquid phase deposition under normal temperature and pressure using $CuCl_2{\cdot}H_2O$, STP, and CNTs as the reactant; | Explosive catalyst; | Zhang, et al., 2011 |
| AAO/CNTs | AAO is simply mixed with templated CNTs; | Nano-detonators; | Pelletier, et al., 2010 |
| Nd-CNTs | Synthesis from nitrogen-doped CNTs using chemical vapor deposition method; | Energetic components; | Zhong, et al., 2010 |
| PbO·CuO/CNTs | Prepared via a microemulsion process; | Catalyst for propellants; | Ren, et al., 2010 |
| MSWCNT | Using a $CO_2$ laser for ablation of the composite graphite target; | Catalyst for propellants; | Assovskiy, et al., 2010 |
| CuO/CNTs | Using sol-infusion method under normal pressure and low temperature (at 100 °C); | catalyst for propellants; | Liu, et al., 2008 |
| nano Cu/CNTs | By liquid reductive deposition method and using the carbon nanotubes as the carrier; | catalyst for propellants; | Liu, et al., 2008 |
| NA/SWNTs | Functionalization is achieved on CVD-produced SWNTs by acidification to -COOH followed by reaction with TC, and then NA; | Energetic component; | Wang, et al., 2003 |

Notes: CNT-OH, hydroxylated CNTs; BAMO-AMMO, 3,3′-bisazido methyloxetane-3-azidomethyl- 3′-methyloxetane; TDI, toluene diisocyanate; TNB, trinitrobenzenes; STP, stannic tetrachloride pentahydrate; AAO, anodic aluminum oxide; BNCP, bis(5-nitrotetrazolato) cobalt (III) perchlorate; TOC, thionyl chloride; NA, 4-nitroaniline.

It was found from the decomposition of HMX/CNTs composites that the CNTs may reduce decomposition $E_a$ and peak temperature ($T_p$) of HMX[248]. About 1 wt.% of CNTs in this mixture would reduce $E_a$ of HMX by more than 70 kJ $mol^{-1}$, resulting in higher decomposition

rate. However, the heat of decomposition and $T_p$ of HMX would decrease with the increase of CNTs content. Similar research has been carried out for hexanitrohexaazaiso wurtzitane (CL-20) and aminonitrobenzodifuroxan (CL-18) using DSC and TG techniques[249,250]. It was shown that CNTs may also bring down initial thermolysis temperature of these explosives. The reason for this phenomenon was suggested to be that CNTs promote homolytic scission of N-NO bond, thereby promoting formation of $NO^{\bullet}$ free radical. It is also the case for AP-based compositions, where the decomposition rate of AP has been promoted above its typical onset temperature.[251]

Table 6. A summary of thermal behavior and decomposition kinetic parameters of various CNMs-based EMs.

| Samples | Exothermic peaks (10 K $min^{-1}$) | | | Kinetic parameters (Kissinger) | | |
|---|---|---|---|---|---|---|
| | $T_o$ / °C | $T_p$ / °C | Δ*H* | $E_a$ | Ln (*A*) | Contributors |
| ε-CL-20/glue | 231.2 | 250.5 | 1495 | na | na | Lan, et al., 2014 |
| ε-CL-20/glue/G | 233.0 | 247.7 | 1027 | na | na | |
| ε-CL-20/glue/GO | 217.2 | 234.3 | 1678 | na | na | |
| ε-CL-20/glue/rGO | 234.3 | 250.6 | 1613 | na | na | |
| RDX | 216.7 | 222.6 | na | 171.7 | 40.84 | Guan, et al., 2014 |
| GAP/FHN | 112.5 | 154.9/242.0 | na | na | na | |
| RDX/FHN | 212.6 | 218.7 | na | 154.8 | 36.94 | |
| HMX | 277.3 | 283.8 | na | 358.2 | 76.95 | |
| HMX/FHN | 279.2 | 281.6 | na | 334.7 | 72.11 | |
| RDX | 208.7 | 240.4 | 499.5 | 174.0 | 36.38 | Jin, et al., 2014 |
| RDX/mNPF | 206.4 | 234.0 | 891.8 | 166.8 | 35.00 | |
| HMX | 276.3 | 278.1 | - | 470.6 | - | Zeng, et al., 2012 |
| HMX/CNTs | 273.2 | 275.9 | - | 397.6 | - | |
| PF | 160.2 | 189.7/247.0 | 2017.7 | na | na | Cataldo, et al., 2013 |
| FED | 150.3 | 202.9 | 1037.7 | na | na | Chen, et al., 2014 |
| FEN | 100.0 | 172.3/360.5 | na | na | na | |
| FPL | 151.3 | 243.6/473.2 | na | na | na | Guan, et al., 2014 |
| FPL/RDX | 189.3 | 206.1 | na | 140.8 | 34.95 | |
| FGAP | 100.3 | 154.9/242.0 | na | na | na | Huang, et al., 2015 |
| FPGN | 435.2 | 473.3/615.3 | 1280 | 170.9 | 36.43 | Gong, et al., 2015 |
| BNCP | 269.6 | 289.9 | na | na | na | Chen, et al., 2013 |
| BNCP/CB | 260.7 | 276.8 | na | na | na | |
| BNCP/CNTs | 263.1 | 280.1[a]/277.8[b] | na | na | na | |
| BNCP/SWCNTs | 262.2 | 278.0 | na | na | na | |
| FOX-12 | 206.3 | 218.5 | 1540 | 258.3 | 59.30 | Liu, et al., 2008 |
| FOX-12/CCNT | 189.5 | 198.3 | 1872 | 178.6 | 42.24 | |
| FOX-12/SCCNT | 192.4 | 204.1 | 1150 | 181.2 | 45.62 | Zhang, et. al, 2011 |
| RDX/PCC | 208.2 | 226.9 | na | 100.7 | 26.29 | Ren, et al., 2010 |
| RDX | 205.2 | 240.2/253.3 | 2546 | 174.0 | 36.38 | An, et al., 2012 |
| RDX/Ag-CNT-1 | 203.7 | 241.0/252.1 | 2451 | na | na | |
| RDX/Ag-CNT-2 | 203.2 | 249.8 | 2120 | na | na | |
| AP | 263.2 | 297.0/406.2 | 621 | na | na | Wang, et al. 2012 |
| AP/GA | 265.1 | 322.5 | 2110 | na | na | |
| AP/GA/$Fe_2O_3$ | 257.8 | 312/348 | 1985 | na | na | Lan, et al., 2015 |
| AP/HTPB | 274.4 | 335.9/405.8 | 1940 | na | na | Liu, et al., 2008 |
| AP/HTPB/CNTs | 266.9 | 328.5/380.9 | 2170 | na | na | |
| AP/HTPB/Cu-CNTs | 271.2 | 353.4 | 2780 | na | na | |
| RDX/nD-1 | 217.9 | 244.6 | 894.6 | 127.5 | 11.30 | Tong, et al., 2009 |
| RDX/nD-2 | 215.1 | 237.3 | 625.6 | 199.9 | 19.10 | |

Notes: $T_o$, onset temperature of the peaks; $T_p$, peak temperature of thermal events; Δ*H*, heat release in $J.g^{-1}$; $E_a$, activation energy; *A*, pre-exponential factor; na, not available; a, CNTs with diameter of 10-20 nm while b, of 60-100 nm; Ag-CNT-1 and -2 means the mass ratio of Ag/CNTs is 19:1 and 9:1, respectively.
*Nomenclatures:* CL-20, 2,4,6,8,10,12-Hexanitro-2,4,6,8,10,12-hexaazaisowurtzitane; FEN, fullerene ethylenediamine nitrate; FED, Fullerene ethylenediamine dinitramide, $H_{12}C_{60}(HNCH_2\ CH_2NH_2{\cdot}HN(NO_2)_2)_{12}$; mNPF, N-methyl-2-(3-nitrophenyl)pyrrolidino- [3',4':1,2] fullerene; PF, polynitro[60]fullerene, $C_{60}(NO_2)_{14}$; FPGN, [60]Fullerene-Poly(glycidyl nitrate); FPL, fullerene phenyl-alanine lead salt; FFGAP, functionalized [60]fullerene-glycidyl azide polymer; FPL, fullerene phenylalanine lead salt; FHN, fullerene hydrazine nitrate; FDN, derivative with molar ratio of $C_{60}$, 2,4-dinitrobenzaldehyde and N-methylglycine 1:2:6; NPF, trinitrophenyl $C_{60}$ derivative; SCCNT, $SnO_2$-$Cu_2O$/CNTs composites; PCC, PbO·CuO/CNTs; CCNT, CuO-CNTs (8.8 nm, 5%); GA, graphene aerogel; nD-1, nD/RDX = 1:8, while it is 1:4 for nD-2.

In fact, porous structure of CNTs bandles, having very large SSA, can be considered as a combustion catalyst nano-carrier, forming many kinds of highly-promising composite catalysts. The synergistic effect of the CNTs with carried catalysts may greatly improve catalytic activity, and the agglomeration problem of nano-sized catalysts could be improved as well. For instance, the catalyst Ag/CNTs can change thermal decomposition mechanism of RDX, where the dominant liquid phase reaction would change to a faster gas phase reaction, resulting in lower $T_p$[221]. The effect is also similar for PbO-CuO/CNTs composite catalyst[230], which has better influence on thermal decomposition of RDX as compared to a parent PbO-CuO. Another two nano-catalysts CuO/CNTs[231] and $SnO_2$-$Cu_2O$/CNTs[239],



 

were shown to decrease $T_p$ of FOX-12 decomposition as well, meanwhile the heat release and $E_a$ were decreased accordingly. When CNTs are used to encapsulate energetic molecules, such as nitromethane (NM), forming NM/CNTs composite material, which has very different thermal behavior in comparison with the parent NM[252]. It has been shown that a transition state (TS) exists for thermal decomposition of NM/CNT(5, 5), while there is no TS for dissociation of C-N bond in a gas phase of a "stand-alone" NM molecule[253]. In fact, SWCNTs can change the molecular structure and electronic charge of $NO_2$ and $CH_3$ groups of NM during its decomposition. The energy barrier of the TS (in the CNT-bound NM) was calculated to be about 198 kJ mol$^{-1}$, which is 21 kJ mol$^{-1}$ lower than that of the aforementioned C-N dissociation of free NM. Meanwhile, the energy barriers for the nitromethane-methyl nitrite rearrangement and H-migration, as well as C-N homolytic dissociation are significantly decreased[254,255]. This is also the case for nitramide encapsulated in SWCNTs[256]. Regarding of some other ingredients of composite propellants, CNTs has little effect on thermal decomposition of phase-stabilised ammonium nitrate (PSAN) and GAP, while it was shown to stabilize HTPB binder[257].

Thermal behavior of ADN could be greatly affected by CNTs-based catalysts. For instance, $Fe_2O_3$/CNTs and Fe·Cu/CNTs may decrease the decomposition $T_p$ of ADN by 12.1°C and 11.6°C, respectively, when just 1 wt.% of a catalyst is used[258]. These results were observed when a large number of hematite phase $Fe_2O_3$ were uniformly filled in the MWCNTs, and the mass fraction of $Fe_2O_3$ in such composite was about 25.8 wt%[204]. In the presence of 10 wt.% $Fe_2O_3$/MWCNTs composites, the second $T_p$ of AP decreased by 116°C, and the first exothermic peak disappeared with 200 kJ mol$^{-1}$ decomposition heat increase.

Graphene, a two-dimensional carbon crystal with monoatomic thickness, is considered to be a basic structural unit of CNTs and graphite. It also has a large SSA, and can form many complexes with energetic molecules. The Ni/graphene nano-composites were prepared via a one-step mixing method, and then their catalytic effect on thermal decomposition of AP was investigated[259]. The results show that when the content of Ni/graphene composites is about 1% of the mixture, the catalytic effect is the most significant. In this case, the second decomposition peak temperature decreased by 97.3 °C, while the first peak disappeared. Later, these researchers used the same methodology to prepare a complex of $Mn_3O_4$ nanoparticles with graphene, which also exhibited a significant catalytic effect on AP decomposition[260]. Similarly, two decomposition peaks in the latter AP fomulation merged into one peak. Meanwhile, the $T_p$ was reduced by 141.9 °C, caused by synergies of $Mn_3O_4$ and graphene. In contrast to graphene, GO has functional groups on its surface. It is easier to combine with the other substances, extending the range of GO-based materials' applications. It was reported that the CuO/GO nano-composites prepared from water/isopropanol solvent are very effective in catalyzing AP decomposition and combustion[261]. In addition, when some other groups were introduced to GO, the catalytic activity may be significantly improved. For instance, the nitrated GO make $T_p$ of AP decomposition decrease by 106 °C[262], while heat of decomposition increases from 875 to 3,236 J g$^{-1}$.

Thermal properties of AN oxidizer, frequently used in propellants and emusion explosives, can also be modified by integration of CNMs[263, 264]. When AN was mixed with activated carbon (AC) or CNTs, violent reactions upon its melting took place. However, mixtures of AN with graphite or with fullerene show only mild exothermic peaks (decomposition), similar to pure AN. It was also found that the formation of carbon dioxide was more distinct for AN/AC and AN/CNTs mixtures than in other mixtures. When BNCP was doped by CB, its $T_p$ decreased from 289.9 to 276.7 °C, while after doping of BNCP with CNTs, the $T_p$ would be significantly further reduced. Besides, there was an obvious endothermic peak, and with the decrease of nanotube diameter, decomposition peak of BNCP becomes more narrow and sharp, accompanied with a shoulder disappearance[52]. In order to make a comparison of the thermal behavior and catalytic effect of different CNMs-based EMs, the thermal decomposition data, as well as kinetic parameters of all abovementioned materials are summarized in Table 6.

As shown in Table 6, addition of flake graphite to the ε-CL-20 induces slightly earlier decomposition of this explosive with much lower heat release, while the addition of GO or rGO to the ε-CL-20 may enhance the decomposition of ε-CL-20/glue fomulation with remarkable improvement in the heat release[265]. However, only rGO additive could improve the thermal stability of ε-CL-20. The catalysts based on fullerene (CBF) would reduce the decomposition $T_p$, apparent $E_a$, and raise the exothermic heat of FOX-12. When the mass ratio of the CBF/FOX-12 is 1-to-5, the decomposition $T_p$ of FOX-12 is reduced by 20.3 °C, while the heat release is increased by 332 J g$^{-1}$. It is 18.08 °C and 148 J g$^{-1}$ for pure CBF[215]. Similarly, the catalytic effect of the Ag/CNTs nanocomposite on the thermal decomposition of RDX was investigated by DSC. It was indicated that the irregularly globose nano-Ag particles, attached to the surface of the CNTs evenly, forming a promising catalyst for RDX. It greatly accelerated the decomposition rate of RDX with reduced $E_a$. It is also the case for PbO·CuO/CNTs catalyst, which can accelerate the decomposition of RDX, and reduce the $T_p$ by 14.1 °C[216]. The nDs can also slightly reduce the $T_p$ of RDX[81]. In contrast, when a fullerene-based catalyst (mNPF) is added to RDX, its $T_p$ drops from 240.4 °C to 234.0 °C, and the corresponding exothermic heat increases from 499.5 to 891.8 J g$^{-1}$. There is another fullerene based catalyst FED, whose catalytic effect hasn't been studied yet. It was shown that FED started to decompose at 150 °C with $T_p$ of 203 °C and enthalpy of 1037.7 J g$^{-1}$. The total mass loss of FED in temperature range 100-800 °C is 49.7%, with intense decomposing of -N($NO_2$)$_2$ and partial decomposition of branched chain.[114] It was further found that FHN can also accelerate decomposition of RDX and HMX. The peak temperatures of the exothermal decomposition of these nitramines were reduced[117] and their corresponding $E_a$ of RDX was decreased by 17 kJ mol$^{-1}$, while that of HMX was reduced by more than 20 kJ mol$^{-1}$. In addition to stabilization of common exlosives, CNTs has also a significant influence on stability of energetic binders. For example, the onset temperature of CNTs/BAMO-AMMO composition was measured to be 236 °C,

which is 7 °C higher than that of the corresponding TME/BAMO-AMMO energetic binders[195].

It was recently reported that energetic derivatives of $C_{60}$-fullerene have very unique thermal properties. For instance, MTNBFP has a very high standard molar enthalpy of formation and it could be a highly-promissing new candidate of primary explosives[113]. The most possible initial dissociation path for MTNBFP is releasing $NO_2$ according to dynamic dissociation energies, which are 58.5, 172.5, and 239.2 kJ $mol^{-1}$, respectively. In terms of energetic polymers based on fullerene, it has been shown that $C_{60}$-PGN is thermally stable up to 200 °C. The decomposition $E_a$ of $C_{60}$-PGN was measured to be 170.9 3 kJ $mol^{-1}$ (by Kissinger method) and 168.3 kJ $mol^{-1}$ (by Ozawa-Doyle method)[120]. $C_{60}$-PGN is more stable than any other known polynitrofullerenes. The $C_{60}$-GAP decomposition shows a three-step thermal process[121], where the first step is due to the reaction of the azide group and fullerene at approximately 150 °C. The second mass loss step is due to the decomposition of the main chain of remaining GAP and N-heterocyclic at approximately 240 °C. The final decomposition step could be attributed to the burning of amorphous carbon or carbon fullerene cage at around 600 °C.

Highly energic polynitro[$C_{60}$]fullerene (PF) starts to decompose below 160 °C, with two peaks at 189.7 and 247.0 °C, with combined heat release of 2,017.7 J $g^{-1}$. The energy content is very comparable to those of HMX and CL-20. Its total mass loss of 47.3% corresponds to the theoretical value of 47.2%, corresponding to the calculated formula of $C_{60}(NO_2)_{14}$. During decomposition, PF releases a mixture of nitrogen oxides: $NO_2$ and NO with minor amounts of $N_2O$. A residue of oxidized carbon was obtained after the main decomposition step. By further releases of $CO_2$ and CO after 700 °C, the residue is reduced to a carbonaceous matter free of oxygenated groups, showing also the presence of a small amount (<10%) of $C_{60}$ fullerene[114]. Theoretical investigation shows that the explosion of PF starts with $NO_2$ group isomerization into C-O-N-O, followed by emission of NO molecules and formation of CO groups on the buckyball surface[266]. Then, NO oxidizes into $NO_2$, and $C_{60}$ structure falls apart, liberating $CO_2$. As a comparison, FEN decomposes just in two steps: the first-stage with 40.8% mass loss (100-250 °C), due to intense scission of $NO_3$- and partial decomposition of branched chain, releasing $H_2O$, $CO_2$, CO, $N_2O$ and $NO_2$. The second-stage has 59.2% of mass loss (250-580 °C), due to decomposition of residual branched chains on a carbon cage, releasing $CO_2$[115]. For comparison of decomposition processes of different energetic fullerene derivatives, their TG/DTG curves under heating rate of 10 °C $min^{-1}$ are shown in Figure 34.

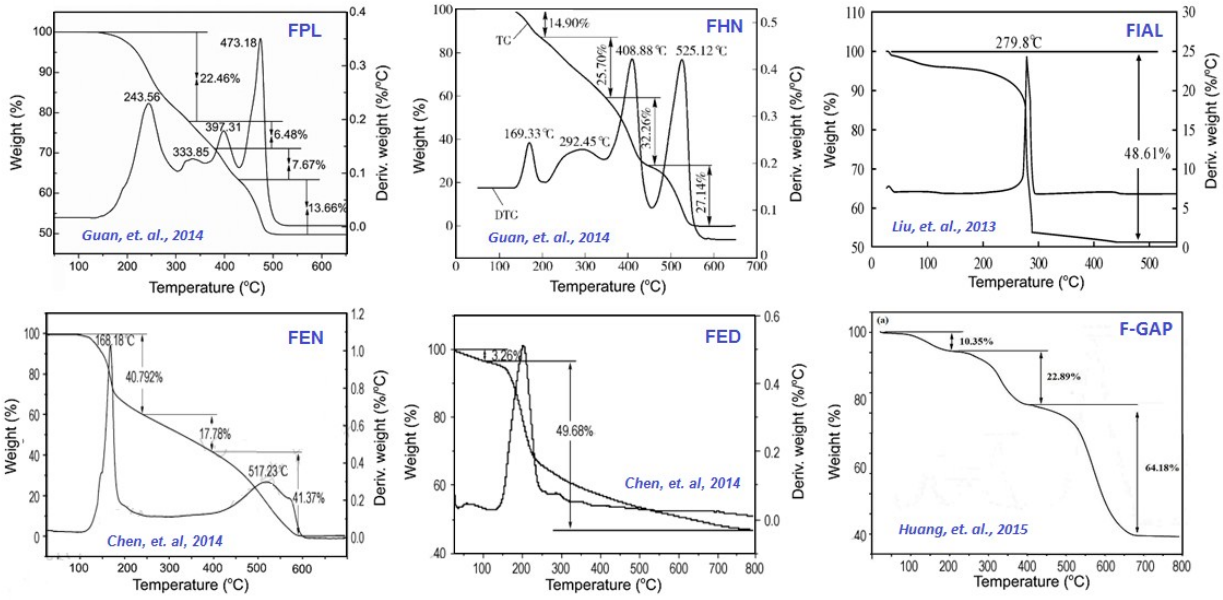


Figure 34, TG-DTG curves of several energetic fullerene derivatives: FPL (fullerene phenylalanine lead salt), FHN, FIAL (fullerene itaconic acid copolymer lead salt), FEN, FED and F-GAP ($C_{60}$-GAP). Recombination of several figures appeared in the listed references 93, 95, 97, and 101 with permission.

According to Figure 34, at least two steps involved in decomposition of these fullerene derivatives, which started at between 100-150 °C. In particular, FPL undergoes a four-step exothermic process started at 135 °C[117], which can reduce decomposition $T_p$ of RDX by more than 20 °C, and decrease $E_a$ by 30 kJ $mol^{-1}$. FHN may undergo at least four steps decomposition, under $N_2$ atmosphere, starting at around 150 °C, while FEN decomposes only in two steps, as descibed above. Moreover, FHN would decompose completely in the air with a trace amount of residue. The FED initialy decomposes in one slow step, with mass loss of 3.3%, followed by a main decomposition step, with mass loss of around 50%. It can also be seen that F-GAP may decompose in three steps under air atmosphere. The first stage of thermal degradation appears at 150 °C, with around 10.4% mass loss. The other two onsets thermolysis appear at 300 °C and 600 °C, with approximately 22.9% and 64.2% total mass losses, respectively. In contrast, the GAP decomposes at approximately 200 °C, with the main gaseous products of CO, HCN, HCHO, and $NH_3$.[267-269] It is indicated that the initial thermal degradation of F-GAP is probably due to the scission of $-N_3$ group *via* the intramolecular or



 

intermolecular cycloaddition of $-N_3$ with fullerene carbon cage, as well as the subsequent nitrogen release. The second step that takes place between 200-400 °C is due to decomposition of GAP's main chain and N-heterocyclic decomposition, while the final mass loss step is caused by decomposition of the fullerene cage (Scheme 12).

As shown in Table 6, the decomposition of AP can be greatly affected by CNMs. For instance, the presence of GA, on one hand, has a catalytic effect on decomposition of AP. On the other hand, the oxidants produced from AP may react with GA, promoting the heat release (Scheme 13)[156]. There was only one exothermic peak observed in DSC for AP/GA nanocomposites (in contrast to two peaks observed for pure AP), which is 83.7 °C lower than the second peak of AP, with a total heat release of 2,110 J $g^{-1}$. It has been shown that the as-prepared AP/GA nanostructured energetic composites have numerous nanoscale pores and their SSA is about 49.2 $m^2g^{-1}$. These properties of the AP/GA result in its accelerated decomposition and more total heat release[157]. Graphene may also change the decomposition mechanism of AP, as shown in Scheme 13. In contrast, the Cu/CNTs catalyst would remarkably decrease the second peak of AP, with higher decomposition heat[210]. The GA/$Fe_2O_3$ nanostructured catalyst dispersed in AP showed a significant catalytic effect in promoting thermolysis of AP. In the latter case, only a single decomposition step was observed, with decreased temperature of the peak and great increase in the total heat release. Thus, the as-prepared GA/$Fe_2O_3$/AP nanostructured energetic composite could be a promising candidate as a component for solid propellants[158]. GA also has great catalytic effect on decomposition of AN[159], whose $T_p$ was decreased by 33.7 °C and the heat release was increased by 532.8 J $g^{-1}$. In comparison to GA and GA/$Fe_2O_3$, the addition of CoAl-MMO and CoAl-MMO/CNT to AP may make the latter decompose in a single exothermic process. For example, in case of CoAl-MMO additive, AP shows a maximum peak temperature of 297 °C. Surprisingly, when using CoAl-MMO/CNT, the second peak temperature of AP is significantly decreased to 271 °C, strongly suggesting that this nanocomposite is the most efficient catalyst for promoting decomposition of the AP[217].

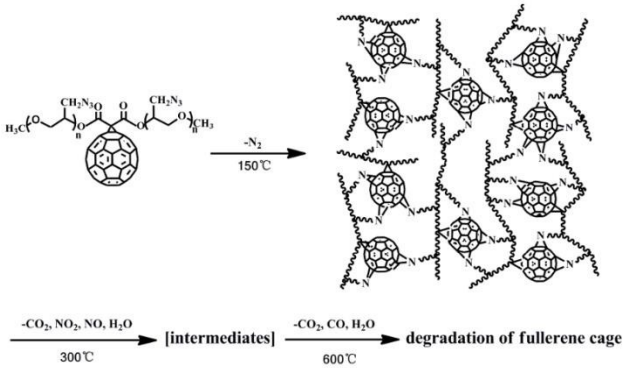


Scheme 12, Thermal decomposition mechanism of $C_{60}$-GAP under air atmosphere (adapted from Huang, et. al., Polymers, 2015, 7, 896-908.) Reprinted from from Ref. 229 with permission of Copyright © 2011, American Chemical Society.

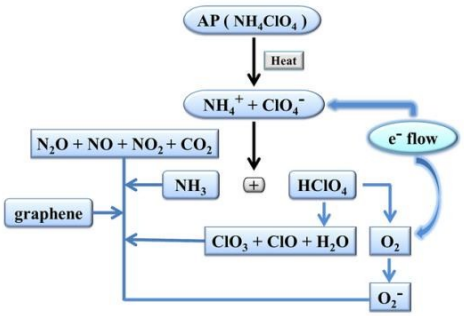


Scheme 13: Thermal decomposition processes of GA/AP nanostructured energetic composite

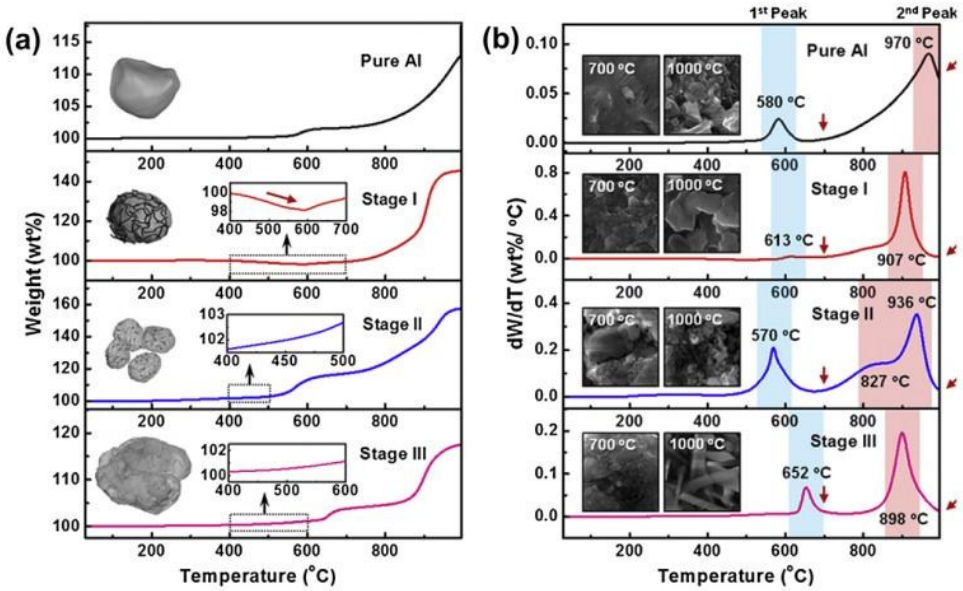


Figure 35, (a) TGA profile under air, at a ramping rate of 5 °C $min^{-1}$ for different stages: Stage I (60 min), Stage II (120 min), and Stage III (180 min). The inset image shows schematics of Al/CNTs mixture morphologies and (b) the corresponding DTG; The inset shows SEM images of Al/CNTs mixtures taken after TGA terminated at 700 and 1000 °C. Note that the scales of y-axes in (b) are different from each other, in order for better visualization of each peak. Reprinted from Ref. 222 with permission of Crown copyright © 2013 Published by Elsevier Ltd.

Based on abovementioned results, one could see that CNTs and its functionalized analogs have strong catalytic effect on energetic compounds such as RDX, FOX-12 and AP. In fact, CNTs may also have great effect on oxidation process of Al, which is a very important ingredient in many propellants and explosives. It was shown that the CNTs can be fully embedded into Al aggregates, forming urchin type Al/CNTs particles. This material has the largest exothermic enthalpy at a lower oxidation temperature for both γ-$Al_2O_3$ and α-$Al_2O_3$ phases[222]. It was attributed to the fast heat transfer into Al particles *via* partially embedded CNTs. The TG curves of Al/CNTs at heating rate of 5 °C $min^{-1}$ are shown in Figure 35. Results presented in Figure 35 show that the exothermic enthalpy of Al oxidation is strongly dependent on the content of CNTs, which increases to -188 kJ $g^{-1}$ at 20 wt.% of CNTs[222]. Moreover, the oxidation process of pure Al particles takes place in the range of 580 to 970 °C (TGA measurements). The first oxidation peak of pure Al at 580 °C is known as γ-$Al_2O_3$ phase formation, while the second peak, near 970 °C is known as α-$Al_2O_3$ phase formation. It is in agreement of typical route of alumina phase transformations: amorphous- $Al_2O_3$ → γ → ($\delta$) → ($\vartheta$) → α-$Al_2O_3$.[270] Typically, amorphous-$Al_2O_3$ transforms to more thermodynamically stable crystalline polymorphs, as the layer thickness reaches a critical value.[271] Once the formation of γ-$Al_2O_3$ phase is completed, the oxide layer thickness reaches a critical thickness to form α-$Al_2O_3$ phase at near 970 °C. However, oxidation behavior of Al/CNTs (10 wt.%) mixture was found to be very different from the pure Al. The weight of Al/CNTs mixture was reduced during the initial stage of oxidation (400-600 °C; Figure 35b). This phenomenon was explained by burning of CNTs, which are located on the surface of Al particles.

The weight increase at near 600 °C was due to the formation of γ-$Al_2O_3$ layer, which was almost nullified by the weight decrease from the CNTs burning. The formation temperature of α-$Al_2O_3$ phase was shifted from 970 to 907 °C, while the weight increase reached 145% (much larger than that of pure Al) due to enhanced oxidation in presence of CNTs. As shown above, although the structure and shape of graphene and CNTs are different, both these namomaterials are capable of facilitating the electron transfer, promoting chemical reactions, as well as catalytic effects. These effects could be further enhanced by addition of other catalysts. The GO, CNTs and fullerene CNMs-based catalysts have large SSAs and thus high reactivity, especially when these nanomaterials are derivatized with additional functional groups.

***Ignition of Pyrotechnics and Thermites*:** A pyrotechnic initiator (igniter) is a device that contains a pyrotechnic composition (oxidants and fuels), used primarily to ignite other more difficult-to-ignite materials, e.g. thermites, gas generators, and solid-fuel rockets[272,273]. The initiator compositions are similar to flash powders, but they are different in their burning rate. Although the explosion of igniters is not favored, they have intentionally-high production of hot particles. Commonly used oxidizers are KP and KN, while typical fuels are Ti, titanium(II) hydride, zirconium, zirconium hydride, and boron[274]. There are many factors that affect the energy output of these compositions, whose performance could be modified by catalysts or energetic additives[275]. It has been found that ignition of BNCP by laser was difficult, but the inclusion of just 5 wt.% of CNTs or CB significantly decreases both the critical energy for ignition and ignition delay time[52]. It indicates that the CNMs and their energetic derivatives have a positive effect on the ignition properties of materials containing them. It has been reported that the EMs mixed with optically active CNTs can be subject to optical initiation by using ordinary light with intensity of several W $cm^{-2}$, on a large surface area[276]. These energetic mixtures could be new ideal candidates for safety apparatus, such as the firing of bolts on space shuttle rockets and aircraft exit doors.

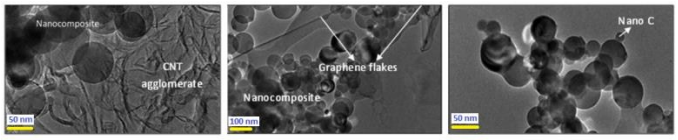


Figure 36, TEM images of Al/Teflon energetic composites combined with CNTs, graphene flakes and nano carbon. Reprinted from Ref. 277 with permission of Copyright © 2012, managed by AIP Publishing LLC.

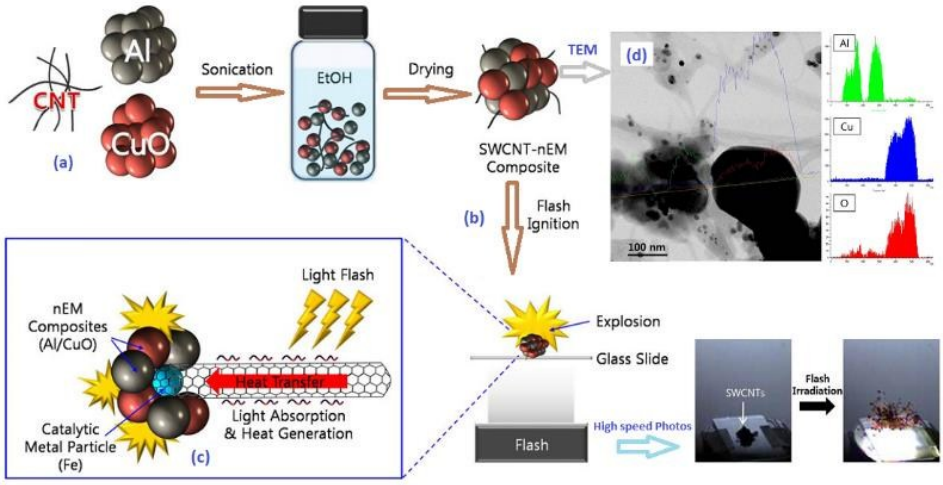


Figure 37, Schematics of (a) the fabrication of SWCNT-nEM composites, (b) the flash ignition of an SWCNT-nEM composite, (c) the optical ignition mechanism of an SWCNT-nEM composite, and (d) scanning TEM image and line scan analysis of SWCNT/Al/CuO nanocomposites. Recombination of several figures from Ref. 280 with permission of Copyright © 2012 The Combustion Institute. Published by Elsevier Inc.

It was further shown that the addition of both CNTs and graphene can significantly enhance the thermal transport properties of energetic composites made of Al and Teflon[277]. However, the composites containing CNTs are much more sensitive to impact. In contrast, although graphene cannot significantly sensitize energetic composites to ignition, it does induce greater overall reactivity. Increasing CNM additives concentration may decrease the overall thermal diffusivity and increase the sites for probable hot spot formation during impact[278]. The TEM images of above mentioned energetic composites containing CNT, graphene and nano-C are shown in Figure 36. In fact, the heat conductivity of polymeric materials can be improved by incorporating of CNTs[279], and it may also be the case for pyrotechnic compositions. According to aforementioned results, the CNTs are more effective than other CNMs in promoting the ignition performance of pyrotechnic compositions. In particular, the SWCNTs is the best choice for this purpose, and it has been demonstrated that the burn rate and pressurization rate of SWCNTs/Al/CuO nanocomposites achieve the maximum values of about 240 $ms^{-1}$ and 5.9 ± 0.8 psi $\mu s^{-1}$, respectively, when the content of SWCNT is just 1 wt.%[280]. The preparation method of SWCNTs/Al/CuO nanocomposites, their morphology and flash irradiation ignition process are shown in Figure 37. The mixing ratio of fuel and oxidizer was fixed at Al:CuO = 3:7 (wt.%). Then, the SWCNTs were added to the nEMs precursor solution in mixing ratios of 1, 2, 5, and 10 wt.%, respectively. The nano-Al particles were firmly attached to the surface of CuO NPs, while the SWCNTs appear to be homogeneously distributed in Al and CuO NPs-based matrix. As the content of SWCNTs increased to more than 2 wt.%, both burn rate and pressurization rate of the as-prepared SWCNT-nEM composites decreased significantly. The researchers belive that it was due to the large amount of SWCNTs in the nEM matrix, which may increase the heat dissipation, resulting in very limited temperature increase for SWCNT-nEM composite, thus hindering the oxidation and subsequent ignition of the nEMs. In the latter case, the remote optical ignition and controlled-explosion reactivity of nEMs was achieved by incorporating less than 2 wt.% of SWCNTs, as optical ignition agent.

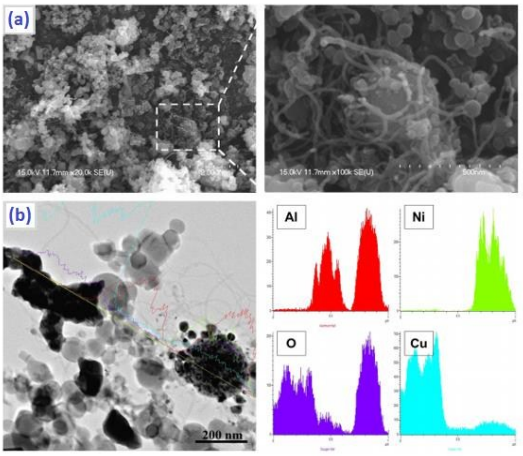


Figure 38, (a) SEM and (b) scanning TEM images of SUCNT/nEM. Reprinted from Ref. 282 with permission of Copyright © 2014 The Combustion Institute, and published by Elsevier Inc.

In addition to ignition by irradiation, the ESD ignition property of pyrotechnics could also be tailored by highly electro-conductive nano-fillers, including CNTs, graphene nano platelets (GNP), and their combinations. It has been found that the ignition and the electrical conductivity of the binary composite of Al and polytetrafluoroethylene (PTFE) can be changed significantly[281]. Instead of GNP, a lower volume fraction of CNTs is adequate to create an electrical conductivity percolation threshold. However, CNT/GNP composite could create a better percolating network. In this way, the compositions that are insensitive to ESD ignition become sensitive due to improvement of electrical conductivity. Based on this strategy, a flash-ignitable nEMs composed of Al/CuO nanoparticles for underwater explosion were invented by using "sea urchin-like" CNTs (SUCNTs)[282]. The underwater ignition of nEMs is a big challenge because water perturbs the reactants prior to ignition and quenches the subsequent combustion. The SUCNTs can absorb the irradiated flash energy and rapidly convert it into thermal energy. Similar to abovementioned Al/CuO system, the maximum burn rate was achieved by adding 1 wt.% of SUCNTs into the nEM matrix. However, the resulting maximum underwater burn rate was found to be only about 34 m $s^{-1}$, which is much lower than burning rate of this composition in air (240 m $s^{-1}$)[280].

***Use of CNMs in Combustion of Propellants***: The combustion properties, including burn rate, pressure exponent, combustion wave and flame structrue, are the most important parameters for propellants[283,284]. In general, the burn rate should be controllable, while the pressure exponent must be smaller than 0.5, for solid rocket applications, and higher than 1.0, for gun propellants. It is a common practice to use burn rate modifiers or combustion catalysts to control the burn rate and pressure exponent of solid propellants. It has been shown that many CNMs derivatives could be used as effective combustion catalysts[285]. The coupled energy balances for a CNTs with an annular coating of reactive metals is solved, where the thermal transport in the nanotube accelerates reaction in the annulus. For the case of Zr metal, the CNTs increase the reaction front velocity from 530 to 5100 mm $s^{-1}$, along the axial direction of the nanotube[286]. This remarkable result offers a proof-of-concept for 1-D anisotropic EMs and could find application in novel propellants. Interestingly, there are large temperature differences (> 1,000 K) between the CNT and the reaction front of annulus. The directional heat conduction in the CNT makes the interfacial heat conductance a less significant factor affecting the heat distribution.

In addition to CTNs, graphene could also enhance the combustion properties of propellants. A comparative study showed[287] that the ignition temperature was lowered and burning rates are increased for the colloidal suspensions of nitromethane with graphene, as compared to the liquid nitromethane monopropellant alone. It has been further reported[288] that the addition of raw fullerene soot (FS), extracted FS (EFS), pure $C_{60}$ and CB additives to nitroglycerine (NG) markedly accelerated its liquid phase decomposition. The effect of these nanomaterials on combustion properties of double-base propellants (DB) has been also evaluated. As indicated earlier, the CNTs have a strong catalytic

effect on decomposition of AP, and it's also a promising combustion catalyst of AP. It was proven that with the increase of CNTs content, burning rate of AP composite would increase with lower pressure exponent ($n$)[251]. Table 7 lists the burn rate and $n$ of different propellants upon using CNMs as the burn rate modifiers. Regarding applications of CNMs additives as catalysts, since the early 1960s, USA began using AC in solid propellants, where Bice[289] and Ives[290] found that AC could promote the burning rate of AN-based propellants. These researchers also reported that a certain amount of carborane/AC composites would increase the burning rate of the same propellant from 5.5 to 9.2 mm $s^{-1}$. Moreover, they showed that the burn rate of aluminized composite propellants may be increased to 25 mm $s^{-1}$ at 7 MPa by using AC as a modifier[291].

A combination of AC with iron oxide can make the propellant burn at a peed of 50 mm $s^{-1}$. Yet, it has a problem of unacceptable large pressure exponent. Later on, it has been proven through the analysis of flame surface by SEM images[292], that the hole in the water encapsuled in AC can reduce melt flow on buring surface of propellant, resulting in higher pressure exponent. Therefore, it would be better to use water-free AC. In addition to AC, the CNTs could also increase the burn rate of HTPB propellant by 20%, while inducing practically no effect on its pressure exponents[293]. Similar findings were observed for NEPE propellant, but the pressure exponent was decreased at low pressure range (e.g. <10 MPa), while it was increased at higher pressure range (15 - 18 MPa)[294].

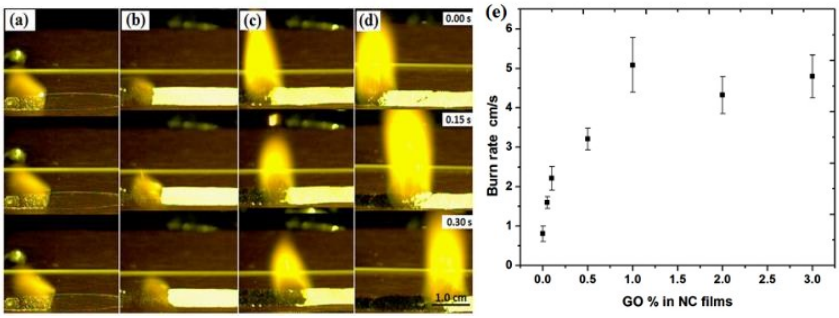


Figure 39, High-speed images of combustion process of pure NC films and GO-NC films under the ambient conditions: (a) Pure NC film; (b) 0.05% GO-NC film; (c) 0.5% GO-NC film; (d) 1% GO-NC film. (e) Comparison of the burn rates of pure NC films and GO-NC films. Reproduced from Ref. 164 with permission from the Royal Society of Chemistry.

Table 7, the effects of CNMs combustion modifiers on burning rates of solid rocket propellants (under $N_2$ atmosphere, 20 °C)

| Propellants | $u$ / (mm·$s^{-1}$) at different pressure | | | | | $n$ (3-11 MPa) | Ref. |
|---|---|---|---|---|---|---|---|
| | 3 MPa | 5 MPa | 7 MPa | 9 MPa | 11 MPa | | |
| AP | 4.70 | 6.33 | 7.39 | 8.93 | 10.14 | 0.586 | |
| AP/CNT(1%) | 7.84 | 9.46 | 11.11 | 12.53 | 13.26 | 0.427 | |
| AP/CNT(2%) | 9.47 | 11.51 | 13.78 | 14.54 | 16.28 | 0.406 | [251] |
| AP/CNT(3%) | 10.64 | 13.63 | 14.83 | 16.39 | 17.86 | 0.386 | |
| AP/CNT(4%) | 13.24 | 15.02 | 16.12 | 17.49 | 18.30 | 0.247 | |
| | 5 MPa | 7 MPa | 9 MPa | 10 MPa | 11 MPa | (5-11 MPa) | |
| AP/HTPB | 5.75 | 7.03 | 7.37 | 8.58 | 9.12 | 0.572 | [206] |
| AP/HTPB/CNT | 6.68 | 7.84 | 8.90 | 9.76 | 10.08 | 0.538 | |
| AP/HTPB/Cu-CNT | 7.93 | 8.92 | 10.00 | 10.48 | 10.85 | 0.408 | |
| | 2 MPa | 4 MPa | 6 MPa | 8 MPa | 12 MPa | (2-8 MPa) | |
| CMDB | 3.71 | 5.88 | 7.87 | 10.23 | 14.30 | 0.721 | |
| CMDB/CB | 3.96 | 6.10 | 7.82 | 9.74 | 13.57 | 0.642 | |
| CMDB/FS | 3.76 | 5.88 | 7.82 | 9.90 | 13.63 | 0.692 | [288] |
| CMDB/EFS | 3.50 | 5.76 | 7.55 | 9.36 | 13.52 | 0.706 | |
| CMDB/$C_{60}$ | 3.57 | 5.72 | 7.49 | 9.49 | 13.46 | 0.697 | |
| DB | 1.22 | 2.36 | 4.55 | 5.93 | 8.53 | 1.171 | |
| DB/PbO-GO | 4.68 | 8.15 | 10.09 | 10.99 | 10.38 | 0.630 | [299] |
| DB/$Cu_2O$-PbO/GO | 8.17 | 11.36 | 12.96 | 14.33 | 16.74 | 0.405 | [300] |
| DB/$Bi_2O_3$/GO | 3.01 | 6.98 | 10.21 | 12.37 | 15.91 | 1.035 | [301] |
| DB/$Cu_2O$ -$Bi_2O_3$/GO | 8.58 | 11.44 | 13.53 | 15.07 | 17.27 | 0.408 | |
| | 8 MPa | 10 MPa | 12 MPa | 16 MPa | 20 MPa | (16-22 MPa) | |
| DBP | 6.49 | 7.81 | 8.99 | 10.30 | 12.24 | 0.783 | [291] |
| DBP/CuO-CNTs | 13.34 | 15.28 | 16.49 | 19.03 | 20.34 | 0.384 | |
| DBP/nano-$Bi_2O_3$ | 6.86 | 8.02 | 8.91 | 10.62 | 12.04 | 0.639 | [290] |
| DBP/$Bi_2O_3$-CNTs | 9.38 | 10.66 | 11.74 | 13.81 | 15.21 | 0.431 | |

Note: Used RDX was a mixture of 80 μm and 50 μm particle sizes, with weight ratio of 1/1; AP particle sizes were in the range of 120-200 μm; the N content in NC was 12.6%; CMDB, RDX/AP/NC/NG/Additives/Catalyst with the mass ratio of 20/10/29/32.5/5.0/3.5; FS, was composed of 10% fullerenes and 90% CB; EFS, containing about 80% $C_{60}$ and 20% $C_{70}$; DBP, double-base propellants containg (NC+NG)/DEP/$C_2$ with the mass ratio of 89/8.5/2.0, where DEP is diethyl phthalate and $C_2$ is a stabilizer; the contents of $Bi_2O_3$ and $Bi_2O_3$-CNTs are 2.5 wt.%.



 

As shown in Table 7, the Cu/CNTs can markedly increase burning rate and decrease the pressure exponent for AP/HTPB propellant[186]. A significant amount of work regarding catalytic effects of CNMs on combustion behavior of solid rocket propellants was done in China by Zhao's group[295-299]. They prepared composite catalysts based on PbO, CuO, $Bi_2O_3$, GO, as well as "Pb-CB" binary catalytic system, to increase the burn rate of DB propellant. It was shown that the "Mesa Burning" could be obtained in pressure range of 8-14 MPa. The PbO -$Cu_2O$ could be jointly supported by CB, forming a "Pb-Cu-CB" three-element catalytic system, so that the burning rate of DB propellant at 2 MPa can be elevated from 2.15 to 8.57 mm $s^{-1}$, with a wider "plateau combustion" pressure range (10-20 MPa)[295].

These researchers also used a combination of $Bi_2O_3$ and GO to replace PbO/GO, as green combustion catalyst[296,297]. It was observed that both $Bi_2O_3$/GO and $Cu_2O$-$Bi_2O_3$/GO catalysts would significantly increase the burning rate of DB propellants and reduce the pressure exponent (Table 7). Although the "Mesa Burning" disappeared upon replacement of PbO by $Bi_2O_3$, the pressure exponents were found to be still acceptable. It was also the case for CNTs-based catalysts where abovementioned oxides were used. There might be another reason for the enhancement of the combustion of nitrocellulose (NC) by GO. In fact, it was found that the burn rate of NC could be significantly increased with the increase of GO content in GO/NC films[141]. The flame structure as well as the burn rate curves is presented in Figure 39.

It is shown in Figure 39 that CNTs, as a carrier, can prevent aggregation of $Bi_2O_3$ or CuO nanoparticles and improve the catalytic efficiency, resulting in much higher burning rate and lower pressure exponent[298,299]. Later on, Liu *et. al.* found that carbon coated Cu-Bi/CNTs powders could function as effective catalysts of DB propellants[300], plateau combustion was obtained within a pressure of 10-22 MPa, with exponent of 0.173, which is very promising for solid rocket motors. In fact, the nano-Cu/CNTs and nano-Ni/CNTs composite catalysts have similar catalytic effect on AP/HTPB propellants[301,302]. It has been stated that when 3 wt.% of such catalysts, including nano CNTs, $Fe_2O_3$/CNTs and Fe·Cu/CNTs, are used, the burn rate of ADN at 4 MPa may increase from 30.49 to 50.59, 39.72 and 38.79 mm $s^{-1}$ and the corresponding pressure exponents decrease from 0.81 to 0.36, 0.67 and 0.75, respectively[258]. In general, use of modified CNMs can improve the combustion properties of propellants[303]. Such modified nanomaterials that include metal oxides, nanometer rare earth materials and nanometer-size oxidizers can increase the burn rates of solid propellants. In addition to increase of the burn rate, aforementioned CNMs and their derivatives could also improve the energy release rate. For instance, the MWCNTs can be used in composition with porous silicon (pSi), impregnated with sodium perchlorate, and it makes pSi explode easily[304].

Except for propellants and explosives, CNMs could be used in nanothermites. Nanothermite formulations that use Al or Mg, as reducing agents and $Fe_2O_3$, $MoO_3$, $WO_3$ *etc.*, as oxidizers, have various applications due to their high energy density and large energy release rate, in comparison to conventional thermites. The addition of boron and CNTs to these nanothermites results in doubling of a gas peak pressure[305], indicating that the boron-CNTs mixtures could be useful for new generation of propellants, explosives and pyrotechnic systems. Recenly, the MWCNTs were coupled with iron oxide nanoparticles, to form new pyrophoric compositions prepared on a basis of water-dispersed CNTs[306].

As mentioned earlier, an addition of CNTs to Zr/$KClO_4$ has a significant impact on light radiation energy of this material. With increase of the CNTs content, the combustion rate and exothermic output of these pyrotechnic mixtures were increased correspondingly[206]. The flash-ignitable nEMs for underwater explosions or for other purposes could be achieved by addition of SUCNTs[282] to Al/CuO nanoparticles or by addition of SWCNTs to pentaerythritol tetranitrate (PETN)[307], as an optical sensitizer. The CNMs absorb the irradiated energy and rapidly convert it into the thermal energy, greatly improving the ignition and burning properties of the pure parent explosive. The same phenomenon was observed for the case of Zr/oxidant/CNTs composites[308]. Except for the CNTs, the functionalized graphene sheet (FGS) is also a promising additive capable of enhancing fuel/propellant combustion. A series of molecular dynamic simulations based on a reactive force field (ReaxFF) show that catalytic activity of FGS in combustion of nitromethane is significant[309]. The derivatives of fullerence have even better catalytic effect than $C_{60}$ and CB on combustion of DB propellants containing RDX. As aforementioned fact, mNPF is a typical example for demonstration of this effect. The burn rates of RDX-CMDB propellants could be greatly improved by addition of mNPF, which grow with the increase of mNPF content. The maximum burning rate can reach up to 19.6 mm $s^{-1}$, when 1.0 wt.% mNPF is used, while the corresponding "plateau combustion" region is in the range between 8 to 22 MPa[310]. The unique structure of CNMs and their energetic derivatives can modify combustion characteristics of propellants, especially when new functional groups or energetic moieties are introduced to their strutures. On one hand, such catalytic effect could be due to special carbon structure allowing facile electron and heat transfer, promoting chemical reactions. On the other hand, the metal oxides catalysts could be dispersed in the inner layer or porous structure of the CNMs. Such dispersion can prevent an agglomeration of nanoparticles, resulting in more uniform catalytically active sites and thus better combustion properties. Moreover, the catalytic efficiency could be further improved by synergistic effects between the CNMs and the carried catalysts.

## Stabilization and Desensitization of EMs by CNMs

***Improvement of Thermal Stability of EMs*:** During development of new EMs, many compounds with high energy content were found to be not sufficiently thermally stable. The stabilization of these EMs is essential for their practical applications. The stabilization of such EMs includes improvement of their molecular stability and crystaline phase stability. There are several strategies for improvement of the thermal stability[311], including (i) recrystallization, in order to exclude the defects, (ii) cocrystalization of unstable compounds with stable ones, (iii) coating of sensitive

crystals with inert materials, and (iv) chemical functionalization of crystal surface with thermally stable groups or compounds. For instance, AN undergoes a polymorphic phase transition near the ambient temperature, affecting the usability of this oxidizer. However, the 1:1 energetic co-crystals of AN with benzo-18-crown-6 (AN-B18C6) wouldn't have this problem[312]. Alternatively, in order to achieve both phase and thermal stabilization of AN, a new material polyvinylpyrrolidone (PVP)-AN glass has been developed, where PVP can separate AN into its ions through an ion-dipole interaction[313].

It has been repoted that ADN could be also stabilized by its coating with some other inert materials[314]. Recently, theoretical investigation showed that the stability of EMs could also be improved by encapsulating them inside CNTs or between graphene layers[315]. Preparations of variety of energetic compounds have been attempted, including FOX-7, RDX, HMX, 3,6-di(hydrazino)-1,2,4,5-tetrazine (DHT), 3,6-diazido-1,2,4,5-tetrazine (DiAT), DAAT, as well as five different N-oxides of DAAT ($DAATO_n$, with n = 1-5). It was found that all of these EMs could be stabilized by 32-53 kcal $mol^{-1}$ by using CNTs with appropriate diameters. Moreover, FOX-7, RDX, and HMX could be confined between graphene layers as well, resulting in stabilization of 28-40 kcal $mol^{-1}$. The stabilization is resulted from the dispersing interactions between the molecules and carbon nanostructures, as well as coulombic interactions, due to charge dissipation, and intermolecular H-bonding.

In addition to stabilization of normal sensitive energetic compounds, it is also possible to stabilize unstable high-nitrogen compounds by using CNTs. Finite temperature simulations demonstrated the stabilization of a polymeric nitrogen ($N_8$) at ambient pressure and room temperature, by confinement inside CNT. If proven experimentally viable, it may open a new path towards stabilization of polynitrogen or polymeric nitrogen compounds under ambient conditions[316,317]. An energy barrier of 1.07 eV was found for the formation of $N_8$/CNT (5,5) from $N_2$/CNT (5,5), while it was 0.2 eV for the dissociation barrier. The reaction pathway snapshots have shown that the transition state is composed of $N_2$ and $N_6$ inside a CNT(5,5)[317].

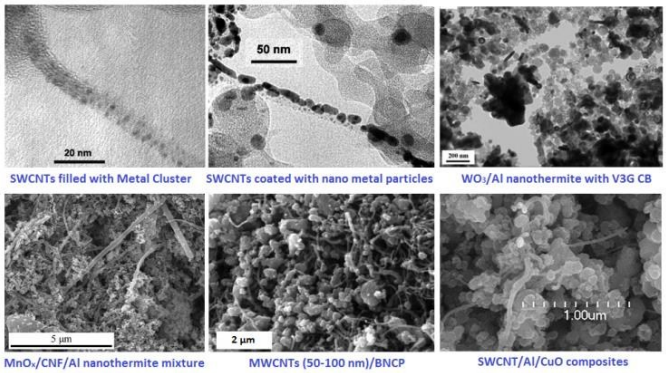


Figure 40, a comparison of SEM morphologies of several MWCNTs and CB based thermites. This combined figure is reproduced from several figures appearing in references 58, 60, 284 and 334 with permission.

Moreover, the simulation of NM with SWCNTs shows that the size-dependent ordered structures of NM with preferred orientations are formed inside the tubular cavities driven by the van der Waals attractions of NM and SWCNT, and together with the dipole-dipole interactions of NM, resulting in a higher local mass density than that of bulk NM[318]. On the basis of these calculations, the stabilization of nitrogen clusters has been proposed. It was demonstrated that the nitrogen clusters could be stabilized by CNTs under various conditions. A linear chain nitrogen cluster could be formed under the plasma conditions and it would be most likely stabilized inside the walls of the CNTs that were used as substrates for synthesis[319]. Later on, a $N_8$ was stabilized on the positively charged sidewalls of MWNTs that were synthesized by cyclic voltammetry (CV) under ambient conditions. It was shown from temperature programmed desorption (TPD) data that MWNT/$N_8$ is thermally stable up to 400 °C[320]. Furthermore, experimental study regarding interaction and energy transport of Al/Teflon nanocomposites with nano-carbon, graphene flakes and CNTs[278], showed that the graphene has the greatest influence on the thermal conductivity (increased by 98%), thermal diffusivity and specific heat of the Al/Teflon matrix.

***Decrease the Sensitivity of EMs*:** Sensitivity refers to explosive phenomena caused by external stimuli that are ordinarily insufficient to produce a detonation, where such stimuli include impact, friction, shock, electrostatic charges and heat. Both experimental and empirical methods were established to determine or predict the sensitivity of EMs[321]. In past decades, great efforts were made to improve the survivability and safety of munitions, during which many new insensitive energetic compounds, as well as mitigatigation techniques, were developed[322-325]. As suggested by many researchers, the important factors determining the sensitivity of EMs, the sub-threshold ignition of EMs involves the generation of hot spots[326]. In fact, various mechanisms have been proposed for the formation of such hot spots, including adiabatic compression of trapped gases in voids, friction involving sliding or impacting surfaces, shear band formation due to mechanical failure, sparks, triboluminescence, and heating at crack tips. In addition of "hot spot" theory, over the years, various methods based on bond dissociation energy, electronic structure properties and energetic transfer rate have been proposed in order to evaluate and interpret the sensitivity of energetic compounds. One may decrease the sensitivity of compound by eliminating or preventing of the hot-spot formation during unwanted stimuli. There are many CNMs and their derivatives capable of decreasing the sensitivity of EMs by suppressing of hotspot formation. It was found that the three types of $C_{60}$ derivatives exhibit different thermal stabilities, while the friction and impact sensitivities of HMX can be reduced from 100% to 70% and even to 60%, respectively, when 1% of $C_{60}$ was added to HMX (Table 8)[327]. For primary explosive BNCP, its mechanical sensitivity could be brought down by addition of CNMs as well, and the impact sensitivity decreases in the following order: BNCP>BNCP/CNTs>BNCP/CB. However, MWCNT-2 with smaller diameter (10-20 nm, Figure 40) would decrease its friction sensitivity[52]. The CNMs are good coating materials for Mg and Al particles. In particular, SWCNTs are the most attractive CNM for coating of small metal nanoparticles and clusters, forming



 

metalized SWCNTs. In this way, the sensitivity of the energetic compositions based on these metals will be decreased[328]. However, when RDX and PETN are doped with CB or CNTs, their laser initiation sensitivity is lowered due to increase in their light absorbance[329]. Although CB could increase the photo-sensitivity of RDX and PETN, it would decrease the mechanical sensitivity of thermites. As mentioned earlier, the mechanical sensitivity of a $WO_3$/Al nanothermite (Figure 40) could be improved by using pristine or chemically modified V3G CB, as an additive[54]. All of the prepared energetic composites were found to be insensitive to impact (with threshold > 50 J, Table 8).

Table 8, the mitigation effect of CNMs on sensitivity of various EMs

| Materials | IS / $H_{50}$ | FS / % | ESD | Ref. |
|---|---|---|---|---|
| BNCP | 10.6 cm | 24 (swing 70°) | Positive-0.99/negative-1.18 | |
| BNCP/MWCNTs-1 | 17.5 cm | 36 | No fire | |
| BNCP/MWCNTs-2 | 24.7 cm | 4 | No fire | [52] |
| BNCP/SWCNTs | 23.1 cm | 54 | No fire | |
| BNCP/CB | 27.1 cm | 90 | Positive-0.49/negative-0.47 | |
| HMX | 100% | 100% | | |
| HMX/1%_$C_{60}$-1 | 100% | 100% | Note: friction: recorded at 90°, 3.92 MPa; | |
| HMX/1%_$C_{60}$-2 | 100% | 90% | impact: 10 kg hammer, 25 cm, 50 mg; Probability out of 30 times; | [327] |
| HMX/1%_$C_{60}$-3 | 60% | 70% | | |
| $WO_3$/Al | > 50 J | 144 N | < 0.14 mJ | |
| $WO_3$/Al/V3G | > 50 J | 252 N | < 0.14 mJ | |
| $WO_3$/Al/TO | > 50 J | 64 N | < 0.14 mJ | [54] |
| $WO_3$/Al/RM | > 50 J | > 360 N | 0.14 mJ | |
| $WO_3$/Al/AM | > 50 J | > 360 N | < 0.14 mJ | |
| $MnO_2$/Al | 31.9 J | > 5 N | 1.0 mJ | |
| $MnO_2$/Al/CNF (mix) | 29.4 | > 360 N | 1800 | [330] |
| $MnO_2$/Al/CNF | 44.2 J | > 360 N | 35 mJ / 5400 mJ (fuel rich) | |
| ε-CL-20 | 100% | 100% | | |
| ε-CL-20/glue | 30% | 36% | Note: the drop hammer is 5 kg, 20 cm height; Friction sensitivity of the samples was recorded at 66° ±1°, 2.45 MPa; Probability out of 30 times; | |
| ε-CL-20/glue/Graphene | 20% | 22% | | [265] |
| ε-CL-20/glue/GO | 25% | 30% | | |
| ε-CL-20/glue/rGO | 22% | 28% | | |
| | Laser sensitivity (Sapphire) mJ | | Laser sensitivity (K9 glass) mJ | |
| PETN | 271 | | 268 | |
| PETN/1%CB | 61.6 | | 43.3 | [329] |
| PETN/1%CNTs | 187.9 | | 266.6 | |

Notes: IS, impact sensitivity; FS, friction sensitivity; $F_s$, Flame sensitivity; $C_{60}$-1, commercially available; $C_{60}$-2, crystallized from pellucid purple carbon disulfide solution; $C_{60}$-3 brown sheet fullerene obtained from pellucid purple carbon disulfide/petroleum ether solution (80 °C, 10 hrs); a) V3G, nanometer-sized graphitized carbon black; RM and AM, carbon milling under air and argon atmospheres; TO, Thermally oxidized carbon nanoparticles.

Unfortunately, the influence of the CNM additives on the electrostatic discharge sensitivity was very limited, due to the low amount of additive used in the preparation of these nanothermites (<5 wt%). It indicates that the ESD desensitization is more related to the percolation effects than to the intrinsic conductivity of the CB. In addition to CB, a "herringbone" carbon nanofiber (CNFs) is another suitable desensitizer for nanothermites (e.g., $MnO_2$/Al) for safer handling[330]. It has been shown that a dramatic decrease in the friction sensitivity (> 360 N), as compared to pure $MnO_2$/Al nanothermite (> 5 N), was found and the ESD sensitivity was also considerably reduced (from 1.0 to 5,300 mJ). Even though, some energetic compounds such as 3-nitro-1,2,4-triazol-5-one (NTO) are quite insensitive, it is still useful to add a certain amount of CNMs (e.g. 1 wt.% of graphene) to increase the processing capability of NTO as an ingredient of PBXs[331]. It also turned out that the mechanical sensitivities of ε-CL-20/glue can be reduced with the incorporation of graphite, GO, and rGO in PBX formulations[265]. Later report shows that GO sheets exhibited better desensitizing effect than $C_{60}$ and CNTs[166]. When 2 wt.% GO sheets are added, the impact sensitivity of as-prepared HMX decreases from 100% to 10%, and the friction sensitivity reduces from 100% to 32%.

## Conclusions and Future directions

As summarized in this review, extensive investigations were and are conducted regarding the design, synthesis, characterization and application of various CNMs or functionalized CNMs in EMs. The widely used CNMs include graphene, GO, rGO, CNTs, activated carbon fiber, EG, as well as functionalized graphene, GO and $C_{60}$-fullerene. Until now, it was shown that EG has been only used in chemical heat pumps, and it may have additional use in the field of EMs e.g., as additive in nanothermites and as a promising flame retardant additive in cladding materials of solid propellant charges. In contrast to EG, $C_{60}$-fullerene could be functionalized with energetic groups, forming a new family of energetic compounds with excellent thermal stability. However, the variety of energetic moieties used for $C_{60}$-fullerene functionalization is still limited and more exploration is required in this field. $C_{60}$-fullerene derivatives could be either used as combustion catalysts, energetic binders, or as additives, depending on the type of functional groups. Their compatibility with other components of explosives and propellants, as well as their sensitivity also needs to be systematically investigated for these nanomaterials practical applications. Graphene and its aerogels could be usually combined with either catalysts or oxidizers using sol-gel method. These novel composite materials are likely to be used as advanced oxidizers and combustion catalysts. Among all the CNMs, only GO and rGO were found to be energetic by themselves. They could be used as matrix to bindmany other energetic compounds including HMX, NC and FOX-7. The common energetic materials could either deposited on a surface of GO or their crystals/particles could be coated with thin layers of GO (rGO). It should be mentioned that development of practically all composite materials based on GO or rGO was reported during the last 3 years. Many other new energetic compounds could be deposited on GO or rGO in order to enhance their performance, as potential combustion catalysts of solid propellants or as additives to propellants and explosives. Similarly to $C_{60}$-fullerene, many functionalized CNTs were developed as combustion catalysts or energetic additives to propellants. Likewise, some of these nanomaterials were also used in new formulations of thermites and ignitors. The preparation procedures of CNM-containing EMs are well developed and include broad variety of synthetic techniques such as microemulsion, hydrothermal, reductive deposition, ultrasonic compositing, CVD, as well as chemical reaction methods. Combination of CNTs with highly sensitive EMs could provide a way for improvement of these EMs sensitivity and performances. However, the encapsulation of sensitive or unstable energetic molecules into CNTs is still extremely challenging and will require much more theoretical and experimental work. The desensitization mechanism of CNMs on EMs is still not very clear, and more theoretical work is needs to address this issue. Although the use of DnDs has become more and more popular in various areas, its application in EMs is just in the infant stage. DnDs could be functionalized with energetic or other function groups, where one of the most challenging issues will be their surface structure characterization.

In summary, it is very clear from the presented above information that use of various CNMs in energetic applications is extremely promising and rewarding, capable of addressing numerous problems in this field and having tremendous growth opportunity in the near future.

## Acknowledgements

The financial support from the Planning and Budgeting Committee (PBC) of the Council for Higher Education in Israeli government is greatly appreciated. This work was also partically supported by the Center for Nanoscience and Nanotechnology and by the Faculty of Exact Sciences in Tel Aviv University.

## References

1. Agrawal, J.P. High Energy Materials Propellants, Explosives and Pyrotechnics. Wiley-VCH., **2010**, ISBN 978-3-527-32610-5, p. 69.
2. David C. S. The Mother of Gunpowder, Oxford University Press, **2013**.
3. Sikder, A.K.; Sikder, N. A review of advanced high performance, insensitive and thermally stable energetic materials emerging for military and space applications, *J Hazard Mater*, **2004**, *112*, 1–15.
4. Klapotke, T.M. High Energy Density Materials ed. Klapotke, T.M., Springer, Heidelberg, **2007**, 85–121.
5. Ying, J.; Guo-gen, X.; Xuan-jun, W. Application of lightweight carbon materials, **2013**, National Defense Industry Press, Beijing.
6. Lulu M.; Amelia H. C.; Hart, S. O.; Robert, V.; Pulickel M.A. Spiers memorial lecture advances of carbon nanomaterials, *Faraday Discuss*., **2014**, *173*, 9.
7. Zhai, Y., Zhu, Z., Dong, S. Carbon-based nanostructures for advanced catalysis, *ChemCatChem*, **2015**, 7 (18), 2806-2815.
8. Comet, M.; Pichot, V.; Siegert, B.; Spitzer, D. Use of nanodiamonds as a reducing agent in a chlorate-based energetic composition, *Propellants Explos. Pyrotech.,* **2009**, *34*, 166-173.
9. P. Jiang-feng, Feng-Qi, Z.; S. Xiu-duo, Z. Wei, Progress of the application of lightweight carbon materials and their composites in solid rocket propellants, *Chin. J. Explos. Propellants*, **2014**, *2*, 1-6.
10. Delhaes, P. Carbon-based Solids and Materials Carbon-based Solids and Materials, ISBN 9781118557617, **2013**, 1-640.
11. Han, W.; Feng-qi, Z.; Shang-wen, L. Function of carbon materials used in solid propellants and their action mechanism. *Chin J. Explos. Propellants*, **2005**, *29*, 32-35.
12. Ying-lei, W.; Feng-Qi, Z.; Jian-hua, Y. New progress of study combustion catalysts used for solid rocket propellants. *Chin. J. Explos Propellants*, **2012**, *35*, 1-8.
13. Heijden, V. D.; Bouma, R. H. B.; Van Der Steen, A. C.; Fischer, H. R. Application and characterization of nanomaterials in energetic compositions, Materials Research Society Symposium - Proceedings, **2003**, *800*, 191-208.
14. Synthesis, characterization and properties of energetic/reactive nanomaterials, Materials Research Society Symposium - Proceedings, **2003**, *800*, 392p.
15. Pokropivny, V.V.; Ivanovskii, A.L. New nanoforms of carbon and boron nitride, Russian Chem. Rev, **2008**, *77*, 837-873.
16. Han, X.; Li, S. Advances in catalytic function of fullerene materials, *Prog. Chem.*, **2006**, *18*, 715-720.
17. Lan, Y.-F.; Li, X.-Y.; Luo, Y.-J. Research progress on application of graphene in energetic materials, *Chin. J. Explos. Propellants*, **2015**, *38*,1-7.
18. Law, C.K. Fuel options for next-generation chemical propulsion, *AIAA J*, **2012**, *50*, 19-36.
19. Ren, C.; Wang, X.-J.; Li, Y.-X.; Wang, J.-L.; Cao, D.-L. Research and application of graphene composites, *Mod. Chem. Industry*, **2015**, *35*, 32-35.



 

20. Ajayan, P.M.; Ebbesen, T.W. Nanometre-size tubes of carbon, *Reports Prog Phys*, **1997**, *60*, 1025-1062.
21. Eklund, P.C.; Rao, A.M.; Zhou, P.; Wang, Y.; Holden, J.M. Photochemical transformation of $C_{60}$ and $C_{70}$ films, *Thin Solid Films*, **1995**, *257*, 2, 185-203.
22. De Volder, M. F. L.; Tawfick, S. H.; Baughman, R. H.; Hart, A. J. Carbon Nanotubes Present and Future Commercial Applications. *Science*, **2013**, *339*, 535–539.
23. Zhang, M.; Fang, S.; Zakhidov, A. A.; Lee, S. B.; Aliev, A. E.; Williams, C. D.; Atkinson, K. R.; Baughman, R. H. Strong, Transparent, Multifunctional, Carbon Nanotube Sheets. *Science*, **2005**, *309*, 1215–1219.
24. Wu, S.; Ge, R.; Lu, M.; Xu, R.; Zhang, Z. Graphene-based nano-materials for lithium-sulfur battery and sodium-ion battery, *Nano Energy*, **2015**,15, 379-405.
25. Geng, D.; Wang, H.; Yu, G. Graphene single crystals Size and morphology engineering, *Adv. Mater.*, **2015**, *27*, 2821-2837.
26. Tománek, D. Interfacing graphene and related, 2D materials with the 3D world, *J. Phys. Condensed Matter.*, **2015**, *27*, 133203.
27. Ge, S.; Lan, F.; Yu, F.; Yu, J. Applications of graphene and related nanomaterials in analytical chemistry, *New J. Chem.,* **2015**, *39*, 2380-2395.
28. Li, Y.; Dong, H.; Li, Y.; Shi, D. Graphene-based nanovehicles for photodynamic medical therapy, Inter J Nanomedicine, **2015**, *10*, 2451-2459.
29. Ding, W.-B.; Wang, L.; Yang, Q.; Xiang, W.-D.; Gao, J.-M.; Amer, W.A. Recent research progress on polymer grafted carbon black and its novel applications, *Inter. Polym. Process.*, **2013**, *28*, 132-142.
30. Novakov, T.; Rosen, H. The black carbon story Early history and new perspectives, *Ambio*, **2013**, *42*, 840-851.
31. Li, X.; Li, Z.; Xia, Y. Test and calculation of the carbon black reinforcement effect on the hyper-elastic properties of tire rubbers, *Rubb. Chem. Tech.*, **2015**, *88*, 98-116.
32. Jacobsson, M.; Wang, F.; Cameron, P.; Neilsen, J.; Nikiel, L.; Wampler, W. Improvements in carcass carbon blacks to enhance compound performance, *Rub. World*, **2015**, *251*, 30-34.
33. Shopin, V.M. Separation of the desired product from aerosol flows in the manufacture of carbon black a review, **2014**, Solid Fuel Chemistry, 48 3, 180-197.
34. Lili Wang, Xiaofeng Wang, Bo Zou, Xiaoyu Ma, Yuning Qu, Chunguang Rong, Ying Li, Ying Su, Zichen Wang, Preparation of carbon black from rice husk by hydrolysis, carbonization and pyrolysis, *Bioresource Tech.*, **2011**, *102*, 8220–8224.
35. Kuo-Huai Kuo, Yu-Hsiang Peng, Wen-Yen Chiu, Trong-Ming Don, A novel dispersant for preparation of high loading and photosensitive CB dispersion, *Inc. J Polym Sci Part A: Polym. Chem*., **2008**, *46*, 6185–6197.
36. Karbiwnyk, C.M.; Miller, K.E. A review of current analytical applications employing graphitized carbon black, *Carbon Black Product., Proper. Uses*, **2011**, 69-92.
37. Li, L.; Li, W.; Qin, D.; Jiang, S.; Liu, F. Application of graphitized carbon black to the quechers method for pesticide multiresidue analysis in Spinach, *J Aoac Int*, **2009**, *92*, 538-547.
38. Horikawa, T.; Zeng, Y.; Do, D.D.; Sotow, K.-I.; Alcántara Avila, J.R. On the isosteric heat of adsorption of non-polar and polar fluids on highly graphitized carbon black, **2015**, *J. Coll. Interf. Sci.*, *439*, 1-6.
39. Yang, X.-Q.; Wang, B.; Liu, S.-E.; Guo, X.-J. Effect of carbon black on burning properties of modified nitramine double base propellant, *Energet. Mater.*, **2004**, *12*, 408.
40. Papirer, E.; Brendle, E.; Ozil, F.; Balard, H. Comparison of the surface properties of graphite, CB and fullerene samples, measured by inverse gas chromatography, *Carbon*, **1999**, *37*, 1265-1274.
41. Kruk, M.; Li, Z.; Jaroniec, M.; Betz, W.R. Nitrogen Adsorption Study of Surface Properties of Graphitized Carbon Blacks, *Langmuir*, **1999**, *15*, 1435-1441.
42. Rwei, S.-P.; Ku, F.-H.; Cheng, K.-C. Dispersion of CB in a continuous phase Electrical, rheological, and morphological studies, *Colloid. Polym. Sci.*, **2002**, *280*, 1110-1115.
43. Shih, Y.-F.; Jeng, R.-J. Carbon black containing interpenetrating polymer networks based on unsaturated polyester/epoxy. I. Dynamic mechanical properties, thermal analysis, and morphology, *J. Appl. Polym. Sci.*, **2002**, *86*, 1904-1910.
44. Wu, G.; Asai, S.; Sumita, M.; Yui, H. Entropy penalty-induced self-assembly in carbon black or carbon fiber filled polymer blends, *Macromolecules*, **2002**, *35*, 945-951.
45. Kowalczyk, P.; Kaneko, K.; Terzyk, A.P.; Tanaka, H.; Kanoh, H.; Gauden, P.A. The evaluation of the surface heterogeneity of carbon blacks from the lattice density functional theory, *Carbon*, **2004**, *42*, 1813-1823.
46. Schröder, A.; Klüppel, M.; Schuster, R.H. Characterisation of surface activity of carbon black and its relation to polymer-filler interaction, *Macromole. Mate. Eng.*, **2007**, *292*, 885-916.
47. Mathew, T.; Datta, R.N.; Dierkes, W.K.; Noordermeer, J.W.M.; Van Ooij, W.J. A comparative investigation of surface modification of CB and silica by plasma polymerization, *Rub. Chem. Tech.*, **2008**, *81*, 209-226.
48. Mathew, T.; Datta, R.N.; Dierkes, W.K.; van Ooij, W.J.; Noordermeer, J.W.M.; Gruenberger, T.M.; Probst, N. Importance of fullerenic active sites in surface modification of carbon black by plasma polymerization, **2009**, *Carbon*, *47*, 1231-1238.
49. Yan, Q.-L.; Zeman, S.; Elbeih, A. Recent advances in thermal analysis and stability evaluation of insensitive plastic bonded explosives PBXs, Thermochim. Acta, **2012**, *537*, 1-12.
50. Duan, Y.-L.; Tong, Y.; Cao, Y.; Huang, F.-L. Phase transition of carbon black shocked by explosion, *Acta Armamentarii*, **2013**, *34*, 169-174.
51. Zhazaeva, E.M.; Pshikhachev, A.G.; Gubzhev, T.A.; Kashirgov, A.A.; Gekkieva, Z.M.; Tkhakakhov, R.B. Surface energetic and strength characteristics of heat treated composites based on butadiene-acrylonitrile elastomer modified with CB, *Inter. Polym.Sci. Tech.*, **2013**, *40*, T33-T37.
52. Chen, L.-K.; Sheng, D.-L.; Yang, B.; Zhu, Y.-H.; Xu, M.-H.; Pu, Y.-L.; Li, Z.-X. Effects of carbon nanotubes and carbon black on sensitivity performances of BNCP, *Chin. J. Energet. Mater.*, **2013**, *21*, 35-38.
53. Yang, B.; Sheng, D.-L.; Chen, L.-K.; Xu, H.-S.; Men, Y.-Y.; Zhu, Y.-H. Performance of carbon black/potassium nitrate propellant for blasting valve, *Chin. J. Energet. Mater.*, **2014**, *22*, 397-400.
54. Arnaud Bach, Pierre Gibot, Loïc Vidal, Roger Gadiou, Denis Spitzer, Modulation of the Reactivity of a $WO_3$/Al Energetic Material with Graphitized CB as Additive, J Energet Mater, **2015**, *33*, 260-276.
55. Shenderova, O.; Panich, A.M.; Moseenkov, S.; Hens, S.C.; Kuznetsov, V.; Vieth, H.-M. Hydroxylated detonation nanodiamond FTIR, XPS, and NMR studies, *J. Phys. Chem. C*, **2011**, *115*, 19005-19011.
56. Amaratunga, G.; Putnis, A.; Clay, K.; Milne, W. Crystalline diamond growth in thin films deposited from a $CH_4$/Arrf plasma, *Appl. Phys. Lett.*, **1989**, *55*, 634-635.
57. Wen, B.; Zhao, J.J.; Li, T.J. Synthesis and crystal structure of n-diamond, *Inter. Mater. Rev.*, **2007**, *52*, 131-151.
58. Krishnan, A.; Dujardin, E.; Treacy, M.M.J.; Hugdahl, J.; Lynum, S.; Ebbesen, T.W. Graphitic cones and the nucleation of curved carbon surfaces, *Nature*, **1997**, *388*, 451-454.
59. Lijima, S.; Ajayan, P.M.; Ichihashi, T. Growth model for carbon nanotubes, *Phys. Rev. Lett*., **1992**, *69*, 3100-3103.
60. Kroto, H.W.; Heath, J.R.; O'Brien, S.C.; Curl, R.F.; Smalley, R.E. $C_{60}$ buckminsterfullerene, *Nature*, **1985**,*318*, 162-163.
61. Howard, J.B.; McKinnon, J.T.; Makarovsky, Y.; Lafleur, A.L.; Johnson, M.E. Fullerenes $C_{60}$ and $C_{70}$ in flames, *Nature*, **1991**, *352*, 139-141.
62. Yin, M.T.; Cohen, M.L. Will diamond transform under megabar pressures? *Phys. Rev. Lett*., **1983**, 50, 2006-2009.
63. Frenklach, M.; Kematick, R.; Huang, D.; Howard, W.; Spear, K.E.; Phelps, A.W.; Koba, R. Homogeneous nucleation of diamond powder in the gas phase, *J. Appl. Phys*., **1989**, *66*, 395-399.
64. Papirer, E.; Brendle, E.; Ozil, F.; Balard, H. Comparison of the surface properties of graphite, CB and fullerene samples, measured by inverse gas chromatography, *Carbon*, **1999**, *37*, 1265-1274.
65. Hirai, H.; Kondo, K.-I. Modified phases of diamond formed under shock compression and rapid quenching, *Science*, **1991**, *253*, 772-774.
66. Howard, J.B.; Chowdhury, K.D.; Vander Sande, J.B. Carbon shells in flames, *Nature*, **1994**,*370,* 603.
67. Cataldo, F. The impact of a fullerene-like concept in carbon black science, *Carbon*, **2002**, *40*, 157-162.
68. Mailhiot, C.; McMahan, A.K. Atmospheric-pressure stability of energetic phases of carbon, *Phys. Rev. B*, **1991**, 44, 11578-11591.

69. Yoo, C.S.; Nellis, W.J.; Sattler, M.L.; Musket, R.G. Diamond like metastable carbon phases from shock-compressed $C_{60}$ films *Appl. Phys. Lett*., **1992**, *61*, 273-275.
70. Peng, J.L.; Bursill, L.A.; Jiang, B.; Orwa, J.O.; Prawer, S. Growth of c-diamond, n-diamond and i-carbon nanophases in carbon-ion-implanted fused quartz, Philosophical Magazine B Physics of Condensed Matter; Statistical Mechanics, Electronic, *Opt. Magnet. Proper*., **2001**, *81*, 2071-2087.
71. Wen, B.; Li, T.; Dong, C.; Zhang, X.; Yao, S.; Cao, Z.; Wang, D.; Ji, S.; Jin, J. Preparation of diamond nanocrystals from catalysed carbon black in a high magnetic field, J. Phys. Condes. Matt., **2003**, *15*, 8049-8054.
72. Bin Wen, Jijun Zhao, Tingju Li, Chuang Dong, Junze Jin, n-diamond from catalysed carbon nanotubes synthesis and crystal structure, *J. Phys. Condes. Matter,* **2005**, *17*, L513–L519.
73. Mironov, E.; Petrov, E.; Koretz, A. Chemical aspect of ultradispersed diamond formation, *Diam. Relat. Mater.*, **2003**, *12*, 1472-1476.
74. Sakovich, G.V.; Zharkov, A.S.; Petrov, E.A. Results of research into the physicochemical processes of detonation synthesis and nanodiamond applications, *Nanotech. Rus.*, **2013**, *8*, 581-591.
75. Gromov, A.A.; Vorozhtsov, S.A.; Komarov, V.F.; Sakovich, G.V.; Pautova, Y.I.; Offermann, M. Ageing of nanodiamond powder Physical characterization of the material, *Mater. Lett.*, **2013**, *91*, 198-201.
76. Dolmatov, V.Yu.; Myllymäki, V.; Vehanen, A. A possible mechanism of nanodiamond formation during detonation synthesis, J. *Sup. hard Mater.*, **2013**, *35*, 143-150.
77. R. K. Barton, A. J. Barratt, Observations on the Reactivity of Pyrotechnic Compositions Containing Potassium Chlorate and Thiourea, *Propellants, Explos. Pyrotech.,* **1993**, *18*, 77.
78. M. Comet, L. Schreyeck, H. Fuzellier, An efficient composition for bengal lights, *J. Chem. Edu.,* **2002**, 79, 70.
79. Comet, M.; Pichot, V.; Siegert, B.; Spitzer, D.; Moeglin, J.-P.; Boehrer, Y. Use of nanodiamonds as a reducing agent in a chlorate-based energetic composition, *Propellants, Explos. Pyrotech*., **2009**, *34*, 166-173.
80. Comet, M.; Pichot, V.; Schnell, F.; Spitzer, D. Oxidation of detonation n-D in a reactive formulation, *Diam. Relat. Mater.*, **2014**, *47*, 35-39.
81. Tong, Y.; Liu, R.; Zhang, T. The effect of a detonation nanodiamond coating on the thermal decomposition properties of RDX explosives, *Phys. Chem. Chem. Phys.*, **2014**, *16*, 17648-17657.
82. Shen, M.-Y.; Li, K.-Y.; Kuan, C.-F.; Kuan, H.-C.; Chen, C.-H.; Yip, M.-C.; Chou, H.-W.; Chiang, C.-L. Preparation of expandable graphite via ozone-hydrothermal process and flame-retardant properties of high-density polyethylene composites, *High Perform. Polym.,* **2014**, *26*, 34-42.
83. Pang, X.-Y.; Duan, M.-W.; Tian, Y.; Zhai, M. Preparation of expandable graphite with phosphoric acid as ancillary intercalation reagent and its antiflame property for linear low density polyethylene, *Asian J. Chem.*, **2013**, *25*, 5390-5394.
84. Kuan, C.-F.; Tsai, K.-C.; Chen, C.-H.; Kuan, H.-C.; Liu, T.-Y.; Chiang, C.-L. Preparation of expandable graphite via $H_2O_2$-hydrothermal process and its effect on properties of high-density polyethylene composites, *Polym. Composit.*, **2012**, *33*, 872–880.
85. Meiling, W.; Jinjiang, Z.; Yunqiao, G.; Xiongbo, Y.; Yajun, G.; Jianwei, Z. Electrochemical Determination of Sunset Yellow Based on an Expanded Graphite Paste Electrode, **2013**, *J. Electrochem. Soc.* 160(8), H459-H462.
86. Wen, Y.; He, K.; Zhu, Y.; Han, F.; Xu, Y.; Matsuda, I.; Ishii, Y.; Cumings, J.; Wang, C. Expanded graphite as superior anode for sodium-ion batteries, Nature Comm., **2014**, *5*, 4033.
87. Ji-hui, L.; Li-li F.; Zhi-xin, J. Preparation of expanded graphite with 160 μm mesh of fine flake graphite, *Mater. Lett*., **2006**, *60*, 746–749.
88. Ba, S.; Jiang, C.; Sun, K.; Sun, Z. Prepared and infrared extinction characteristics of micron expanded graphite, *Adv. Mater. Res.*, **2011**, *308-310*,710-714.
89. Gao, L.; Gong, Y.-X.; Ma, L. Effect of expansion time on the microstructure of an expanded natural flake graphite, New Carbon Mater., **2006**, *21*, 139-143.
90. Balat, M.; Spinner, B. Optimization of a chemical heat pump Energetic density and power, *Heat Recov. Sys. CHP*, **1993**, *13*, 277-285.
91. Zamengo, M.; Ryu, J.; Kato, Y. Thermochemical performance of magnesium hydroxide-expanded graphite pellets for chemical heat pump, *Appl. Therm. Eng.*, **2014**, *64*, 339-347.
92. Wu, X.; Wang, L.; Wu, C.; Wang, G.; Jiang, P. Flammability of EVA/IFR APP/PER/ZB system, and EVA/IFR/synergist $CaCO_3$, NG, and EG, composites, *J. Appl. Polym. Sci.*, **2012**, *126*, 1917-1927.
93. Zhang, Q.; Yan, J.; Li, T.-P.; Wang, J. Preparation of magnetic expanded graphite by Sol-gel method and its electromagnetic properties, *Adv. Mater. Res.*, **2011**, 295-297, 93-97.
94. Birkett, P.R. Fullerene chemistry, *Ann. Rep. Prog. Chem. – Sect. A*, **1999**, *95*, 431-451.
95. Maurizio P. Fullerene chemistry for materials science applications, J. Mater. Chem., **1997**, 7, 1097-1109.
96. Kenichiro I. Molecular Catalysis for Fullerene Functionalization, *Chem. Rec. MBLA Spec. Is*., 2011, 11, 5, 226–235.
97. Nazario, M.; Nathalie, S.; Jean-François, N. Advances in Molecular and Supramolecular Fullerene Chemistry, *Electrochem. Soc. Interf.,* **2006**, 29-33.
98. Li, K.; Schuster, D. I.; Guldi, D. M.; Herranz, M. A.; Echegoyen, L. Convergent Synthesis and Photophysics of [60]Fullerene/Porphyrin-Based Rotaxanes, *J. Am. Chem. Soc*., **2004,** *126*, 3388.
99. Nakamura, Y.; Minami, S.; Iizuka, K.; Nishimura, J. Preparation of Neutral [60]Fullerene-Based [2]Catenanes and [2]Rotaxanes Bearing an Electron-Deficient Aromatic Diimide Moiety, *Angew. Chem. Int. Ed.*, **2003**, *42*, 3158.
100. Cardinali, F.; Mamlouk, H.; Rio, Y.; Armaroli, N.; Nierengarten, J.-F. Fullerohelicates: a new class of fullerene-containing supermolecules, *Chem. Commun*., **2004**, 1582.
101. Felder, D.; Heinrich, B.; Guillon, D.; Nicoud, J.-F.; Nierengarten, J.-F. A Liquid Crystalline Supramolecular Complex of $C_{60}$ with a Cyclotriveratrylene Derivative, *Chem. Eur. J.,* **2000**, *6*, 3501.
102. Guldi D. M.; Martin, N. Fullerene architectures made to order; biomimetic motifs — design and features, *J. Mater. Chem*., **2002**, *12*, 1978.
103. Hahn, U.; Elhabiri, M.; Trabolsi, A.; Herschbach, H.; Leize, E.; van Dorsselaer, A., et al. Supramolecular click chemistry with a bisammonium-$C_{60}$ substrate and a ditopic crown ether host, *Angew. Chem. Int. Ed.,* **2005**, *44*, 5338.
104. Delia, S.; Roberto, S. Coordination Modes and Different Hapticities for Fullerene Organometallic Complexes, *Molecules*, **2012**, *17*, 7151-7168.
105. Osuna, S.; Swart, M.; Solà, M. The reactivity of endohedral fullerenes. What can be learnt from computational studies? *Phys. Chem. Chem. Phys*., **2011**, *13*, 3585–3603.
106. Yang, S.; Liu, F.; Chen, C.; Jiao, M.; Wei, T. Fullerenes encaging metal clusters-Clusterfullerenes, *Chem. Commun*., **2011**, *47*, 11822–11839.
107. Y. Matsuo, K. Kanaizuka, K. Matsuo, Y.-W. Zhong, T. Nakae, and E. Nakamura, Photocurrent-Generating Properties of Organometallic Fullerene Molecules on an Electrode, *J. Am. Chem. Soc*., **2008**, *130*, 5016–17.
108. Wang, N.; Li, J.; Ji, G. Synthesis of trinitrophenyl $C_{60}$ derivative, *Propellants, Explos., Pyrotech.*, **1996,** *21*, 317-319.
109. Jin, B.; Peng, R.-F.; Shu, Y.-J.; Zhong, F.-C.; Chu, S.-J. Study on the synthesis of new energetic fullerene derivative, Chinese *J. High Press. Phys.*, **2006**, *20*, 220-224.
110. Jin, B.; Peng, R.-F.; Tan, B.-S.; Huang, Y.-M.; Shu, Y.-J.; Chu, S.-J.; Fu, Y.-B. Synthesis and characterization of nitro fulleropyrrolidine derivatives, *Chin. J. Energet. Mater*., **2009**, *17*, 287-292.
111. Tingting W., Heping Z. Synthesis, charge-separated state characterization of N-methyl-2-4'-N-ethylcarbozole,-3-fulleropyrrolidine and its derivatives, *Frontiers Chem. China*, **2006**, *1*, 161-169.
112. Tan, B.; Peng, R.; Li, H.; Jin, B.O.; Chu, S.; Long, X. Theoretical investigation of an energetic fullerene derivative, J Comput Chem., **2010**, *31*, 2233-2237.
113. Cataldo, F.; Ursini, O.; Angelini, G. Synthesis and explosive decomposition of polynitro[60]fullerene, *Carbon*, **2013**, *62*, 413-421.
114. Chen, B.-L.; Jin, B.; Peng, R.-F.; Zhao, F.-Q.; Yi, J.-H.; Han, W.-J.; Guan, H.-J.; Chu, S.-J. Synthesis and characterization of fullerene-ethylenediamine nitrate, *Chin. J. Energet. Mater*., **2014**, *22*, 186-191.
115. Liu, Q.-Q.; Jin, B.; Peng, R.-F.; Zhao, F.-Q.; Xu, S.-Y.; Chu, S.-J. Preparation and characterization of fullerene itaconic acid copolymer lead salt, *Chin. J. Explos. Propellants*, **2013**, *36*, 64-69.



 

116. Chen, B.-L.; Jin, B.; Peng, R.-F.; Zhao, F.-Q.; Yi, J.-H.; Guan, H.-J.; Bu, X.-B.; Chu, S.-J. Synthesis, characterization and thermal decomposition of fullerene-ethylenediamine dinitramide, *Chin. J. Energet. Mater*., **2014**, *22*, 467-472.
117. Guan, H.-J.; Peng, R.-F.; Jin, B.; Liang, H.; Zhao, F.-Q.; Bu, X.-B.; Han, W.-J.; Chu, S.-J. Preparation and thermal performance of fullerene-based lead salt, *Bull. Korean Chem. Soc.*, **2014**, *35*, 2257-2262.
118. Hu, Z.; Zhang, C. H.; Huang, Y. D.; Sun, S. F.; Guan, W. C.; Yao, Y. H. Photodynamic anticancer activities of water-soluble $C_{60}$ derivatives and their biological consequences in a HeLa cell line, *Chem-Biol. Interact*., **2012**, *195*, 86-94.
119. Guan, H.-J.; Jin, B.; Peng, R.-F.; Zhao, F.-Q.; Han, W.-J.; Chen, B.-L.; Chu, S.-J. The preparation and thermal decomposition performance of fullerene hydrazine nitrate, *Acta Armamentarii*, **2014**, *35*, 1756-1764.
120. Gong, W.; Jin, B.; Peng, R.; Deng, N.; Zheng, R.; Chu, S. Synthesis and Characterization of [60]Fullerene-Polyglycidyl nitrate, and Its Thermal Decomposition, *Indust. Eng.g Chem. Res.*, **2015**, *54*, 2613-2618.
121. Huang, T.; Jin, B.; Peng, R.F.; Chen, C.D.; Zheng, R.Z.; He, Y.; Chu, S.J. Synthesis and characterization of [60]fullerene-glycidyl azide polymer and its thermal decomposition, *Polymers*, **2015**, *7*, 896-908.
122. Novoselov, K. S.; Geim, A. K.; Morozov, S. V.; Jiang, D.; Zhang, Y.; Dubonos, S. V. et al. Electric field effect in atomically thin carbon films, *Science*, **2004**, *306*, 666-669.
123. Allen, M. J.; Tung, V. C.; Kaner, R. B. Honeycomb Carbon: A review of graphene, *Chem. Rev.,* **2010**, *110*, 132-145.
124. Tang, Q.; Zhou, Z.; Chen, Z. Graphene-related nanomaterials tuning properties by functionalization, *Nanoscale*, **2013**, *5*, 4541-4583.
125. Li, X.; Cai, W.; An, J.; Kim, S.; Nah, J.; Yang, D.; Piner, R.; Velamakanni, A.; Jung, I.; Tutuc, E.; Banerjee, S. K.; Colombo, L.; Ruoff, R. R. Large-area synthesis of high-quality and uniform graphene films on copper foils, *Science*, **2009**, *324*, 1312-1314.
126. Mattevi, C.; Kima, H.; Chhowalla, M. A review of chemical vapour deposition of graphene on copper, *J. Mater. Chem*., **2011**, *21*, 3324-34.
127. Vallés, C., Drummond, C., Saadaoui, H., Furtado, C.A., He, M., Roubeau, O., Ortolani, L., et al. Solutions of negatively charged graphene sheets and ribbons. *J Am Chem Soc*, **2008**, 130 (47), 15802-15804.
128. Morishita, T., Clancy, A.J., Shaffer, M.S.P. Optimised exfoliation conditions enhance isolation and solubility of grafted graphenes from graphite intercalation compounds, *J Mater Chem A*, **2014**, 2 (36), 15022-15028.
129. Compton, O. C.; Nguyen, S. T. Graphene Oxide, Highly reduced graphene oxide, and graphene versatile building blocks for carbon-based materials, *Small*, **2010**, *6*, 711-723.
130. Chen, D.; Feng, H.; Li, J. Graphene oxide Preparation, functionalization, and electrochemical applications, *Chem. Rev*, **2012**, *112*, 6027-6053.
131. Dreyer, D. R.; Park, S.; Bielawski, C. W.; Ruoff, R. S.; The chemistry of graphene oxide, *Chem. Soc. Rev.*, **2010**, *39*, 228-240.
132. Gilje, S.; Han, W.; Wang, M.; Wang, K. L.; Kaner, R. B. A Chemical route to graphene for device applications, *Nano Lett.,* **2007**, *7*, 3394-98.
133. Pyun, J. Graphene Oxide as Catalyst Application of Carbon Materials beyond Nanotechnology, *Angew. Chem. Int. Ed*., **2011**, *50*, 46-48.
134. Yeh, T-F.; Syu, J-M.; Cheng, C.; Chang, T-H.; Teng, H. Graphite Oxide as a Photocatalyst for Hydrogen Production from Water, Adv. *Funct. Mater*., **2010**, *20*, 2255-62.
135. Dreyer, D. R.; Jia, H-P.; Bielawski, C. W. Graphene Oxide: A Convenient Carbocatalyst for Facilitating Oxidation and Hydration Reactions, *Angew. Chem. Int. Ed*., **2010**, *49*, 6813-16.
136. Song, Y. J.; Chen, Y.; Feng, L. Y.; Ren, J. S.; Qu, X. G. Selective and quantitative cancer cell detection using target-directed functionalized graphene and its synergetic peroxidase-like activity, *Chem. Commun*., **2011**, *47*, 4436-38.
137. Guo, Y. J.; Deng, L.; Li, J.; Guo, S. J.; Wang, E. K.; Dong, S. J.; Hemin–Graphene Hybrid Nanosheets with Intrinsic Peroxidase-like Activity for Label-free Colorimetric Detection of Single-Nucleotide Polymorphism, *ACS Nano*, **2011**, *5*, 1282-90.
138. Wang, Y.; Li, Z.; Wang, J.; Li, J.; Lin, Y. Graphene and Graphene Oxide biofunctionalization and applications in biotechnology, *Trends Biotechnol*., **2011**, *29*, 205-212.
139. Sanchez, V. C.; Jachak, A.; Hurt, R. H.; Kane, A. B. Biological Interactions of Graphene-Family Nanomaterials: An Interdisciplinary Review, *Chem. Res. Toxicol*., **2012**, *25*, 15-34.
140. Kim, J.; Cote, L. J.; Franklin Kim, F.; Yuan, W.; Shull, K. R.; Huang, J. Graphene oxide sheets at interfaces, *J. Am. Chem. Soc*., **2010**, *132*, 8180-86.
141. Sha, J.; Lin-sheng X., Yu-lu M., Jing-jie H., Zhang X., Guo-xun Z., Shu-mei D.; Yan-yun W. Low-temperature expanded graphite for preparation of graphene sheets by liquid-phase method, *J. Phys. Conf. Ser.* **2009**, *188*, 012040.
142. Yongqiang, D; Congqiang, C; Xinting, Z; Lili, G; Zhiming, C; Hongbin, Y; Chunxian, G; Yuwu, C; Chang-Ming, L. One-step and high yield simultaneous preparation of single- and multi-layer graphene quantum dots from CX-72 carbon black, *J. Mater. Chem;* **2012**, *22*, 8764-8766.
143. B.C. Brodie, On the atomic weight of graphite, *Philos. Trans. R. Soc. Lond;* **1859**, *14*, 249–259
144. W.S. Hummers, R.E. Offeman, Preparation of graphitic oxide, *J. Am. Chem. Soc;* **1958**, *80*, 1339
145. D.C. Marcano, D.V. Kosynkin, J.M. Berlin, A. Sinitskii, Z. Sun, A. Slesarev, et al. Improved synthesis of graphene oxide, *ACS Nano*, **2010**, *4*, 4806–4814
146. Chen, J.; Li, Y.; Huang, L.; Li, C.; Shi, G. High-yield preparation of graphene oxide from small graphite flakes via an improved Hummers method with a simple purification process, *Carbon*, **2015**, *81*, 826-834.
147. P.S.V. Jimenez, Thermal Decomposition of Graphite Oxidation Products DSC Studies of Internal Combustion of Graphite Oxide, Mater. Res. Bull; **1987**, *22*, 601—608.
148. Wong, C.H.A.; Jankovský, O.; Sofer, Z.; Pumera, M. Vacuum-assisted microwave reduction/exfoliation of graphite oxide and the influence of precursor graphite oxide, *Carbon*, **2014**, *77*, 508-517.
149. Krishnan, D.; Kim, F.; Luo, J.; Cruz-Silva, R.; Cote, L.J.; Jang, H.D.; Huang, J. Energetic graphene oxide challenges and opportunities, *Nano Today*, **2012**, *7*, 137-152.
150. Garcia, J. C.; de Lima, D. B.; Assali, L. V. C.; Justo, J. F; Group IV graphene- and graphane-like nanosheets. *J. Phys. Chem. C*, **2011**, *115*, 13242–13246.
151. Yamada, Y.; Miyauchi, M.; Jungpil, K. et al. Exfoliated graphene ligands stabilizing copper cations, *Carbon*, **2011**, *49*, 3375–3378.
152. Yamada, Y.; Suzuki, Y.; Yasuda, H.; Uchizawa, S.; Hirose-Takai, K.; Sato, Y.; Suenaga, K.; Sato, S; Functionalized graphene sheets coordinating metal cations. *Carbon*, **2014**, *75*, 81–94.
153. Zhang, C.; Cao, X.; Xiang, B. Sandwich complex of TATB/graphene: An approach to molecular monolayers of explosives, *J. Phys. Chem. C*, **2010**, *114*, 22684-22687.
154. Li, Z.-M.; Zhou, M.-R.; Zhang, T.-L.; Zhang, J.-G.; Yang, L.; Zhou, Z.-N. The facile synthesis of graphene nanoplatelet-lead styphnate composites and their depressed electrostatic hazards, *J. Mater. Chem. A*, **2013**, *1*, 12710-12714.
155. Liu, R.; Zhao, W.; Zhang, T.; Yang, L.; Zhou, Z.; Zhang, J. Particle refinement and graphene doping effects on thermal properties of potassium picrate, Journal of Thermal Analysis and Calorimetry, **2014**, *118*, 561-569.
156. Wang, X.-B.; Li, J.-Q.; Luo, Y.-J. Preparation and thermal decomposition behaviour of ammonium perchlorate/graphene aerogel nanocomposites, *Chin. J. Explos. Propellants*, **2012**, *35*, 76-80.
157. Wang, X.-B.; Li, J.-Q.; Luo, Y.-J.; Huang, M. A Novel ammonium perchlorate/graphene aerogel nanostructured energetic composite preparation and thermal decomposition, *Sci. Adv. Mater.*, **2014**, *6*, 530-537.
158. Lan, Y.; Jin, M.; Luo, Y. Preparation and characterization of graphene aerogel/$Fe_2O_3$/ammonium perchlorate nanostructured energetic composite, *J. Sol-Gel Sci. Tech.,* **2015**, *74*, 161-167.
159. Yang S, Feng X, Mullen K, Sandwich-like, graphene-based titania nanosheets with high surface area for fast lithium storage, *Adv Mater*, **2011**, *2331*, 3575–3579
160. Lan, Y.-F.; Luo, Y.-J. Preparation and characterization of graphene aerogel/ammonium nitrate nano composite energetic materials, *Chin. J. Explos. Propellants*, **2015**, *38*, 15-18.

161. Thiruvengadathan, R.; Chung, S.W.; Basuray, S.; Balasubramanian, B.; Staley, C.S.; Gangopadhyay, K.; Gangopadhyay, S. A versatile self-assembly approach toward high performance nanoenergetic composite using functionalized graphene, **2014**, *Langmuir, 30*, 22, 6556-6564.
162. Wang, Y.; Liu, H.; Cheng, H.; Zu, M.; Wang, J. Corrosion behavior of pyrocarbon coatings exposed to $Al_2O_3$-$SiO_2$ gels containing ammonium nitrate, *Corrosion Science*, **2015**, *94*, 401-410.
163. Cai, H.; Tian, L.; Huang, B.; Yang, G.; Guan, D.; Huang, H. 1,1-Diamino-2,2-dintroethene FOX-7, nanocrystals embedded in mesoporous carbon FDU-15, *Microporous and Mesoporous Materials,* **2013**, *170*, 20-25.
164. Ferrari, A.C.; Bonaccorso, F.; Fal'ko, V.; et al.; Science and technology roadmap for graphene, related two-dimensional crystals, and hybrid systems, *Nanoscale*, **2015**, *7*, 4598-4810.
165. Zhang, X.; Hikal, W.M.; Zhang, Y.; Bhattacharia, S.K.; Li, L.; Panditrao, S.; Wang, S.; Weeks, B.L. Direct laser initiation and improved thermal stability of nitrocellulose/graphene oxide nanocomposites, *Appl. Phys. Lett*., **2013**, *102*, 141905.
166. McCrary, P.D.; Beasley, P.A.; Alaniz, S.A.; Griggs, C.S.; Frazier, R.M.; Rogers, R.D. Graphene and graphene oxide can "lubricate" ionic liquids based on specific surface interactions leading to improved low-temperature hypergolic performance, *Angrew. Chem. - Inter Ed*, **2012**, *51*, 9784-9787.
167. Zhang, Y.; Shao, Z.; Gao, K.; Wu, X.; Liu, Y. Tensile properties of nitrate glycerol ether cellulose/graphene oxide nanocomposites, *Integ. Ferroelect*., **2014**, *154*, 147-153.
168. Li, R.; Wang, J.; Shen, J.P.; Hua, C.; Yang, G.C. Preparation and characterization of insensitive HMX/graphene oxide composites, *Propellants, Explos., Pyrotech*., **2013**, *38*, 798-804.
169. Li, Y.; Alain-Rizzo, V.; Galmiche, L.; Audebert, P.; Miomandre, F.; Louarn, G.; Bozlar, M.; Pope, M.A.; Dabbs, D.M.; Aksay, I.A. Functionalization of Graphene Oxide by Tetrazine Derivatives: A Versatile Approach toward Covalent Bridges between Graphene Sheets, *Chem. Mater*., **2015**, *27*, 4298-4310.
170. Endo M. Takuya H., Yoong-Ahm K., Large-scale production of carbon nanotubes and their applications, *Pure Appl. Chem.*, **2006**, 78, 1703–1713.
171. Li, W. Z.; Xie, S. S.; Qian, L. X.; Chang, B. H.; Zou, B. S.; Zhou, W. Y. et al., Large-Scale Synthesis of Aligned Carbon Nanotubes, *Science*, **1996**, *274*, 1701–1703.
172. Ren, Z. F.; Huang, Z. P.; Xu, J. W.; Wang, J. H.; Bush, P.; Siegal, M. P.; Provencio, P. N. Synthesis of Large Arrays of Well-Aligned Carbon Nanotubes on Glass, *Science*, **1998**, *282*, 1105–1107.
173. Fan, S.; Chapline, M. G.; Franklin, N. R.; Tombler, T. W.; Cassell, A. M.; Dai, H. Self-Oriented Regular Arrays of Carbon Nanotubes and Their Field Emission Properties, *Science*, **1999**, *283*, 512–514.
174. Zheng, B.; Lu, C.; Gu, G.; Makarovski, A.; Finkelstein G.; Liu, J. Efficient CVD Growth of Single-Walled Carbon Nanotubes on Surfaces Using Carbon Monoxide Precursor, *Nano Lett*., **2002**, *2*, 895–898.
175. Hata, K.; Futaba, D. N.; Mizuno, K.; Namai, T.; Yumura M.; Iijima, S. Water-Assisted Highly Efficient Synthesis of Impurity-Free Single-Walled Carbon Nanotubes, *Science*, **2004**, *306*, 1362–1364.
176. M. Terrones, N. Grobert, J. Olivares, J. P. Zhang, H. Terrones, K. Kordatos, W. K. Hsu, J. P. Hare, P. D. Townsend, K. Prassides, A. K. Cheetham, H. W. Kroto and D. R. M. Walton, Controlled production of aligned-nanotube bundles, *Nature*, **1997**, *388*, 52–55.
177. Cao, A.; Wei, B.; Jung, Y.; Vajtai, R.; Ajayan P. M.; Ramanath, G. Growth of aligned carbon nanotubes on self-similar macroscopic templates, *Appl. Phys. Lett*., **2002**, *81*, 1297–1299.
178. Wei, B. Q.; Vajtai, R.; Jung, Y.; Ward, J.; Zhang, R.; Ramanath, G.; Ajayan, P. M. Microfabrication technology Organized assembly of carbon nanotubes, *Nature*, **2002**, *416*, 495–496.
179. Jung, Y. J.; Wei, B.; Vajtai ,R.; Ajayan, P. M.; Homma, Y.; Prabhakaran, K.; Ogino, T. Mechanism of Selective Growth of Carbon Nanotubes on $SiO_2$/Si Patterns, Nano Lett., **2003**, *3*, 561–564.
180. Cao, A.; Dickrell, P. L.; Sawyer, W. G.; Ghasemi-Nejhad, M. N.; Ajayan, P. M. Super-Compressible Foamlike Carbon Nanotube Films, Science, **2005**, *310*, 1307–1310.
181. Cao, A.; Veedu, V. P.; Li, X.; Yao, Z.; Ghasemi-Nejhad, M. N.; Ajayan, P. M. Multifunctional brushes made from carbon nanotubes, *Nat. Mater.,* **2005**, *4*, 540–545.
182. Dean, C.R.; Young, A.F.; Meric, I.; Lee, C.; Wang, L.; Sorgenfrei, S.; Watanabe, K.; Taniguchi, T.; Kim, P.; Shepard, K.L.; Hone, J. Boron nitride substrates for high-quality graphene electronics, *Nature Nanotech*., **2010**, *5*, 722-726.
183. Arnold, M.S.; Green, A.A.; Hulvat, J.F.; Stupp, S.I.; Hersam, M.C. Sorting carbon nanotubes by electronic structure using density differentiation; Nature nanotechnology, **2006**, *1*, 60-65.
184. Lin, Y.-M.; Dimitrakopoulos, C.; Jenkins, K.A.; Farmer, D.B.; Chiu, H.-Y.; Grill, A.; Avouris, Ph. 100-GHz transistors from wafer-scale epitaxial graphene, Science, **2010**, *327*, 662.
185. Novoselov, K.S.; Fal'Ko, V.I.; Colombo, L.; Gellert, P.R.; Schwab, M.G.; Kim, K. A roadmap for graphene, *Nature*, **2012**, *490*, 192-200.
186. Morozov, S.V.; Novoselov, K.S.; Katsnelson, M.I.; Schedin, F.; Elias, D.C.; Jaszczak, J.A.; Geim, A.K. Giant intrinsic carrier mobilities in graphene and its bilayer, *Phys. Rev. Lett*., **2008**, *100*, 016602.
187. Sutter, P.W.; Flege, J.-I.; Sutter, E.A. Epitaxial graphene on ruthenium, *Nature Mater*., **2008**, *7*, 406-411.
188. Utschig, T.; Schwarz, M.; Miehe, G.; Kroke, E. Synthesis of carbon nanotubes by detonation of, 2,4,6-triazido-1,3,5-triazine in the presence of transition metals, *Carbon*, **2004**, *42*, 823-828.
189. Kroke, E.; Schwarz, M.; Buschmann, V.; Miehe, G.; Fuess, H.; Riedel, R. Nanotubes formed by detonation of C/N precursors, *Adv Mater*, **1999**, *11*, 158-161.
190. Shearer, S.J.; Turrell, G.C.; Beyant, J.I.; Brooks III, R.L. Vibrational spectra of cyanuric triazide, *J. Chem. Phys*., **1968**, *48*, 1138-1144.
191. Ye, C.; Gao, H.; Boatz, J.A.; Drake, G.W.; Twamley, B.; Shreeve, J.M. Polyazidopyrimidines High-energy compounds and precursors to carbon nanotubes, *Angew. Chem. – Inter.Ed.,* **2006**, *45*, 7262-7265.
192. Koch, E.-C. Metal/fluorocarbon pyrolants VI. Combustion behaviour and radiation properties of magnesium/polycarbon monofluoride, pyrolant, *Propellants, Explos. Pyrotech*., **2005**, *30*, 209-215.
193. Ćirić-Marjanovic, G.; Pašti, I.; Mentus, S. One-dimensional nitrogen-containing carbon nanostructures, *Prog. Mater. Sci*., **2014**, *69*, 61-182.
194. Zhang, C.; Li, J.; Luo, Y.; Zhang, X.; Zhai, B. Preparation and properties of carbon nanotubes modified glycidyl azide polymer binder film, *Polym. Mater. Sci. Eng*., **2013**, *29*, 105-108.
195. Chi Z., Jie L., Yun-Jun L., Bin Z. Preparation and property studies of carbon nanotubes covalent modified BAMO-AMMO energetic binders*, J Energet Mater,* **2015**, *33*, 305-314.
196. Yan Q.-L., Zeman S., Elbeih A., Thermal behavior and decomposition kinetics of Viton A bonded explosives containing attractive cyclic nitramines, *Thermochim. Acta*, **2013**, *562*, 56-64.
197. Yan Q.-L., Zeman S., Zhang T.-L., Elbeih A., Non-isothermal decomposition behavior of Fluorel bonded explosives containing attractive cyclic nitramines, *Thermochim. Acta*, **2013**, *574*, 10–18.
198. Lin, C.-M.; Liu, J.-H.; Liu, S.-J.; Huang, Z.; Li, Y.-B.; Zhang, J.-H. Characterization viscoelastic properties of multi-walled carbon Nanotubes/F2314 composites using DMA method, *Chin. J. Energet. Mater*., **2015**, *23*, 140-145.
199. Qian, X.-M.; Deng, N.; Wei, S.-F.; Li, Z.-Y. Catalytic effect of carbon nanotubes on pyrotechnics, *Chin. J. Energet. Mater*., **2009**, *17*, 603-607.
200. Guo, R.; Hu, Y.; Shen, R.; Ye, Y.; Wu, L. A micro initiator realized by integrating $KNO_3$/CNTs nanoenergetic materials with a Cu microbridge, *Chem. Eng. J*., **2012**, *211-212*, 31-36.
201. Yan H., Rui G., Yinghua Y., Ruiqi S., Lizhi W., Peng Z., Fabrication and electro-explosive performance of carbon nanotube energetic igniter, *Sci. Tech. Energ. Mater.,* **2012**, *73*, 116-123.
202. Guo, R.; Hu, Y.; Shen, R.; Ye, Y. Electro-explosion performance of $KNO_3$-filled carbon nanotubes initiator, *J. Appl. Phys.*, **2014**, *115*, 174901.
203. Currano, L.J.; Churaman, W.; Becker, C.; Morris, C.J.; Reddy, L.M.; Ihnen, A.; Ajayan, P.; Lee, W.Y. Energetic materials for integration on chip, Proceedings - 14th International Detonation Symposium, IDS, **2010**, 30-36.



 

204. Pelletier, V.; Bhattacharyya, S.; Knoke, I.; Forohar, F.; Bichay, M.; Gogotsi, Y. Copper azide confined inside templated carbon nanotubes, Adv. Funct. Mater., **2010**, *20*, 3168-3174.
205. Choi, W.; Hong, S.; Abrahamson, J. T.; Han, J.-H.; Song, C.; Nair, N.; Baik, S.; Strano, M. S. Chemically driven carbon-nanotube- guided thermopower waves, *Nat. Mater.*, **2010**, *9*, 423-429.
206. Liu, L.-M.; Kang, X.-L.; Yi, Y.; Zhang, H.-F.; Luo, J.-S.; Tang, Y.-J. Influence of CNTs on thermal behavior and light radiation properties of Zr/$KClO_4$ pyrotechnics, *Chin. J. Energet. Mater.*, **2014**, *22*, 75-79.
207. Labhsetwar, N.; Doggali, P.; Rayalu, S.; Yadav, R.; Mistuhashi, T.; Haneda, H. Ceramics in environmental catalysis Applications and possibilities, *Chin. J. Catalyst.*, **2012**, *33*, 1611-1621.
208. Dong, X.-F.; Li, Y.; Xiong, X.-F.; Cao, D.-L. Preparation and performance of copper-lead-carbon composite burning rate catalyst, *Chin. J. Explos. Propellants*, **2011**, *34*, 69-73.
209. Van Devener, B.; Perez, J.P.L.; Jankovich, J.; Anderson, S.L. Oxide-free, catalyst-coated, fuel-soluble, air-stable boron nanopowder as combined combustion catalyst and high energy density fuel, *Ener Fuels*, **2009**, *23*, 6111-6120.
210. Liu, Y.; Jiang, W.; Liu, J.-X.; Wang, Y.; Liu, G.-P.; Li, F.-S. Study of catalyzing thermal decomposition and combustion of AP/HTPB propellant with nano Cu/CNTs, *Acta Armamentarii*, **2008**, *29*, 1029-1033.
211. Liu, X.; Hong, W.-L.; Zhao, F.-Q.; Tian, D.-Y.; Zhang, J.-X.; Li, Q.-S. Synthesis of CuO/CNTs composites and its catalysis on thermal decomposition of FOX-12, *J. Sol. Rock. Tech.*, **2008**, *31*, 508-511, 526.
212. Assovskiy, I.G.; Berlin, A.A. Metallized carbon nanotubes, *Inter. J. Energet. Mater. Chem. Propul.*, **2009**, *8*, 281-289.
213. Wang, F.; Arai, S.; Endo, M. Metallization of multi-walled carbon nanotubes with copper by an electroless deposition process, *Electrochem. Comm.*, **2004**, *6*, 1042-1044.
214. Wang, R.; Li, Z.; Ma, Y.; Zhao, F.; Pei, C. Preparation of high filling ratio $Fe_2O_3$/MWCNTs composite particles and catalytic performance on thermal decomposition of ammonium perchlorate, *Mic. Nano Lett.*, **2014**, *9*, 787-791.
215. Zhang, J.-X.; Hong, W.-L.; Zhao, F.-Q.; Liu, J.-H.; Tian, D.-Y.; Zhu, X.-Y.; Ma, Y.-Q. Synthesis of $SnO_2$-$Cu_2O$/CNTs catalyst and its catalytic effect on thermal decomposition of FOX-12, *Chin. J. Explos. Propellants*, **2011**, *34*, 47-51.
216. Ren, H.; Liu, Y.-Y.; Jiao, Q.-J.; Fu, X.-F.; Yang, T.-T. Preparation of nanocomposite PbO·CuO/CNTs via microemulsion process and its catalysis on thermal decomposition of RDX, *J. Phys. Chem. Sol.*, **2010**, *71*, 149-152.
217. Fan, G.; Wang, H.; Xiang, X.; Li, F. Co-Al mixed metal oxides/carbon nanotubes nanocomposite prepared via a precursor route and enhanced catalytic property, **2013**, *J. Sol. State Chem.*, *197*, 14-22.
218. Pang, W.; Fan, X.; Zhao, F.; Xu, H.; Zhang, W.; Yu, H.; Li, Y.; Liu, F.; Xie, W.; Yan, N. Effects of different metal fuels on the characteristics for HTPB-based fuel rich solid propellants, Propellants, Explos. Pyrotech., **2013**, 386, 852-859.
219. Wu X.-G.; Yan, Q.-L.; Guo, X.; Qi, X.-F.; Li, X.-J. Wang, K.-Q. Combustion efficiency and pyrochemical properties of micron-sized metal particles as the components of modified double-base propellant. *Acta Astro.*, **2011**, *687-8,* 1098-1112.
220. Sylvain, D.; Patric, B.; Nicole, G.; Sebastien, C.; Serge, T. Flash-ignitable energetic material, US Patent, No.20040040637 A1, Mar 4, **2004**.
221. An, T.; Cao, H.-Q.; Zhao, F.-Q.; Ren, X.-N.; Tian, D.-Y.; Xu, S.-Y.; Gao, H.-X.; Tan, Y.; Xiao, L.-B. Preparation and characterization of Ag/CNTs nanocomposite and its effect on thermal decomposition of cyclotrimethylene trinitramine, *Acta Physo.–Chim. Sin.*, **2012**, *28*, 2202-2208.
222. Jeong, H.Y.; So, K.P.; Bae, J.J.; Chae, S.H.; Ly, T.H.; Kim, T.H.; Keum, D.H.; Kim, C.K.; Hwang, J.S.; Choi, Y.J.; Lee, Y.H. Tailoring oxidation of Al particles morphologically controlled by carbon nanotubes, *Energy*, **2013**, *55*, 1143-1151.
223. Rai, A.; Lee, D.; Park, K.; Zachariah, M.R. Importance of phase change of aluminum in oxidation of aluminum nanoparticles, *J. Phys. Chem. B*, **2004**, 108, 14793-14795.
224. Blobaum, K.J.; Reiss, M.E.; Plitzko Lawrence, J.M.; Weihs, T.P. Deposition and characterization of a self-propagating $CuO_x$/Al thermite reaction in a multilayer foil geometry, *J. Appl. Phys.*, **2003**, *94*, 2915-2922.
225. Esawi, A.M.K.; Morsi, K.; Sayed, A.; Taher, M.; Lanka, S. Effect of carbon nanotube CNT, content on the mechanical properties of CNT-reinforced aluminium composites, *Compos. Sci. Tech.*, **2010**, *70*, 2237-2241.
226. Wang, Y.; Malhotra, S.; Iqbal, Z. Nanoscale energetics with carbon nanotubes, *Mater. Res. Soc. Sym. – Proc.,* **2003**, *800*, 351-359.
227. Forohar, F.; Whitaker, C.M.; Uber, I.C.; Bellitto, V. Synthesis and Characterization of Nitro-Functionalized Single-Walled Carbon Nanotubes, *J. Energet. Mater.*, **2012**, *30*, 55-71.
228. Ji, X.-T.; Bu, J.-H.; Ge, Z.-X.; Li, T.-Q.; Su, H.-P.; Liu, Q.; Zhu, Y.; Xiao, X. Preparation and characterization of tetrazolyl-functionalized single walled carbon nanotubes, *Chin. J. Energet. Mater.,* **2015**, *23*, 99-102.
229. Abrahamson, J.T.; Song, C.; Hu, J.H.; Forman, J.M.; Mahajan, S.G.; Nair, N.; Choi, W.; Lee, E.-J.; Strano, M.S. Synthesis and energy release of nitrobenzene-functionalized single-walled carbon nanotubes, *Chem. Mater.*, **2011**, *23*, 4557-4562.
230. Wang, L.; Yi, C.; Zou, H.; Gan, H.; Xu, J.; Xu, W. Adsorption of the insensitive explosive TATB on single-walled carbon nanotubes, *Mol. Phys.*, **2011**, *109*, 1841-1849.
231. Wang, L.; Wu, J.; Yi, C.; Zou, H.; Gan, H.; Li, S. Assemblies of energetic 3,3'-diamino-4,4'-azofurazan on single-walled carbon nanotubes, *Comput. Theo. Chem.*, **2012**, *982*, 66-73.
232. Zhong, Y.; Jaidann, M.; Zhang, Y.; Zhang, G.; Liu, H.; Ioan Ionescu, M.; Li, R.; Sun, X.; Abou-Rachid, H.; Lussier, L.-S. Synthesis of high nitrogen doping of carbon nanotubes and modeling the stabilization of filled DAATO/CNTs 10,10, for nanoenergetic materials, *J. Phys. Chem. Sol.,* **2010**, *71*, 134-139.
233. Hiskey, M. A.; Chavez, D. E; Naud, D. Preparation of 3,3'-azobis6-amino-1,2,4,5-tetrazine, US Patent 6342589, **2002**, United States Department of Energy, USA.
234. Tang, C.C.; Bando, Y.; Golberg, D.; Xu, F.F. Structure and nitrogen incorporation of carbon nanotubes synthesized by catalytic pyrolysis of dimethylforma-mide, *Carbon*, **2004**, *42*, 2625–2633.
235. Huang, K.; Pisharath, S.; Ng, S.-C. Preparation of polyurethane-carbon nanotube composites using 'click' chemistry, *Tetrahed. Lett.*, **2015**, *56*, 577-580.
236. Jiang, K. A.; Eitan, L.S.; Schadler, P.M.; Ajayan, R.W.; Siegel, N.; Grobert, et al., Selective attachment of gold nanoparticles to nitrogen-doped carbon nanotubes, *Nano Lett.*, **2003**, *3*, 275–277.
237. Abou-Rachid, H.; Hu, A.; Timoshevskii, V.; Song, Y.; Lussier, L.-S. Nanoscale high energetic materials A polymeric nitrogen chain N8 confined inside a carbon nanotube, *Phys. Rev. Lett.*, **2008**, *100*, 196401.
238. Zhang, G.-Q.; Liu, X.-B.; Huang, M. Review on energetic nitroguanidine derivatives, *Chin. J. Energet. Mater.*, **2013**, *21*, 668-674.
239. Gao, H.; Shreeve, J.M. Azole-based energetic salts, *Chem. Rev.*, **2011**, *111*, 7377-7436.
240. Nair, U.R.; Asthana, S.N.; Rao, A.S.; Gandhe, B.R. Advances in high energy materials, 2010, *Defense Sci. J.*, *60*, 137-151.
241. Sinditskii, V.P.; Egorshev, V.Yu.; Serushkin, V.V.; Levshenkov, A.I.; Berezin, M.V.; Filatov, S.A.; Smirnov, S.P. Evaluation of decomposition kinetics of energetic materials in the combustion wave, *Thermochim. Acta*, **2009**, *496*, 1-12.
242. Talawar, M.B.; Sivabalan, R.; Mukundan, T.; Muthurajan, H.; Sikder, A.K.; Gandhe, B.R.; Rao, A.S. Environmentally compatible next generation green energetic materials GEMs, *Journal of Hazardous Materials*, **2009**, *161*, 589-607.
243. Korobeinichev, O.P.; Paletskii, A.A.; Volkov, E.N. Flame structure and combustion chemistry of energetic materials, *Russian J. Phys. Chem. B*, **2008**, *2*, 206-228.
244. Beckstead, M.W.; Puduppakkam, K.; Thakre, P.; Yang, V. Modeling of combustion and ignition of solid-propellant ingredients, *Prog. Energ. Combust. Sci.*, **2007**, *33*, 497-551.
245. S. Zeman, Q.-L. Yan, M. Vlcek, Recent advances in the study of the initiation of energetic materials using characteristics of their thermal decomposition, Part I. cyclic nitramines, *Cent. Eur. J. Energ. Mater.*, **2014**, *112*, 173-189.

246. S. Zeman, Q.-L. Yan, A. Elbeih, Recent Advances in the study of the initiation of energetic materials using the characteristics of their thermal decomposition, Part II. Using simple differential thermal analysis, *Cent. Eur. J. Energ. Mater*., **2014**, *113*, 285-294.
247. Q.-L. Yan, S. Zeman, J.-G. Zhang, P. He, T. Musil, M. Bartošková, Multi-stage decomposition of 5-aminotetrazole derivatives kinetics and reaction channels for the rate-limiting steps, *Phys. Chem. Chem. Phys.,* **2014**, *16*, 24282–24291.
248. ZENG Gui-yu, LIN Cong-mei, ZHOU Jian-hua, Influences of Carbon Nanotubes on the Thermal Decomposition Behavior of HMX*, Chin. J. Explos. Propellants*, **2012**, *356*, 55-57.
249. YU Xian-feng. The effect of carbon nanotubes on the thermal decomposition of CL-20, *Chin. J. Explos. Propellants*, **2004**, *273*, 78-80.
250. ZHANG Wei, LI Meng-meng, LI Jie, Effect of carbon nanotubes on thermal decomposition of aminomitrobenzodifuroxan, *J. Combus.t Sci. Tech.*, **2004**, *101*, 92-95.
251. GU Ke-zhuang, LI Xiao-dong, YANG Rong-jie. Catalytic action on combustion and thermal decomposition of AP with CNTs, *Chin. J. Explos. Propellants*, **2006**, *291*, 48-51.
252. Wang, L.-X.; Wu, Z.-B.; Tuo, X.-L.; Zou, H.-T.; Xu, J.; Yi, C.-H.; Xu, W.-L. Theoretical study on thermal decomposition of nitromethane confined inside an armchair 5, 5, single-wall carbon nanotube, *Chin. J. Energet. Mater*., **2009**, *17* 5, 518-522.
253. Wang, L.; Xu, J.; Yi, C.; Zou, H.; Xu, W. Theoretical study on the thermal decomposition of nitromethane encapsulated inside single-walled carbon nanotubes, *J. Mol. Struct. THEOCHEM*, **2010**, *940*, 76-81.
254. Wang, L.; Yi, C.; Zou, H.; Xu, J.; Xu, W. Rearrangement and thermal decomposition of nitromethane confined inside an armchair 5, 5, single-walled carbon nanotube, *Chem. Phys.*, **2010**, *367*, 120-126.
255. Wang, L.; Zou, H.; Yi, C.; Xu, J.; Xu, W. Finite-Length Effect of Carbon Nanotubes on the Encapsulation and Decomposition of Nitromethane ONIOM Calculation, *Curr. Nanosci.*, **2011**, *7*, 1054-1060.
256. Wang, L.; Yi, C.; Zou, H.; Xu, J.; Xu, W. On the isomerization and dissociation of nitramide encapsulated inside an armchair 5,5, single-walled carbon nanotube, *Mater. Chem. Phys.*, **2011**, *127*, 232-238.
257. Reshmi, S.; Catherine, K.B.; Reghunadhan Nair, C.P. Effect of carbon nanotube on the thermal decomposition characteristics of selected propellant binders and oxidisers, *Inter. J. Nanotech.*, **2011**, *8*, 979-987.
258. Li, X.-D.; Yang, R.-J. Combustion and thermal decomposition of ammonium dinitramide catalyzed by carbon nanotubes, *New Carbon Mater*., **2010**, *25*, 444-448.
259. Li Na, Cao Minhua, Wu Qingyin, A facile one-step method to produce Ni/graphenenanocomposites and their application to the thermal decomposition of ammonium perchlorate. *CrystEngComm*, **2012**, *142*, 428-434.
260. Li, Na; Geng, Zhenfeng; Cao, Minhua, Well-dispersed ultrafine $Mn_3O_4$ nanoparticles on graphene as a promising catalyst for the thermal decomposition of ammonium perchlorate. *Carbon*, **2013**, *54*, 124-132.
261. Zhu Junwu, Zeng Guiyu, NieFude, Decorating graphene oxide with CuO nanoparticles in a water-isopropanol system, *Nanoscale*, **2010**, *26*, 988-994.
262. Wenwen Zhang, Qingping Luo, Xiaohui Duan, et al. Nitrated graphene oxide and its catalytic activity in thermal decomposition of ammonium perchlorate. *Mater. Res. Bull.*, **2014**, *50*, 73-78.
263. Izato, Y.-I.; Miyake, A.; Echigoya, H. Influence of the physical properties of carbon on the thermal decomposition behavior of ammonium nitrate and carbon mixtures, *Sci. Tech. Energet. Mater.*, **2009**, *70*, 101-104.
264. Miyake, A.; Izato, Y.-I. Thermal decomposition behaviors of ammonium nitrate and carbon mixtures, *Inter. J. Energet. Mater. Chem. Propul*., **2010**, *9*, 523-531.
265. Yu, L.; Ren, H.; Guo, X.-Y.; Jiang, X.-B.; Jiao, Q.-J. A novel ε-HNIW-based insensitive high explosive incorporated with reduced graphene oxide, *J Therm Anal Calorim*, **2014**, *117*, 1187–1199.
266. Chaban, V.V.; Fileti, E.E.; Prezhdo, O.V. Buckybom, reactive molecular dynamics simulation, *J. Phys. Chem. Lett*., **2015**, *6*, 913-917.
267. Fazhoğlu, H.; Hacaloğlu, J. The effect of triethanolamine on thermal decomposition of GAP, *J. Macromol. Sci. A*, **2002**, *7*, 759–768.
268. Fazlıoğlu, H.; Hacaloğlu, J. Thermal decomposition of glycidyl azide polymer by direct insertion probe mass spectrometry. *J. Anal. Appl. Pyrolysis*, **2002**, *2,* 327–338.
269. Jin, B.; Shen, J.; Peng, R.F.; Shu, Y.J.; Tan, B.S.; Chu, S.J.; Dong, H.S. Synthesis, characterization, thermal stability and sensitivity properties of the new energetic polymer through the azidoacetylation of polyvinyl alcohol, *Polym. Degrad. Stab*; **2012**, *4*, 473–480.
270. Levin I, Brandon D. Thermodynamic stability of Metastable alumina polymorphs crystal structures and transition sequences, *J. Am. Ceram. Soc.* **1998**; *81*, 1995-2012.
271. Jeurgens L, Sloof W, Tichelaar F, Mittemeijer E.; Amorphous oxidefilms on metals application to aluminum oxide films on aluminum substrates, *Phys. Rev. B*, **2000**, *62*, 4707-19.
272. Ren, L.; Chu, E.; Zhang, G.; Bai, Y.; Shi, C.; Sun, L. Development discussion on metrology of initiators and pyrotechnics, Proceedings - 4th International Conference on Computational and Information Sciences, ICCIS, **2012**, 6300819, 1120-1122.
273. Zhu, P.; Zhou, X.; Shen, R.-Q.; Ye, Y.-H.; Hu, Y. Electrical-explosion performance of dielectric structure pyrotechnic initiators prepared by Al/CuO reactive multilayer films, *Chin. J. Energet. Mater*., **2011**, *19*, 366-369.
274. Zhu, P.; Shen, R.; Fiadosenka, N.N.; Ye, Y.; Hu, Y. Dielectric structure pyrotechnic initiator realized by integrating Ti/CuO-based reactive multilayer films, *J. Appl. Phys*., **2011**, *109*, 084523.
275. Hinkel, T.J.; Salazar, F. Material properties effects on pyrotechnic initiator output, 44th AIAA/ASME/SAE/ASEE Joint Propulsion Conference and Exhibit, **2008**.
276. Manaa, M.R.; Mitchell, A.R.; Garza, P.G.; Pagoria, P.F.; Watkins, B.E. Flash ignition and initiation of explosives-nanotubes mixture, *J. Am. Chem. Soc.,* **2005**, *127*, 13786-787.
277. Kappagantula, K.; Pantoy, M.L.; Hunt, E.M. Impact ignition of aluminum-teflon based energetic materials impregnated with nano-structured carbon additives, *J. Appl. Phys.*, **2012**, *112*, 024902.
278. Kappagantula, K.; Pantoya, M.L. Experimentally measured thermal transport properties of aluminum- polytetrafluoroethylene nanocomposites with graphene and carbon nanotube additives, *Inter. J. Heat Mass Trans.*, **2012**, *55*, 817-824.
279. W. Hong, N. Tai, Investigations on the thermal conductivity of composites reinforced with carbon nanotubes, *Diam. Relat. Mater.,* **2008**, *17*, 1577–1581.
280. Kim, J.H.; Ahn, J.Y.; Park, H.S.; Kim, S.H. Optical ignition of nanoenergetic materials: the role of single-walled carbon nanotubes as potential optical igniters, *Combust. Flame*, **2013**, *160*, 830-834.
281. Collins, E.S.; Skelton, B.R.; Pantoya, M.L.; Irin, F.; Green, M.J.; Daniels, M.A.; Ignition sensitivity and electrical conductivity of an aluminum fluoropolymer reactive material with carbon nanofillers, *Combust. Flame*, **2015**, *162*, 1417-1421.
282. Kim, J.H.; Kim, S.B.; Choi, M.G.; Kim, D.H.; Kim, K.T.; Lee, H.M.; Lee, H.W.; Kim, J.M.; Kim, S.H. Flash-ignitable nanoenergetic materials with tunable underwater explosion reactivity: the role of sea urchin-like carbon nanotubes, *Combust. Flame*, **2015**, *162*, 1448-1454.
283. Wang, Y.-L.; Wei, Z.-X.; Kang, L. Progress on combustion catalysts of solid propellant, *Chin. J. Energet. Mater.,* **2015**, *23,* 89-98.
284. Chai, Y.-P.; Zhang, T.-L. Advances on burning rate catalyzer of composite solid propellant at home and abroad, *J Sol. Rock. Tech.*, **2007**, *30*, 44-47.
285. Han, X.; Li, S. Advances in catalytic function of fullerene materials, *Prog. Chem.*, **2006**, *18,* 715-720.
286. Abrahamson, J.T.; Nair, N.; Strano, M.S. Modelling the increase in anisotropic reaction rates in metal nanoparticle oxidation using carbon nanotubes as thermal conduits, *Nanotechn.*, **2008***, 19*, 195701.
287. Sabourin, J.L.; Dabbs, D.M.; Yetter, R.A.; Dryer, F.L.; Aksay, I.A. Functionalized graphene sheet colloids for enhanced fuel/propellant combustion, *ACS Nano*, **2009**, *3,* 3945-3954.
288. X. Han, T.F. Wang, Z.K. Lin, D.L. Han, S.F. Li, F.Q. Zhao, L.Y. Zhang, RDX/AP-CMDB Propellants Containing Fullerenes and Carbon Black Additives, *Defence Sci. J.*, **2009**, *59*, 284-293.
289. Bice Charles C. Propellants with improved burning rate. US patent, **1962**, US 3018204 A.



 

290. Ives Edwin K. Catalyzed propellant compositions of high burning rate. US patent, **1966**, US 3240640 A.
291. VermaSumit, Ramakrishna P A. Activated charcoal A novel burn rate enhancer of aluminized composite propellants. *Combust. Flame*, **2010**, *157*, 1202-1210.
292. Verma, S.; Ramakrishna, P. A. Investigations on activated charcoal, a burn-rate enhancer in composite solid propellant[J]. Journal of Propulsion and Power, **2013**, *295*, 1214-1219.
293. Li X.D.; Yang R.-J.; Li X.-X. The functional additveis CNTs, conference paper in Propellants Explos. Proced., **2004**, Xi'an Modern Chemistry Research Institute, 228-231.
294. R.-Z. Hu; Y. Wang; J. Zheng. The application of nano-sized materials in solid propellants, The, 24th annual conference in Professional Committee of solid rocket propellant of Chinese Society of Astronautics. Xiang Fan, China, **2003**, 144-149.
295. Zhao F.-Q.; Yi J.-H. Preparation method of $Cu_2O$-PbO/GO composites; Chinese patent, **2013**, CN 1003007947 A.
296. Tan Q.-L.; Hong W.-L.; Xiao X.-B. Preparation of $Bi_2O_3$/GO and its combustion catalytic performance on double-base propellant, *Nanosci. Nanotech.*, **2013**, *106*, 22-27.
297. Hong W.-L.; Shi H.-B.; Zhao F.-Q. Preparation method of $Cu_2O$-$Bi_2O_3$/GO composites, Chinese patent, **2013**, CN 102895979A.
298. Hong W.-L.; Xue Y.-F.; Zhao F.-Q. Preparation of $Bi_2O_3$/CNTs Composite and Its Combustion Catalytic Effecton Double-base Propellant, *Chin. J. Explos. Propellants*, **2012**, *6*, 7-11.
299. Hong W.-L.; Zhu X.-Y.; Zhao F.-Q. Preparation of CuO/CNTs and its combustion catalytic activity on double-base propellant, *Chin. J. Explos. Propellants,* **2010**, *336,* 83-86.
300. Liu J.-H.; Hong W. L.; Zhu X.-Y. A preparation method for Cu-Bi/CNTs composite coated by carbon particles. Chinese patent, 2010, CN 101757927A.
301. Liu Y.; Jiang W.; Liu J.-X. A study of catalyzing thermal decomposition and combustion of AP/HTPB propellant with nano Cu/CNTs. *Acta Armamentarii*, **2008**, *299*, 1029-1033.
302. Zhang X.-J.; Jiang W.; Song D. Liu J.-X. Preparation and catalytic activity of Ni/CNTs nanocomposites using microwave irradiation heating method. Mater. Lett., **2008**, *621*, 2343–2346.
303. Li, F.; Jiang, W.; Guo, X.; Liu, L.; Li, M.; Chen, W.; Wu, S. Application of nanometer materials for solid propellants, *Inter. J. Energet. Mater. Chem. Propul.*, **2011**, *10*, 67-83.
304. Malec, C.D.; Voelcker, N.H.; Shapter, J.G.; Ellis, A.V. Carbon nanotubes initiate the explosion of porous silicon, **2010**, *Mater. Lett*., 64, 2517-2519.
305. Martirosyan, K.S.; Wang, L.; Luss, D. Tuning the gas pressure discharge of nanoenergetic materials by boron and carbon nanotubes additives, Technical Proceedings of the, 2011 NSTI Nanotechnology Conference and Expo, NSTI-Nanotech, **2011**, *1*, 323-326.
306. Doorenbos, Z.; Groven, L.; Haines, C.; Kapoor, D.; Puszynski, J. Novel pyrophoric substrates with a tunable energetic output, AIChE Annual Meeting, Conference Proceedings, **2010**.
307. Manaa, M.R.; Mitchell, A.R.; Garza, P.G.; Pagoria, P.F.; Watkins, B.E. Flash ignition and initiation of explosives-nanotubes mixture, *J. Am. Chem. Soc*., **2005**, *127*, 13786.
308. Zhang, C.; Wen, Y.; Xue, X. Self-enhanced catalytic activities of functionalized graphene sheets in the combustion of nitromethane Molecular dynamic simulations by molecular reactive force field, *ACS Appl. Mater. Interf.*, **2014**, *6*, 12235.
309. X.; Xiang; S.-B.; Xiang; Z.; Wang; X.; Wang; G. Hua, Photo-responsive behaviors and structural evolution of carbon-nanotube-supported energetic materials under a photoflash, *Mater. Lett.*, **2012**, *88*, 27-29.
310. Jin, B.; Peng, R.; Zhao, F.; Yi, J.; Xu, S.; Wang, S.; Chu, S. Combustion effects of nitrofulleropyrrolidine on RDX-CMDB propellants, *Propellants, Explos. Pyrotech.,* **2014**, *39*, 874-880.
311. Huagn, M.; Tan, B.-S. Some strategies on the stabilization of high-energy explosives, *Chin. J. Energet. Mater*., **2014**, *22*, 134-135.
312. Lee, T.; Chen, J.W.; Lee, H.L.; Lin, T.Y.; Tsai, Y.C.; Cheng, S.-L.; Lee, S.-W.; Hu, J.-C.; Chen, L.-T. Stabilization and spheroidization of ammonium nitrate Co-crystallization with crown ethers and spherical crystallization by solvent screening, *Chem. Eng. J.*, **2013**, 2*25*, 809-817.
313. Lang, A.J.; Vyazovkin, S. Phase and thermal stabilization of ammonium nitrate in the form of PVP-AN glass, *Mater. Lett.*, **2008**, 62, 1757-1760.
314. Zhang, Z.; Wang, B.; Ji, Y.; Liu, Z.; Liu, Q. Thermal Stabilization of Ammonium Dinitramide ADN, Proceedings of the, International Autumn Seminar on Propellants, Explosives and Pyrotechnics, IASPEP, *Theory Practice Energet. Mater.*, **2003**, *5*, 259-262.
315. Smeu, M.; Zahid, F.; Ji, W.; Guo, H.; Jaidann, M.; Abou-Rachid, H. Energetic molecules encapsulated inside carbon nanotubes and between graphene layers DFT calculations, *J. Phys. Chem. C*, **2011**, *115*, 10985-10989.
316. Abou-Rachid, H.; Hu, A.; Timoshevskii, V.; Song, Y.; Lussier, L.-S. Nanoscale high energetic materials: A polymeric nitrogen chain $N_8$ confined inside a carbon nanotube, *Phys. Rev. Let.,* **2008**, *100*, 196401.
317. Ji, W.; Timoshevskii, V.; Guo, H.; Abou-Rachid, H.; Lussier, L. Thermal stability and formation barrier of a high-energetic material $N_8$ polymer nitrogen encapsulated in 5,5, carbon nanotube, *Appl. Phys. Lett*., **2009**, *95*, 021904.
318. Liu, Y.; Lai, W.; Yu, T.; Ge, Z.; Kang, Y. Structural characteristics of liquid nitromethane at the nanoscale confinement in carbon nanotubes, *J. Mol. Mod.*, **2014**, *20*, 8.
319. Benchafia, E.M., Yu, C., Sosnowski, M., Ravindra, N.M., Iqbal, Z. Plasma synthesis of nitrogen clusters on carbon nanotube sheets, *JOM*, **2014**, *66*, 608-615.
320. Wu, Z., Benchafia, E.M., Iqbal, Z., Wang, X. $N_8$ polynitrogen stabilized on multi-wall carbon nanotubes for oxygen-reduction reactions at ambient conditions *Angew. Chem. – Inter. Ed*., **2014**, *53*, 12555-12559.
321. Yan, Q.-L.; Zeman, S. Theoretical evaluation of sensitivity and thermal stability for high explosives based on quantum chemistry methods a brief review, *Int. J. Quant. Chem.*, *113*, **2013**, 1049-1061.
322. Pandey AK. Damage prediction of RC containment shell under impact and blast loading. *Struc.t Eng. Mech.*, **2010**, *366*, 729-44.
323. Urtiew PA, Tarver CM. Shock initiation of energetic materials at different initial temperatures review, *Combust. Explos. Shock Waves*, **2005**, *416*, 766-76.
324. Keshavarz M. H. Overview on theoretical prediction of 3,6-bis-3,5-dinitro-1,2,4-triazolyl'-1,2,4,5-tetrazine as a high performance explosive. *Chin. J. Energet. Mater.,* **2007**, *155*, 551-4.
325. Walley, S. M.; Field, J. E.; Greenaway M. W. Crystal sensitivities of energetic materials a review, *Mater. Sci. Tech.*, **2006**, *22*, 402-413.
326. Wu, C. J.; Piggott, T.; Yoh, J.; Reaugh, J. Numerical Modeling of Impact Initiation of High Explosives, UCRL-TR-221760, June 1, **2006**.
327. Jin, B.; Peng, R.; Chu, S.; Huang, Y.; Wang, R. Study of the desensitizing effect of different [60]fullerene crystals on cyclotetramethylene tetranitramine HMX, *Propellants, Explos. Pyrotech.,* **2008**, 33, 454-458.
328. Assovskiy, I.G. Metallized SWCNT-promising way to low sensitive high energetic nanocomposites, *Propellants, Explos. Pyrotech*., **2008**, *33*, 51-54.
329. Xu, J.; Wu, L.-Z.; Shen, R.-Q.; Ye, Y.-H.; Hu, Y. Effects of dopants and confined windows on laser initiation sensitivity of explosives, *Chin. J. Explos. Propellants*, **2011**, *34*, 77-79, 85.
330. Siegert, B.; Comet, M.; Muller, O.; Pourroy, G.; Spitzer, D. Reduced-sensitivity nanothermites containing manganese oxide filled carbon nanofibers, *J. Phys. Chem. C,* **2010**, *114*, 19562-19568.
331. Zecheru, T.; Rotariu, T.; Matache, L.-C.; Sava, A.-C.; Lungu, R.-M.; Voicu, A.; Cosereanu, L. Synthesis and applications of 3-nitro-1,2,4-triazol-5-one based hybrid energetic compositions, *Revista de Chimie*, **2014**, *65*, 1186-1189.